

Yield Stress Materials in Soft Condensed Matter

Daniel Bonn and Jose Paredes

*Van der Waals-Zeeman Institute,
Institute of Physics,
University of Amsterdam,
Science Park 904,
1098 XH Amsterdam,
The Netherlands*

Morton M. Denn

*Benjamin Levich Institute for Physico-Chemical Hydrodynamics,
City College of New York,
New York, NY 10031,
USA*

Ludovic Berthier

*Laboratoire Charles Coulomb, UMR 5221,
CNRS and Université Montpellier, Montpellier,
France*

Thibaut Divoux

*Centre de Recherche Paul Pascal, UPR 8641,
115 av. Dr. Schweitzer, 33600 Pessac,
France*

Sébastien Manneville

*Université de Lyon,
Laboratoire de Physique,
École Normale Supérieure de Lyon,
CNRS UMR 5672,
46 Allée d'Italie,
69364 Lyon cedex 07,
France*

We present a comprehensive review of the physical behavior of yield stress materials in soft condensed matter, which encompasses a broad range of soft materials from colloidal assemblies and gels to emulsions and non-Brownian suspensions. All these disordered materials display a nonlinear response to an external mechanical forcing, which results from the existence of a finite force threshold for flow to occur, the yield stress. We discuss both the physical origin and the rheological consequences associated with this nonlinear behavior. We give an overview of the different experimental techniques developed to measure the yield stress. We discuss extensively the recent progress concerning a microscopic description of the flow dynamics of yield stress materials, emphasizing in particular the role played by relaxation timescales, the interplay between shear flow and aging behavior, the existence of inhomogeneous shear flows and shear bands, wall slip, and non-local effects in confined geometries. We finally review the status of modeling of the shear rheology of yield stress materials in the framework of continuum mechanics.

CONTENTS

		stress	10
I. A short introduction: What are yield stress materials?	2	D. Thixotropy in yield stress fluids	11
II. General concepts about yield stress fluids	3	E. Theoretical considerations on yield stress materials	13
A. Popular rheological models for yield stress materials	3	1. Why a theory of yield stress solids is difficult	13
B. Physical origin of the yield stress in soft materials	4	2. Flow curves from theories	14
1. Simple colloidal systems: Soft glassy materials	4	III. How the yield stress is determined classically:	
2. Non-Brownian suspensions: Jammed materials	5	Measurement techniques	17
3. Role of attractive forces: Colloidal gels	7	A. General overview of yield stress determination under drag flow	17
C. Is the yield stress real?	9	B. Yield stress measured starting from the solid state	18
1. Lessons from a historical debate	9	1. Shear-start up experiments	18
2. Theoretical insight on the existence of a yield		2. Creep experiments	20

3. Large-amplitude oscillatory shear (LAOS) experiments	20
C. Yield stress measured starting from the liquid state	22
1. Extrapolation of the flow curve in the limit of vanishing shear rates	22
2. Flow cessation experiments	23
D. Comparison between the different methods	23
E. Yield stress or yield strain?	24
IV. Flow dynamics of yield stress fluids	24
A. Distinction between simple and thixotropic yield stress fluids	25
1. From flow curve measurements	25
2. From “viscosity bifurcation”	26
3. From local measurements	26
B. What causes steady-state shear banding?	29
1. Competition between aging and shear rejuvenation	29
2. Simple theoretical models	29
3. Flow-concentration coupling	31
C. Wall slip related effects	32
1. Impact on flow curve measurements	32
2. Physical origin of wall slip in yield stress fluids	33
3. How to deal with wall slip in practice?	35
D. “Hot topics”	36
1. How do yield stress materials creep prior to fluidization?	36
2. How do yield stress materials behave in confined geometries?	36
3. What is the origin and scaling of the yielding timescales?	38
V. Towards a continuum treatment of yield stress materials	40
A. Rheology	40
1. Properly invariant 3-D models	40
2. Extensional flow	41
3. Normal Stresses	42
B. Fluid Mechanics	43
1. Analytical approaches	43
2. Computational issues	43
3. The conceptual starting point	45
4. Comparison with experiments in non-viscometric flows	46
C. Structure and Viscoelasticity	46
1. Structural continuum models	46
2. Viscoelastic modeling	48
VI. Conclusion	50
Acknowledgments	51
References	51

I. A SHORT INTRODUCTION: WHAT ARE YIELD STRESS MATERIALS?

Many of the materials we encounter in our daily life are neither perfectly elastic solids nor simple Newtonian fluids, and attempts to describe these materials as being either fluid or solid often fail. Try for instance to determine which material has the higher “viscosity” between whipped cream or thick syrup. When moving a spoon through these two materials we would clearly conclude that syrup is the more viscous fluid, but if we leave these two fluids at rest, the syrup will readily flatten and become horizontal under the force of gravity while whipped cream will retain its shape for a long time. In that case,



FIG. 1 Comparing the flow properties of whipped cream and thick maple syrup. Slowly stirring both materials with a spoon suggests that syrup is more viscous, but the conclusion is the opposite when observing the flattening of two piles of material. So which fluid is more viscous? The question is ill-posed. The flow properties of whipped cream cannot be reduced to a single viscosity value because it is a yield stress material, whereas syrup is simply a very viscous fluid.

we would instead conclude that whipped cream is more viscous than syrup (Fig. 1). This apparent contradiction stems from the fact that the syrup is a Newtonian fluid, whereas whipped cream is not a true fluid at all, and its flow properties cannot simply be reduced to a single number, such as the viscosity. Whipped cream does not flow if the imposed stress is below a threshold value, but it can flow rather easily after this value is exceeded. This threshold rheology is the defining feature of *yield stress materials*. Classical examples of yield stress materials include paints, foams, wet cement, cleansing creams, mayonnaise, tooth paste, etc.

This long list of ordinary products demonstrates that yield stress materials are widely used in pharmaceutical and cosmetic applications. Other application fields include oil industry, where estimating the minimum pressure requested to restart a gelled crude oil pipeline is crucial (Chang *et al.*, 1999). The yield stress is also relevant for instance to the concrete and the dairy product industries, where its value is related to the size of air bubbles that remain trapped in the material and affect its final properties (van Aken, 2001; Kogan *et al.*, 2013). Therefore, the physical, and more particularly, the flow properties of these types of materials are important for their formulation and handling. In this sense, it is of paramount importance to characterize more quantitatively the force threshold to obtain a flowing material, *the yield stress*, as this represents the characteristic force needed to make the material flow.

We wish to review the recent progress concerning both the fundamental understanding of the yield stress and its practical determination in a broad range of materials across soft condensed matter. The existence of a threshold for flow suggests that these materials respond in a highly nonlinear manner, which has dramatic impact on their dynamical properties under flow, which we also review extensively. These problems are of key importance both for fundamental purposes and for numerous practical situations involving amorphous solids across a broad

spectrum of hard and soft condensed matter.

The manuscript is structured as follows. We first give in section II a general overview of the various physical concepts and issues raised by the existence of a yield stress, with emphasis on model system and theoretical approaches. In section III, we provide a critical review of the traditional rheological techniques used for measuring the yield stress. Section IV is devoted to the most recent developments and “hot topics” regarding flow dynamics of yield stress fluids, including time-dependence, shear banding and wall slip. Finally, we turn towards the general, fully three-dimensional approach of yield stress materials required for describing flows in complex geometries.

II. GENERAL CONCEPTS ABOUT YIELD STRESS FLUIDS

A. Popular rheological models for yield stress materials

Quantifying the steady state flow properties of non-Newtonian fluids requires the measurement of an entire function, the *flow curve*, since the shear viscosity is not a unique number. For a simple shear geometry, the flow curve is a representation of the dependence of the shear stress, σ , on the shear rate, $\dot{\gamma}$. For a Newtonian fluid, these functions are linearly related, $\sigma = \eta\dot{\gamma}$, where η is a constant viscosity. For a yield stress material, the viscosity becomes formally a function of the shear rate, $\sigma = \eta(\dot{\gamma})\dot{\gamma}$, and the flow curve $\sigma = \sigma(\dot{\gamma})$ is not a simple straight line crossing the origin.

The most elementary model capturing the existence of a finite yield stress is the Bingham model (Bingham, 1922):

$$\sigma < \sigma_y \Rightarrow \dot{\gamma} = 0, \quad (1)$$

$$\sigma \geq \sigma_y \Rightarrow \sigma = \sigma_y + \eta_p \dot{\gamma}, \quad (2)$$

where $\sigma_y > 0$ is the yield stress, and η_p a model parameter describing the slope of the flow curve in the fluid region, which is defined by $\dot{\gamma} > 0$. The Bingham model is equivalently described by an effective viscosity which is asymptotically equal to η_p at large stresses, and diverges continuously as the stress decreases towards the yield stress: $\eta_{\text{eff}}(\dot{\gamma}) \equiv \sigma/\dot{\gamma} = \eta_p + \sigma_y/\dot{\gamma}$.

In Fig. 2(a) the flow curve of whipped cream is shown, and it can be seen that the Bingham model gives a reasonable description of this measured flow curve with a yield stress of about $\sigma_y \approx 33$ Pa. In Fig. 2(b) the flow curves of whipped cream and syrup are shown together. This shows that an answer to the question of which material has the higher viscosity actually depends on the relevant shear rates (stresses): for shear rates (stresses) above 4 s^{-1} (33 Pa), syrup is the more viscous material, but for shear rates (stresses) below that value, whipped cream is by far the more viscous material. Therefore, it

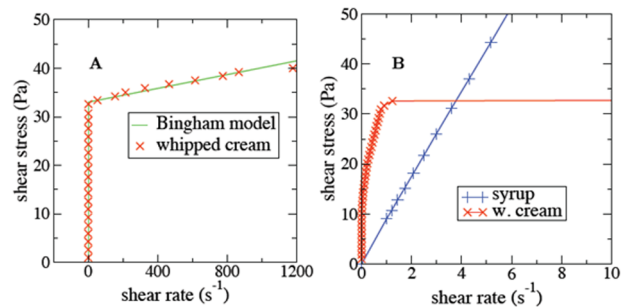


FIG. 2 (a) The Bingham model provides a reasonable fit to the flow curve of whipped cream. The yield stress is seen to be about $\sigma_y \approx 33$ Pa. (b) The flow curves of syrup and whipped cream at low shear rates. Data points are connected by lines. For stresses above 33 Pa, whipped cream flows more easily, while the opposite is true below 33 Pa. Using this enlarged scale, one can see that the flow curve of whipped cream is not well described by the Bingham model at low shear rates.

makes little sense to compare these two “fluids”, as only one of them is in fact really a fluid.

Comparing Figs. 2(a) and (b) also shows that whereas the Bingham model gives an excellent fit to the flow curve of whipped cream for a certain range of shear rates [Fig. 2(a)], it fails once the resolution is improved [Fig. 2(b)]. From the latter plot, one would conclude that the yield stress is about $\sigma_y \approx 10$ Pa, rather than 33 Pa. This highlights one of the practical problems encountered when working with complex fluids: before a question about the flow properties of a complex material can be satisfactorily answered one needs to carefully consider the exact experimental protocol as well as the range and resolution of shear rates/stresses over which the data are analyzed.

Two popular generalizations of the Bingham fluid model in shear flow are the Herschel-Bulkley (Herschel and Bulkley, 1926) and Casson equations, given respectively as

$$\text{Herschel - Bulkley : } \sigma = \sigma_y + K\dot{\gamma}^n, \quad \sigma \geq \sigma_y, \quad (3)$$

$$\text{Casson : } \sigma^{1/2} = \sigma_y^{1/2} + (\eta_p \dot{\gamma})^{1/2}, \quad \sigma \geq \sigma_y(4)$$

where K and n are additional parameters. Obviously, the Bingham model is a specific instance of the Herschel-Bulkley equation, obtained by imposing $n = 1$.

The Herschel-Bulkley model is very popular as it offers more flexibility for fitting experimental data than the Bingham model. It describes both the yield stress regime, $\sigma \approx \sigma_y$, at low shear rate, and a power-law shear-thinning behavior, $\sigma \approx K\dot{\gamma}^n$, with $n < 1$ for larger shear rates. Across a large variety of systems, the shear-thinning exponent n is found to have a value in the range $n = 0.2 - 0.8$. Frequently, n changes very little with either the density or the temperature (Vinogradov *et al.*, 1978) of the material, so that it appears as a relevant “material parameter”, as found for instance for microgels

(Gutowski *et al.*, 2012; Nordstrom *et al.*, 2010; Oppong *et al.*, 2006; Roberts and Barnes, 2001), emulsions (Bécu *et al.*, 2006; Mason *et al.*, 1996), and foams (Gilbreth *et al.*, 2006; Höhler and Cohen-Addad, 2005; Pratt and Dennin, 2003; Princen and Kiss, 1989). The crossover between the yield stress regime and the shear thinning regime occurs for a typical shear rate $\dot{\gamma}^* \approx (\sigma_y/K)^{1/n}$. It is therefore tempting to interpret the corresponding timescale $1/\dot{\gamma}^*$ as a relevant microscopic timescale for the material (Bonnecaze and Cloitre, 2010). Finally, we remark that the Herschel-Bulkley equation predicts the existence of a diverging timescale τ governing the relaxation to steady state in stress-controlled experiments in the vicinity of the yield point, i.e. for $\sigma \gtrsim \sigma_y$, since one gets: $\tau \sim \dot{\gamma}^{-1} \approx [K/(\sigma - \sigma_y)]^{1/n}$, which readily suggests a “critical” interpretation of the yielding transition observed in steady state simple shear flows (Chaudhuri and Horbach, 2013; Divoux *et al.*, 2012). This point will be discussed extensively in Sec. IV.D.

B. Physical origin of the yield stress in soft materials

A central question on the behavior of yield stress materials concerns the elucidation of its physical origin. Ideally, one would like to know under what conditions a given system will exhibit a yield stress, what are the microscopic mechanisms responsible for the emergence of a yield stress, and whether general rules can be formulated to predict for instance the value of the yield stress as a function of the composition and structural organization of the material from the knowledge of the microscopic constituents and interactions between them.

In the soft condensed matter literature, the emergence of a finite yield stress is frequently referred to as a “jamming transition” (Liu and Nagel, 2001). In fact, the two concepts are often taken as being nearly equivalent, such that “jammed” then simply means that a material does not flow unless a finite stress is applied. This idea is graphically captured by the “jamming phase diagram”, first proposed by Liu and Nagel, which illustrates the idea that a broad range of dense amorphous materials (from foams and grains to dense liquids) share important similarities (Liu and Nagel, 1998). In fact, we ourselves follow this general line of thought in writing a review article on yield stress materials in soft condensed matter, because we implicitly assume that they form a coherent family, which is defined by the emergence of a finite yield stress as either temperature or density is varied.

However, whereas the construction of the jamming phase diagram implicitly suggests that all amorphous solids undergo a “jamming transition” between fluid and solid states, this view does not capture well the variety of phase transitions which account for the existence of solid behaviour in soft condensed materials. In the following, we describe three important types of yield stress materi-

als whose solid behavior originates from different types of phase transitions (or sharp dynamical crossovers), which are usually described by distinct types of theoretical approaches as well. Of course, these distinctions do not imply that the rheology of these materials is different, and it still makes sense to talk about the “rheology of yield stress materials” in a general sense, as we do throughout this review. This is because several aspects of their rheology mainly depend on the existence of the yield stress, independently of the physical ingredients and parameters controlling its value.

1. Simple colloidal systems: Soft glassy materials

Suspensions of nearly-hard sphere colloidal particles are amongst the most studied experimental systems in soft condensed matter (Pusey and van Meegen, 1986), as they represent good model systems to study a large variety of physical phenomena also occurring in atomic and molecular systems, from first-order crystallisation to glassy dynamics (Royall *et al.*, 2013). For colloidal particles, thermal fluctuations and Brownian motion play a key role, since they ensure that the system may reach thermal equilibrium. However, when colloidal hard spheres are compressed, they undergo a colloidal glass transition that shares important similarities with the glass transition observed upon decreasing the temperature in molecular supercooled liquids (Pusey and van Meegen, 1987). Experimentally, above a “glass transition” packing fraction of about $\phi_G \approx 0.58 - 0.60$ (in three dimensional suspensions), the equilibrium relaxation time of the colloidal suspension becomes so large that the particles do not significantly diffuse over a typical experimental timescale and the system is effectively dynamically arrested (Brambilla *et al.*, 2009). Above ϕ_G , colloidal particles simply perform localized back and forth “vibrational” motion inside the cage formed by their neighbors. This empirical definition of the glass transition density demonstrates that its actual location is not very well-defined experimentally, in the sense that deciding whether a material is “solid” or simply “very viscous” depends on the observation timescale (or the explored range of shear rates in steady state flow curves). In particular, this implies that the (disputed!) question of the (continuous or discontinuous) nature of the emergence of a yield stress in soft glassy materials can in fact receive no sharp answer, the question being ill-posed.

The rheological consequences of the glass transition are readily observed in the flow curves shown in Fig. 3(a) (Petekidis *et al.*, 2004). An extended Newtonian regime is observed for $\phi < \phi_G$, which defines a density dependent viscosity, $\eta(\phi)$ that is seen to increase very rapidly as the density increases towards ϕ_G . A finite yield stress σ_y emerges as the glass transition is crossed for $\phi > \phi_G$, which increases as the colloidal glass concentration is in-

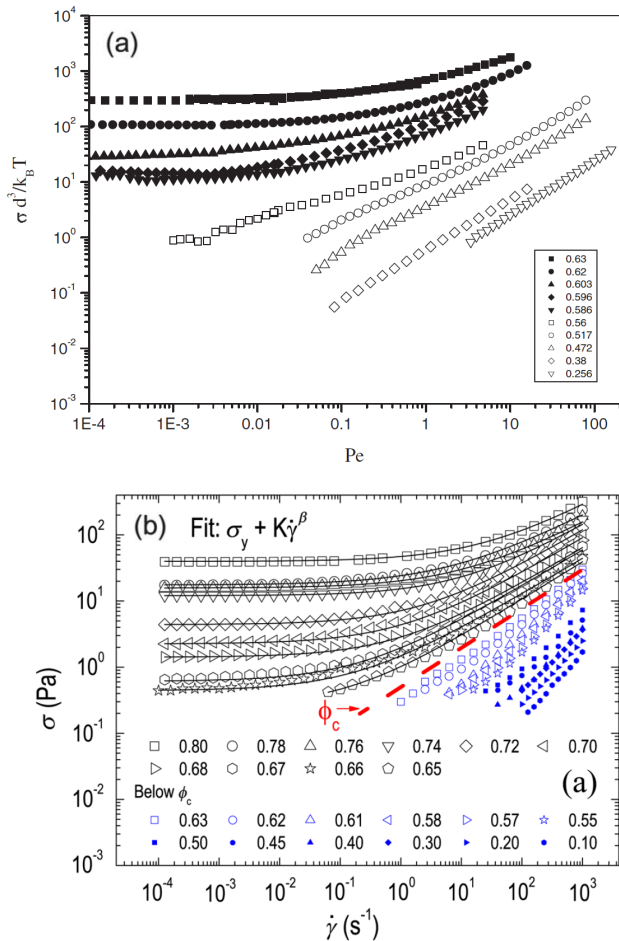


FIG. 3 (a) Soft glassy rheology. Evolution of the flow curves across the thermal colloidal glass transition for a suspension of PMMA hard spheres of size $a \approx 200$ nm. Extracted from (Petekidis *et al.*, 2004). (b) Jamming rheology. Evolution of the flow curves for an oil-in-water emulsion with droplet size $a \approx 3.2 \mu\text{m}$ across the athermal jamming transition. Extracted from (Paredes *et al.*, 2013). Although the emergence of solid behaviour in both cases is conceptually very different, the flow curves of both materials are surprisingly similar.

creased further. In the vicinity of the glass transition, $\phi \approx \phi_G$, a shear-thinning regime is observed, where $\sigma \simeq \dot{\gamma}^n$ with $n < 1$, underlying the general fact that the rheology of glassy suspensions occurs mostly out of the viscous regime. In fact, accurate measurements of the viscosity in hard sphere suspensions are scarce, and often limited to a modest dynamic regime (Cheng *et al.*, 2002). In the glass phase, the flow curve is typically well described by the Herschel-Bulkley law, which efficiently incorporates both the yield stress and shear-thinning behaviors in a single empirical model.

Similar flow curves are observed in many systems undergoing a glass transition, from dense molecular liquids (Berthier and Barrat, 2002) to colloidal suspensions with soft and hard repulsion between the particles (Nordstrom

et al., 2010; Petekidis *et al.*, 2004; Siebenb rger *et al.*, 2012). In all these systems, a finite yield stress emerges experimentally when the shear viscosity becomes so large (when changing density or temperature) that the system cannot flow anymore on experimentally accessible time scales. Physically, the yield stress results from the fact that particles move too slowly and cannot rearrange the structure fast enough to relax the stress introduced by an external deformation. Therefore, a simple criterion for the emergence of a yield stress is when the timescale for equilibrium relaxation, usually called “alpha-relaxation” timescale, τ_α , becomes slower than the timescale of the external deformation, given by $1/\dot{\gamma}$. In the regime where $\tau_\alpha \dot{\gamma} \gg 1$, spontaneous relaxation cannot occur over the rheologically relevant time window and the system appears solid. Empirically, τ_α closely follows the behavior of the Newtonian viscosity, $\tau_\alpha \propto \eta(\phi)$.

In such glassy materials, the yield stress is typically a function of temperature and density. This dependence simplifies considerably for the hard sphere model, because the hard sphere potential contains no energy scale. In that case, the relevant stress scale controlling solidity is $\sigma_T = k_B T/a^3$, where k_B is Boltzmann’s constant, T the temperature and a the particle diameter, so that the yield stress can be rewritten as $\sigma_y = \sigma_T f(\phi)$, where $f(\phi < \phi_G) = 0$. This behavior emphasizes the entropic origin of the solidity in colloidal hard spheres, and therefore the crucial role played by thermal fluctuations in the emergence of a yield stress in colloidal particles with purely repulsive interactions (Ikeda *et al.*, 2012; Petekidis *et al.*, 2004).

Finally, when the colloidal glass is compressed much above the glass transition, the interparticle distance decreases and particles eventually come into near contact as the “random close packing” packing fraction is approached (Bernal and Mason, 1960). As a consequence, the colloidal glass becomes stiffer, and this results also in a strong increase of the yield stress, which appears to diverge as a power law, $\sigma_y \sim \sigma_T(\phi_J - \phi)^{-\gamma}$, with an exponent $\gamma \approx 1$ and where the jamming density $\phi_J > \phi_G$ is the topic we discuss next. As also discussed in the next section, this functional form shows that the yield stress vanishes for fully non-Brownian suspensions of hard particles due to the entropic prefactor $\sigma_T = k_B T/a^3$, such that suspensions of non-Brownian hard particles do not belong to the family of yield stress materials.

2. Non-Brownian suspensions: Jammed materials

When the typical size a of the colloidal particles increases, Brownian motion becomes negligible and thermal fluctuations are less relevant. This is because the typical time scale for a Brownian particle to diffuse over a distance comparable to its own size scales as a^2/D_0 , where D_0 is the single particle diffusion constant. For

an observation time scale of the order of one second, the crossover size typically occurs for a particle diameter of about $a \approx 1\mu\text{m}$.

Non-Brownian suspensions of soft particles, such as foams and large emulsion droplets, become solid when the density is increased above a critical packing fraction, which now corresponds to a genuine “jamming transition”; in that case, glassy dynamics is not observed. For soft repulsive spherical particles in three dimensions, the transition takes place near the random close packing density, $\phi_J \approx 0.64 - 0.66$. Apart from experimental difficulties, an important source of the uncertainty concerning the jamming density is size polydispersity. It is empirically found that ϕ_J increases systematically with the size polydispersity of the sample (Hermes and Dijkstra, 2010; Torquato and Stillinger, 2010).

By contrast with the glass transition, thermal fluctuations play strictly no role in this process, and the emergence of solid behavior can be obtained in model systems at $T = 0$. Rather, it is the contact network between particles which becomes able to support a macroscopic stress if the packing fraction is large enough. The key concept is the existence of a sufficiently large number of contacts between the particles to maintain mechanical equilibrium (van Hecke, 2010). A second major difference from the glass transition is that the jamming transition can in principle be defined and located with arbitrary precision, as its definition does not rely on an observation timescale, although of course additional experimental difficulties might intervene (van Hecke, 2010; Ikeda *et al.*, 2013). The reason is that the emergence of solidity does not result from the competition between an equilibrium relaxation timescale defined at rest and a finite shear rate, as for glasses, because non-Brownian suspensions have no spontaneous dynamics at rest. The jamming transition and existence of a yield stress in soft materials can therefore be described as “static” transitions resulting from a sharp qualitative change in the microstructural properties of the material (Parisi and Zamponi, 2010).

Another important consequence of the absence of thermal fluctuations is the fact that the jamming transition, unlike the glass transition, necessarily takes place far from thermal equilibrium. In particular, this implies that the preparation protocol of the non-Brownian packings in the vicinity of the jamming transition becomes a relevant parameter controlling the location of the transition (Donev *et al.*, 2004), but, quite importantly, not its physical nature and properties (Chaudhuri *et al.*, 2010a).

In experiments and model systems studied in computer simulations, it is found that the yield stress emerges continuously with increasing packing fraction past the jamming transition (Durian, 1995). This has been found for foams and emulsions, which are well-described (at least near the transition) by simple models of soft repulsive spheres interacting via truncated harmonic or Hertzian

potentials of the form $V(r < a) = \frac{\epsilon}{\alpha}(1 - r/a)^\alpha$, where ϵ is an energy scale governing the mechanical property (essentially the softness) of the particles. In that case, the relevant stress scale controlling the behaviour of the yield stress is of energetic (rather than entropic) nature: $\sigma_0 = \epsilon/a^3$. As a result, the yield stress can now be written $\sigma_y = \sigma_0 g(\phi)$, where $g(\phi < \phi_J) = 0$.

A robust finding for the behavior of the yield stress close to jamming is a power-law increase: $\sigma_y = \sigma_0(\phi - \phi_J)^\beta$ for $\phi \geq \phi_J$ (Durian, 1995; Olsson and Teitel, 2007). There is no yield stress below jamming. The exponent β can be seen as a critical exponent characterizing the rheology of jammed materials. Although the exact value of β is still under discussion, even in simple models, the exponent depends sensitively from the exact form of the repulsion between the particles, as quantified for instance by the exponent α in the pair repulsion $V(r)$. This is reasonable, as softer particles (with larger α values) should be easier to deform for a given degree of compression $(\phi - \phi_J)$, and should thus have a larger exponent β . The simplest assumption, which relies on dimensional analysis, is that $\beta = \alpha - 1$. This is close to numerical results, but small systematic deviations, $\beta \gtrsim \alpha - 1$, have been reported in several numerical studies (Hatano, 2010; Kawasaki *et al.*, 2015; Olsson and Teitel, 2012). More work is therefore needed to assess the precise value of this exponent.

The evolution of the steady state flow curves for soft non-Brownian suspensions across the jamming transition is reported for the case of an emulsion in Fig. 3(b), from (Paredes *et al.*, 2013). The similarity with the soft glassy rheology in Fig. 3(a) is striking, as the material crosses over from a Newtonian fluid at low enough density and shear rate to a yield stress solid above jamming, where the flow curves are again well-described by the Herschel-Bulkley model with a shear-thinning exponent $n < 1$. Exactly at the jamming density, a power-law shear-thinning behavior is observed. A detailed discussion of the exponent appearing in the Herschel-Bulkley law can be found in (Olsson and Teitel, 2012). Notice, however, that a careful determination of n requires a power-law fit to $(\sigma - \sigma_y)$ as a function of $\dot{\gamma}$. It is found in simple numerical models that such a plot actually displays two distinct power-law regimes with two different exponents, n at small shear rates, and n' at larger shear rates (Kawasaki *et al.*, 2015; Lerner *et al.*, 2012; Olsson and Teitel, 2011, 2012). It is likely that fitting of experimental flow curves is dominated by the second of these two exponents, and comparison to theory is thus somewhat delicate. Additionally, at finite shear rates, it is also possible that other ingredients, such as the friction law between particles (Bonnecaze and Cloitre, 2010; Katgert *et al.*, 2009, 2008) or energy dissipation of the interstitial liquid (or in Plateau borders for foams (Schwartz and Princen, 1987) start to play a significant role and affect the value of the shear-thinning exponent.

It is also interesting to consider the limit of infinitely hard non-Brownian suspensions (such as wet cement), which are also often described as possessing a yield stress. As should be clear from the above discussion, a yield stress can only exist in non-Brownian repulsive objects if they can be compressed strictly above the jamming density $\phi > \phi_J$. This is by definition not possible when particles are truly hard, such as granular suspensions, which only exist in the fluid state, $\phi < \phi_J$ (Andreotti *et al.*, 2013). Careful measurements on suspensions of spherical particles (Fall *et al.*, 2010b) have indeed revealed that if the particles and suspending liquid are carefully density matched, there is no yield stress up to random close packing, where all the particles start to touch each other. However, as soon as there is the slightest density mismatch, the particles cream or sediment, so that $\phi \rightarrow \phi_J$, which is indeed the only density where hard particles can be fully arrested.

Another consequence of the hard particle limit is that no time scale can be constructed from the particle interaction, and the flow curves obtained at constant density therefore simplify considerably and become fully Newtonian. This limit is thus very different from the flow curves shown in Fig. 3. In that regime, the rheology is therefore described by simpler constitutive laws (with no yield stress) that have been very carefully studied and validated by many experiments in the community of granular media (Andreotti *et al.*, 2013; MiDi, 2004).

We summarize our discussions of the yield stress in repulsive particle systems concerning the relative role of thermal fluctuations and particle softness in the context of glassy and jamming rheologies in Fig. 4 (Ikeda *et al.*, 2013). This figure depicts the evolution with temperature T and packing fraction ϕ of the yield stress for a three-dimensional assembly of harmonic repulsive particles, determined using computer simulations. This figure demonstrates the emergence of a yield stress in thermalized colloidal assemblies, at a packing fraction ϕ_G , which depends weakly on the particle softness. Softness can be quantified by the adimensional temperature scale $k_B T/\epsilon$, which compares thermal energy to particle repulsion. Colloidal PMMA hard spheres are typically characterized by $k_B T/\epsilon \sim 10^{-8}$, whereas soft microgels are usually much softer, $k_B T/\epsilon \sim 10^{-4}$, emulsions being typically intermediate, $k_B T/\epsilon \sim 10^{-6}$. All these systems display a yield stress above the colloidal glass transition. In soft systems such as foams, $k_B T/\epsilon \sim 10^{-8}$ is again small because thermal fluctuations become irrelevant for such big particles, and the emergence of the yield stress is associated with the jamming transition, with no influence of thermal fluctuations on the rheology. The jamming transition controls the $T \rightarrow 0$ limit of the jamming phase diagram in Fig. 4. Such a diagram is experimentally useful as it allows one to locate systems such as microgels, emulsions, foams and colloidal hard spheres on the same graph, and to elucidate the origin of the yield stress ob-

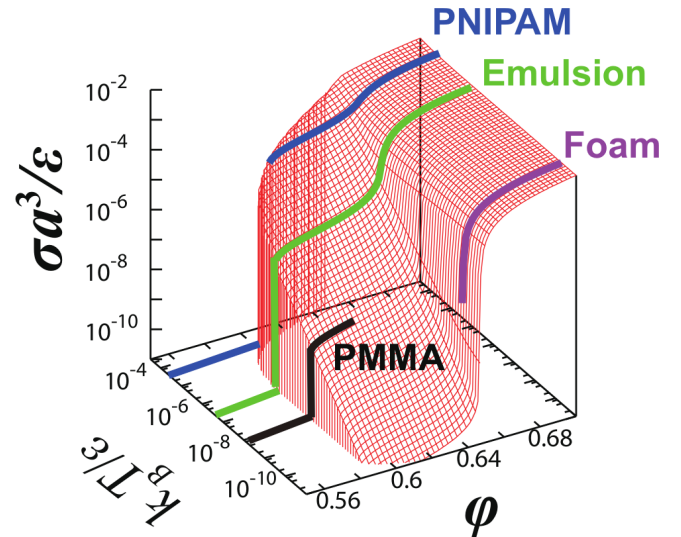


FIG. 4 Three-dimensional “jamming phase diagram” showing the reconstructed yield stress surface from numerical simulations as a function of the thermodynamic parameters temperatures and density in a dimensionless representation (particle softness $k_B T/\epsilon$, volume fraction ϕ , and stress $\sigma a^3/\epsilon$) for a model of soft harmonic particles (Ikeda *et al.*, 2013). The thick lines represent the location of typical experimental measurements in various materials. Foams are mainly sensitive to jamming physics, PMMA hard spheres to glass physics, emulsions display an interesting interplay between glass and jamming transitions, while PNIPAM microgels undergo a colloidal glass transition far from the jamming limit.

served in rheological experiments.

3. Role of attractive forces: Colloidal gels

In the previous section, only repulsive forces were described from a theoretical perspective, in which case temperature can only compete with the particle softness, and the main control parameter is the packing fraction. The situation becomes more complex when attractive forces are also playing a role. Of course, adhesion and attractive forces are relevant for a large number of model systems and real materials. For instance, dense liquids do not interact via hard sphere potentials, but typically also possess longer-range attractive forces, modelled for instance via a Lennard-Jones potential (Hansen and McDonald, 2006). In colloidal systems, attractive forces can be easily induced and tuned, as colloid-polymer mixtures (Royall *et al.*, 2013). Regarding real materials, many systems, such as clay suspensions, or more generally, colloidal gels, are Brownian systems with attractive interactions between the colloidal particles (Larson, 1999).

Regarding the glass transition phenomenon in simple atomic liquids, attractive forces only weakly affect the physics, in the sense that they contribute quantitatively to the relaxation dynamics and details of the phase dia-

gram, but do not change the physical behavior qualitatively (Berthier and Tarjus, 2009, 2011).

Attractive forces in simple liquids start to change the physics when they are strong enough to induce a nontrivial dynamical arrest in a regime that would otherwise be characterized by a simple fluid behavior. The simplest case is when very strong bonds are present, which might result in a percolating gel structure. In that case, a percolating particle network may form in the system, which can sustain a finite stress, very much as in chemical gels (Larson, 1999). Therefore, a yield stress emerges and coincides with a percolation transition. When the gel is dense enough, such a network can confer a macroscopic elasticity to the system and hence be responsible for a yield stress. This of course only happens if the interactions are strong enough: if the thermal energy is sufficient to break and reform bonds within the network, for a small applied stress the system will eventually flow at long times, and the system is simply viscoelastic (it is a “transient” gel).

Percolation only represents one of the possible routes to the production of physical gels, and several other examples have been studied in recent years (Zaccarelli, 2007). A well studied example is the case of colloidal gels that are formed by increasing the strength of short-ranged adhesive depletion forces, starting from an initially purely repulsive system. It is empirically found that “nonequilibrium gels” can be formed over a broad range of densities as the adhesion between particles is increased (Lu *et al.*, 2008; Manley *et al.*, 2005; Royall *et al.*, 2008). These gels are heterogeneous, dynamically arrested structures, which thus behave mechanically as soft solids. The current understanding of the gelation process is that adhesion induces the analog of a liquid-gas phase separation in the colloidal systems, which may phase separate into a colloid-rich and colloid-poor phases. However, because the attraction is very short-ranged, the coexistence curve on the colloid-rich region at large density may hit the colloidal glass transition. The emergence of slow, glassy dynamics may be able, in some cases, to slow down dramatically and even fully arrest the kinetics of the phase separation process (Foffi *et al.*, 2005; Lu *et al.*, 2008; Testard *et al.*, 2011). At long times, the system may thus acquire a percolating bicontinuous structure which is mechanically rigid and does not flow if a small shear stress is applied. Whereas a lot of work has been dedicated to the study of the formation of these nonequilibrium gels, as reviewed in (Zaccarelli, 2007), comparatively few studies have been performed to understand the resulting flow curves in such materials. These “attractive glasses” or gel systems should be analysed more carefully, as they are good candidates to understand the competition between shear and aging in thixotropic materials discussed in other parts of this review from a more microscopic viewpoint.

Whereas colloidal gels are formed when strong adhe-

sive interactions are added to semi-dilute colloids with repulsive, nearly hard sphere colloids, the behaviour of attractive colloids at large density has also attracted a large experimental interest in the recent decade (Puertas and Fuchs, 2009; Sciortino and Tartaglia, 2005). In this situation, a complex physical interplay is to be expected, as this corresponds to a competition between the non-equilibrium kinetic arrest arising at moderate densities (leading to gelation), and the glassy physics emerging at large densities without adhesive interaction (leading to glass formation). Early studies have advocated that this competition produces a novel state of arrested matter, named “attractive glass” (Dawson *et al.*, 2000; Fabbian *et al.*, 1999; Pham *et al.*, 2002; Sciortino, 2002), actively studied both numerically and experimentally (Pham *et al.*, 2004, 2002; Puertas *et al.*, 2005; Sciortino *et al.*, 2003; Zaccarelli *et al.*, 2005). Because the dynamics is controlled by at least two microscopic length-scales (the adhesion range responsible for initiating phase separation, and the cage size responsible for the glassy dynamic arrest), complex relaxation patterns have been predicted (Dawson *et al.*, 2000; Fabbian *et al.*, 1999) and observed (Pham *et al.*, 2004; Zaccarelli *et al.*, 2005), including in rheological studies (Koumakis and Petekidis, 2011). Whereas early interpretation relied on the existence of an underlying peculiar form of glass singularity predicted by mode-coupling theory (Dawson *et al.*, 2000; Fabbian *et al.*, 1999), more recent work has shown that such singularity is not needed for complex time dependences to occur (Chaudhuri *et al.*, 2010b), whereas the existence of a genuine attractive glass phase has also been called into question (Royall *et al.*, 2015; Zaccarelli and Poon, 2009).

Finally, the role of attractive forces in non-Brownian suspensions is also relevant but has a different nature, as the adhesive forces cannot compete, by construction, with thermal fluctuations. A few studies have explored the emergence of solidity in athermal adhesive particle systems, to understand in particular how the jamming transition is affected when adhesion is present (Chaudhuri *et al.*, 2012a; Irani *et al.*, 2014; Lois *et al.*, 2008). In particular, because adhesion creates bonds between particles, it seems physically clear that adhesive forces can only enhance solidity above jamming, and in this dense regime, adhesion acts as a small perturbation. On the other hand, it appears that solid behavior can be maintained in a density regime even below the jamming transition, $\phi < \phi_J$, which opens a novel regime for solid behavior with no analog for purely repulsive systems. In particular, a recent numerical study suggests that a small amount of attractive force is indeed able to generate a material with a finite yield stress below the jamming transition, with a potentially interesting interplay between the imposed shear flow and the microstructure of the system, eventually giving rise to large scale flow inhomogeneities (Irani *et al.*, 2014). This points to a

possible mechanism for shear banding, which we discuss further below.

C. Is the yield stress real?

1. Lessons from a historical debate

Yield stress materials have been studied for nearly a century (Barnes, 1999), but a consensus on mechanical behavior is only slowly emerging. The classical description, initiated by Bingham, is that there is no steady flow if the shear stress is less than a critical value (the yield stress), and the stress is a monotonically increasing function of the shear rate above that value. In practice, however, measurement of the shear stress as a function of shear rate is fraught with a number of difficulties as shown by (Barnes and Nguyen, 2001; Nguyen and Boger, 1992). These difficulties make the very concept of a yield stress somewhat ambiguous, and this has led to controversial statements about the status of a finite yield stress to characterize amorphous solids. Let us try to disentangle the various conceptual, theoretical, and practical issues.

For a number of years, there has been a controversy about whether or not the yield stress marks a transition between solid and fluid states, or a transition between two fluid states with drastically different viscosities. Numerous experimental studies were published that apparently demonstrate that these materials flow as very viscous Newtonian liquids at low stresses (Barnes, 1999; Macosko, 1994), as well as many replotted data sets shown in (Barnes, 1999). These works suggest that yield stress materials submitted to a shear stress smaller than the apparent yield stress may eventually reach a steady flow situation, in stark contradiction with the Bingham description. Possibly the earliest work that seriously questions the solidity of yield stress fluids below the yield stress is a 1985 paper by (Barnes and Walters, 1985), where they showed data on Carbopol microgels apparently demonstrating the existence of a finite viscosity plateau at very low shear stresses—rather than an infinite viscosity below the yield stress. (Barnes, 1999) published another paper on the subject, titled “*The yield stress—a review or ‘πανταρει’ everything flows?*” where he presents numerous viscosity vs. shear stress curves displaying finite viscosity plateaus at low stress values, thus suggesting that yield stress materials should rather be described as Newtonian fluids with a very large viscosity. Following the initial publication by Barnes a number of papers appeared, discussing the definition of yield stress fluids, whether such things existed or not, and how to demonstrate either way (Astarita, 1990; Barnes, 2007, 1999; Evans, 1992; Hartnett and Hu, 1989; Schurz, 1990; Spaans and Williams, 1995). The outcome of this debate has been that the rheology community presently

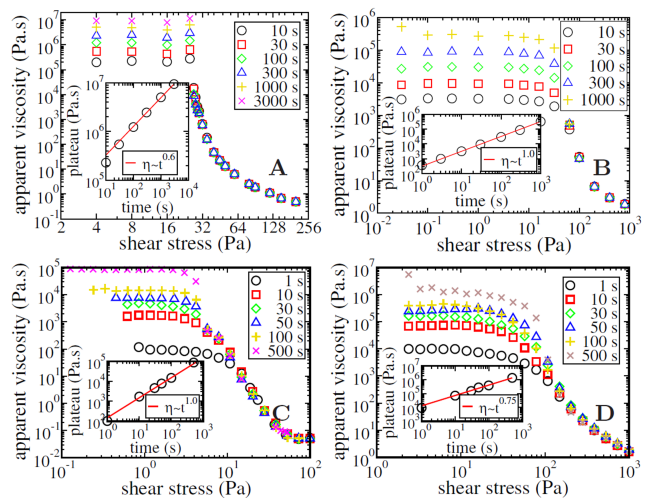


FIG. 5 Viscosity vs shear stress in various materials. For each material and each measurement time the resulting viscosity-stress curve resembles that of (Barnes, 1999), but the values of the low stress viscosity plateaus increase with measurement time. The insets show that the plateaus increase as power laws with time, with exponents in the range 0.6–1.0, depending on the system, indicating that the measured viscosities do not correspond to steady state shear flows for shear stress below the yield stress. A) 0.2% wt. carbopol microgel. B) Hair gel. C) Foam. D) Emulsion. Extracted from (Møller *et al.*, 2009a).

holds two coexisting and conflicting views: (i) the yield stress marks a transition between a liquid state and a solid state, and (ii) the yield stress marks a transition between two fluid states that are not fundamentally different, but simply have very different viscosities. Recalling that the Bingham model provides a diverging viscosity as the shear rate decreases, these two views should be distinguished by the existence (or absence) of a time-independent Newtonian viscosity regime at extremely small flow rates. It is therefore experimentally very challenging to distinguish between these two pictures.

(Møller *et al.*, 2009a) reproduced the experiments used to demonstrate Newtonian limits at low stresses and could also observe the apparent viscosity plateaus at low stresses. However, their conclusion was that such curves can be very misleading and that extreme caution should be taken before concluding that a true viscosity plateau exists. Figure 5 shows that viscosity curves have a low-stress viscosity plateau. However, while all measurements collapse at high stresses, below some critical stress they no longer do. Below this stress, the apparent viscosity values depend in fact on the delay time t between the application of the stress and the viscosity measurement. The insets show that the viscosity value of the low-stress viscosity plateau increases as a power of the delay time. It is clear that each of the several curves, when seen individually, greatly resembles the curves of Barnes and others, and that such curves can be mislead-

ing since one assumes that the data represent measurements in steady state while in fact the flows may well be changing with time, as is the case here. If we remove all the points from the flow curve that do not correspond to steady states, we are left with a simple Herschel-Bulkley material with a finite yield stress corresponding to the critical stress mentioned above. Note that this cannot be an evaporation or aging effect since all measurements were done on the same sample after it had been allowed to relax after the previous experiment. Since evidently no steady state shear is observed one should not, contrary to what is suggested by Barnes, take the instantaneous shear rate at any arbitrary point in time to be proof of a high-viscosity Newtonian limit at low stresses for these materials. These data also confirm that the large viscosity values obtained at low stress correspond to shear rates of the order of 10^{-6}s^{-1} or less, which are clearly reaching the accuracy limits of ordinary rheometers.

Perhaps the most ubiquitous problem encountered by scientists and engineers dealing with everyday materials such as food products, powders, cosmetics, crude oils, or concrete is that the yield stress of a given material has turned out to be very difficult to determine (Barnes, 1999; Møller *et al.*, 2006; Mujumdar *et al.*, 2002). Indeed, (James *et al.*, 1987; Nguyen *et al.*, 2006; Zhu *et al.*, 2001) demonstrated that a variation of the yield stress of more than one order of magnitude can be obtained, depending on the way it is measured. The huge variation in the obtained value for the yield stress cannot be attributed to different resolution powers of different measurement techniques, but hinges on more fundamental problems raised by the existence of the yield stress. This is of course well-known to rheologists, but since no reasonable and easy way of introducing a variable yield stress is generally accepted, researchers and engineers often choose to work with the yield stress nonetheless, and treat it as if it were a material constant which is just experimentally tricky to determine, or as (Nguyen and Boger, 1992) put it: “*Despite the controversial concept of the yield stress as a true material property ... there is generally acceptance of its practical usefulness in engineering design and operation of processes where handling and transport of industrial suspensions are involved.*”

2. Theoretical insight on the existence of a yield stress

Can theory and simulations shed light on the debate regarding the existence of a true yield stress in amorphous materials? This is a difficult problem which cannot have a simple generic answer, as this amounts to asking first whether genuine amorphous solid states exist, and second whether such states can support a finite shear stress without flowing over arbitrarily long timescales. Moreover, as detailed above, different materials exhibit solid properties for distinct fundamental reasons under various

experimental conditions and for various particle interactions.

Clearly, the existence of a “real” yield stress in materials undergoing a glass transition is at least as ambiguous as answering the question about the existence of a genuine fluid-to-glass phase transition, which remains an open fundamental question. While there exist theoretical approaches and simple models where the glassy phase is entered through a genuine thermodynamic singularity accompanied by a diverging viscosity, there are also theoretical perspectives based on the opposite idea that the glass region is accessed by a dynamic crossover, and where the equilibrium relaxation timescale does not necessarily diverges (Berthier and Biroli, 2011). Notice that this fundamental question is *in practice* not very relevant, as glassy phases are experimentally produced by going through a dynamic crossover in a non-equilibrium manner, as explained in Sec. II.B.1. As a consequence, in the vicinity of the experimental glass transition, flow curves might display an apparent yield stress value when measured over a given window of shear rates, even though the material might eventually flow at very long times. Of course, deeper in the glassy region, when the relaxation time has become larger than any relevant experimental timescale, the distinction between a slowly flowing fluid and a kinetically arrested material is practically largely irrelevant.

Note, however, that since the relaxation time is very large, a system prepared in the glass region slowly ages with time because thermal fluctuations allow a slow exploration of its complex free energy landscape (Berthier and Biroli, 2011). Importantly, this implies also that the rheological properties of glasses might depend on the timescale used to perform the measurements. For instance, the yield stress of the system has been observed to increase logarithmically with the preparation time in model systems (Varnik *et al.*, 2004). Additionally, the aging behaviour observed in glasses at rest might be affected in a nontrivial manner by an imposed shear flow, possibly resulting in a steady-state situation where aging is arrested by the external shear flow, a situation coined “shear rejuvenation” (Bonn *et al.*, 2002b; Cloitre *et al.*, 2000; Ianni *et al.*, 2007; Viasnoff and Lequeux, 2002). The role played by the preparation protocol and by the aging dynamics is similarly crucial for colloidal gels that might be formed through nonequilibrium processes, such as kinetically arrested phase separation. In that case, it is unclear how such a nonequilibrium competition is affected by an externally imposed shear stress, which could for instance either “mix” the material or break the bicontinuous structure and accelerate the phase separation.

Now, a different question to ask is the following: Assuming that genuine amorphous *phases* exist (where for instance ergodicity is truly broken and the Newtonian viscosity is infinite), is it necessarily obvious that such phases display a finite yield stress? To answer this

question one should ask whether there exists a physical dynamical process allowing the system to relax and flow in a finite time scale after a finite shear stress has been imposed. This problem was studied in (Sausset *et al.*, 2010). Using a simple nucleation-type argument, a stress-dependent free energy barrier for relaxation was constructed, which can then be crossed using thermal fluctuations. By connecting the constructed activation timescale to the imposed stress, a limiting flow curve $\sigma(\dot{\gamma})$ was obtained, which in three spatial dimensions is of the form

$$\dot{\gamma} = \frac{\sigma}{G\tau_0} \exp \left[-c \left(\frac{\sigma_0}{\sigma} \right)^4 \right], \quad (5)$$

where G is the elastic shear modulus, c a constant and $\sigma_0(T)$ a temperature-dependent stress scale. The details of the derivation of Eq. (5) do not really matter, but the result in Eq. (5) demonstrates the existence of a lower bound for the resulting shear rate for a finite shear stress $\sigma > 0$. This argument suggests therefore that the *shear rate is actually finite at any imposed shear stress* even in the “solid” phase. This result is not inconsistent with the existence of measured flow curves with an apparent yield stress, as it predicts that the shear stress decreases logarithmically slowly with the shear rate. It might therefore be very difficult to detect such behavior in an experiment to discriminate for instance from a Herschel-Bulkley functional form with a finite yield stress. An interesting additional comment on this result is that it is not specific to amorphous materials, but applies equally to ordered systems, such as crystalline materials. This discussion shows that despite the translational symmetry breaking observed during the formation of the crystal, which contrasts with the absence of such a symmetry breaking in amorphous solids, a yield stress is conceptually not better defined in ordered systems. Therefore, the absence of a real yield stress is not due to the “messy” nature of soft amorphous materials but is more profound.

Finally, notice that the reasoning leading to Eq. (5) and the conclusion that a finite yield stress cannot exist even in dynamically arrested phases heavily relies on a barrier crossing argument, and therefore on the presence of thermal fluctuations. Therefore, the situation might be different in non-Brownian suspensions undergoing a jamming transition. For soft jammed particle systems such as foams and large droplet emulsions, the transition to the jammed phase is not a dynamic crossover and the “solidity” cannot be destroyed by thermal fluctuations. In that case, there is a priori no deep argument against the existence of a finite yield stress—such that the flow curves shown in Fig. 3(a) might be true examples of genuine yield stress materials. Of course, as noticed several times, these experimental results do not seem to differ dramatically from other measurements in thermal materials, which again questions the practical relevance of the present theoretical discussion.

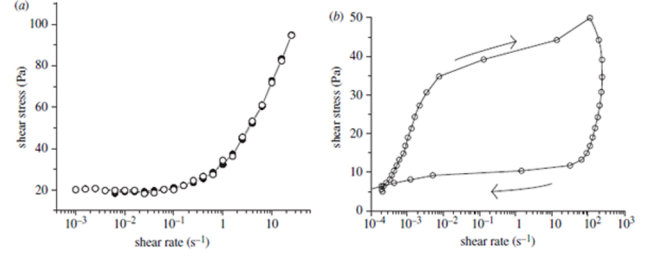


FIG. 6 (a) The behavior of 0.1% wt. carbopol microgel under increasing and decreasing shear stresses shows that this material is non-thixotropic (filled circle, up; open circle, down). (b) Thixotropy of a 10% wt. bentonite solution under an increasing and then decreasing stress ramp

D. Thixotropy in yield stress fluids

One common observation about most yield stress fluids is that they possess a yield stress because there is some microscopic structural organization in the material that confers a macroscopic elasticity to the system. If such structured materials are forced to flow, it may very well be that the microscopic structure is (partly) destroyed by the flow, entailing a reversible decrease of the viscosity in time: the system is then said to be *thixotropic* (Mewis and Wagner, 2009). Once the flow has stopped, one consequently has a different material with likely a different yield stress value. These difficulties have resulted in lengthy discussions of whether the concept of the yield stress is useful for thixotropic fluids and how it should be defined and subsequently determined experimentally. Although the same microstructure gives rise to both the yield stress and thixotropy, the two phenomena are often considered separately. For instance, Barnes wrote two different reviews on the yield stress and thixotropy, each without considering the other (Barnes, 1997, 1999).

Schematically, it is important to realize that yield stress fluids may come in two distinct flavors: thixotropic and non-thixotropic (or “simple”) yield stress fluids. A simple yield stress fluid is one for which the shear stress (and hence the viscosity) depends only on the imposed shear rate, while for thixotropic fluids the viscosity depends more generally on the shear history of the sample. The distinction is simple to make in principle: one can for instance measure the flow curve by using up and down stress ramps. Figure 6(a) shows that if the material is a “simple” yield stress fluid, the data for increasing and decreasing shear stresses coincide: the material parameters do not depend on flow history. On the other hand, Fig. 6(b) shows that if the material is thixotropic, in general the flow will have significantly “liquefied” the material at high stresses, and the branch obtained upon decreasing the stress is significantly below the one obtained while increasing the stress. In that case, one should then also specify better the protocol used to measure flow curves, for instance indicating the rate at which the stress is

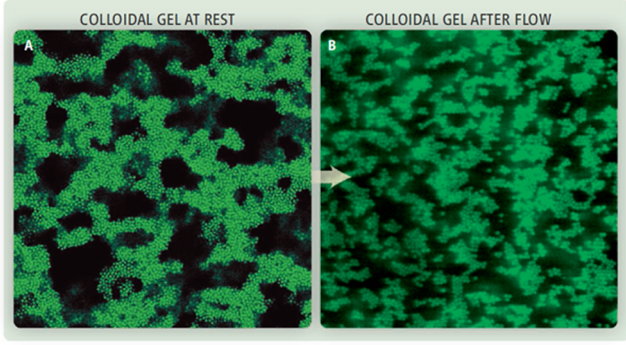


FIG. 7 A colloidal gel (A) at rest, with a percolated structure and a yield stress of 5 Pa, and (B) just after flow, with individual flocs and no measurable yield stress [from (Bonn and Denn, 2009)].

ramped up and down, as this might also influence the outcome of the experiment.

Figure 7 shows a direct observation of the effect of stress-dependent structural organization in a colloidal gel. Here, the gel is made up of $1.3 \mu\text{m}$ fluorescent PMMA particles and $3 \cdot 10^7$ Mw polystyrene in a mixture of decalin and cyclohexyl bromide. At rest (A), the gel exhibits a percolated structure and exhibits a yield stress of about 5 Pa. Just after flow (B), the gel has broken up into individual flocs and there is no measurable yield stress.

Thus, for “simple” yield stress fluids there is no problem in principle in determining the yield stress. However for thixotropic materials there is, since any flow liquefies the material and thus decreases the yield stress. As thixotropy is by definition reversible, this also means that when left at rest after shearing, the yield stress will increase again as the material solidifies. In that case, experimental protocols should be made more precise.

A very striking demonstration of how the simple yield stress fluid picture often fails predicting the flow of actual yield stress fluids even qualitatively is *avalanche behavior*, which has been observed for thixotropic yield stress fluids (Coussot *et al.*, 2002a). One of the simplest tests to determine the yield stress of a given fluid is the inclined plane test (Coussot and Ancely, 1999; Coussot and Boyer, 1995). In this experiment, a large amount of the material is deposited on a plane that is subsequently slowly tilted to some angle, θ , where the fluid starts flowing. According to the Herschel-Bulkley and Bingham models, the material will start flowing when an angle is reached for which the tangential gravitational force per unit area at the bottom of the pile is larger than the yield stress, $\rho g h \sin \theta > \sigma_y$, with ρ the density of the material, g the gravitational acceleration and h the height of the deposited material. In reality, however, inclined plane tests on a clay suspension reveal that for a given pile height there is a critical slope above which the sample

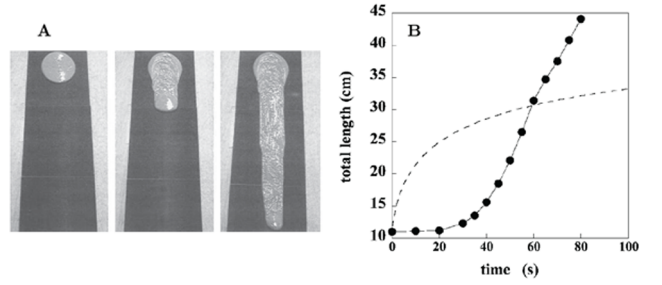


FIG. 8 A: Avalanche-like flow of a clay suspension over an inclined plane covered with sandpaper. The experiment was performed just above the critical angle below which the fluid behaves like a solid (Coussot *et al.*, 2002b). While any simple yield stress fluid model would predict only infinitesimal spreading of the pile when the yield stress is slightly exceeded, in reality an avalanche results. B: Distance covered by the fluid front in an inclined plane experiment (Coussot *et al.*, 2002b). The Herschel-Bulkley model is seen to provide a very poor fit (dashed line) to the experimental points that evolve in the “opposite” manner.

starts flowing, and once it does, the thixotropy leads to a decrease in viscosity which accelerates the flow, since fixing the slope corresponds to fixing the stress (Coussot *et al.*, 2002a). This in turn leads to an even more pronounced viscosity decrease and so on. An avalanche results, which transports the fluid over large distances. By contrast, a simple yield stress fluid model predicts that the fluid moves only infinitesimally when the critical angle is slightly exceeded, since the pile need only flatten a bit for the tangential gravitational stress at the bottom of the pile to drop below the yield stress.

In Fig. 8, pictures and quantitative data from an inclined plane experiment on a bentonite suspension are shown (Coussot *et al.*, 2002a). Once the fluid gets going, it accelerates and eventually covers large distances rather than only spreading slightly as predicted by simple yield stress models. In the same figure the Herschel-Bulkley model is seen to provide a very poor fit to the data.

To summarize, two qualitatively different systems can be distinguished in terms of their physical properties:

- “Simple” yield stress fluids: emulsions, foams and carbopol microgels (Bertola *et al.*, 2003; Møller *et al.*, 2009b; Ovarlez *et al.*, 2013a).
- Thixotropic yield stress fluids: particle and polymer gels (Møller *et al.*, 2008), attractive glasses (Møller *et al.*, 2009b), “soft” colloidal glasses (Bonn *et al.*, 2002a), adhesive emulsions (Ragouilliaux *et al.*, 2007), dry granular systems (Cruz *et al.*, 2002), pastes (Huang *et al.*, 2005), hard-sphere colloidal glasses (Møller *et al.*, 2009a).

Note that this separation into two main families is at present mostly driven by empirical considerations. It would be interesting to understand this distinction at

a more fundamental level, while simultaneously devising and studying experimental model systems where both behaviors could be observed and controlled, for instance by devising materials that are only weakly thixotropic and where “simple” yield stress behavior could be continuously recovered in some controlled limit.

E. Theoretical considerations on yield stress materials

1. Why a theory of yield stress solids is difficult

The yield stress is a defining characteristic of a broad range of amorphous solids. It represents a robust mechanical signature of the emergence of solid behavior in many atomic, molecular and soft condensed materials undergoing a transition between fluid and solid states. From a physical viewpoint, the existence of a yield stress implies that the material does not flow spontaneously unless a driving force of finite amplitude is applied, which represents a very intuitive definition of “solidity”. While properly defining and measuring a yield stress is a debated experimental issue, as emphasized throughout this review, in theoretical work one usually identifies the yield stress as the shear stress measured in steady-state shear flow in the limit where the deformation rate goes to zero,

$$\sigma_y = \lim_{\dot{\gamma} \rightarrow 0} \sigma(\dot{\gamma}). \quad (6)$$

Thus, the challenge for theory does not lie in the practical definition of the yield stress or its best quantitative determination, but in the conceptual difficulty to treat theoretically the nonlinear mechanical properties of disordered solids.

The yield stress is generically difficult to analyze theoretically because it stems from the strongly nonlinear response of an arrested solid to an applied deformation. It marks a transition point between flowing states for $\sigma > \sigma_y$ and arrested states when $\sigma < \sigma_y$. As should be clear from the discussion of the physical mechanisms responsible for the existence of a finite yield stress in condensed matter systems in Sec. II.B, even describing the mere emergence of amorphous solids from a microscopic perspective is already an important open challenge. Therefore, additionally predicting quantitatively the mechanical properties of these materials during steady state deformation, namely the value of the yield stress and its dependence on control parameters are even more difficult tasks, which involve dealing with strongly nonequilibrium and strongly nonlinear processes in these complex materials. This is clearly a very hard problem to tackle from a microscopic perspective.

An additional difficulty can be appreciated by comparing the situation of disordered materials to the one of crystalline solids. Crystals are formed through a phase transition across which translational invariance is broken. Because the broken symmetry is easily identified,

it is also not difficult to recognize the associated defects (such as dislocations) directly from the structure of an imperfect crystalline system. It is well established that nonlinear flow and mechanical deformation in crystalline materials are mostly driven by these defects.

This analogy immediately begs the following questions: What are the “defects” in an amorphous material that is formed without breaking any obvious symmetry? Are there at least equivalent localized structures allowing us to efficiently describe flow and mechanical deformation in amorphous solids? These are two long-standing questions in the literature of the rheology of amorphous materials, which have received some constructive answers in the last decades, mostly from numerical and experimental studies (Barrat and Lemaitre, 2011).

It has been demonstrated by many different studies that flow in amorphous materials occurs in very localized “zones”, sometimes identified as “shear transformation zones” (Falk and Langer, 1998). These zones are best observed in studies of amorphous systems which are sheared so slowly that individual events can be resolved in space and time, such as computer simulations in quasi-static shear conditions (Maloney and Lemaitre, 2006), or confocal microscopy experiments on slowly deformed colloidal glassy systems (Schall *et al.*, 2007). It is observed that flow occurs mostly near those zones comprising a small number of particles (say, 5 to 10) undergoing the largest irreversible rearrangements. However, because the material is globally an elastic solid, these local plastic events additionally induce a long-range redistribution of the stress field in their surroundings (Picard *et al.*, 2004), which can in turn couple to a different zone, or trigger further relaxation elsewhere in the system. An example of such an event detected in the numerical simulation of a slowly sheared glass model (Tanguy *et al.*, 2006) is shown in Fig. 9.

This phenomenology is well established from observations on different systems, and it clearly suggests theoretical pathways to understand better the mechanical properties of yield stress amorphous solids or to provide simple theoretical models for flow in disordered solids. In particular, an important modeling effort currently builds on these results to construct mesoscopic elasto-plastic descriptions of the rheology of amorphous materials (Baret *et al.*, 2002; Bocquet *et al.*, 2009; Cheddadi *et al.*, 2011; Picard *et al.*, 2002, 2005; Rodney *et al.*, 2011). These models are coarse-grained descriptions in the sense that no attempts are made to describe the microscopic origins of the yield stress, but they rather build on its existence to explore the consequences of deforming a material assumed to behave as a disordered solid. An advantage of such models is that they can open the possibility to explore the large-scale consequences of the dynamics of shear transformation zones. For instance, it has been observed numerically that elastic deformation in the vicinity of a local rearrangement induces long-range spa-

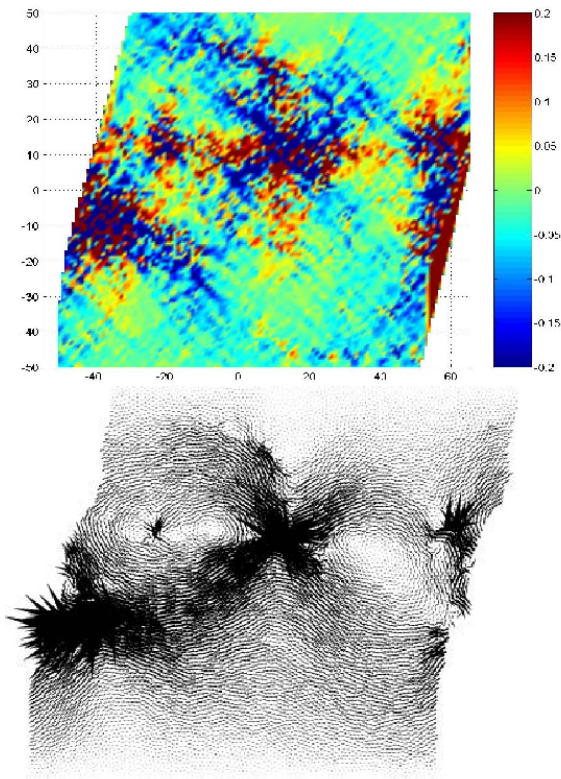


FIG. 9 Changes in the local shear stresses during a localized plastic event (top), and associated displacement field (bottom) observed in the numerical simulation of a quasi-statically sheared model of atomic glass. Adapted from (Tanguy *et al.*, 2006).

tial correlations, which may induce correlations between plastic events (Martens *et al.*, 2012; Vandembroucq and Roux, 2011). These correlations have been observed to lead to system-spanning avalanches in quasi-static deformations that are sometimes also described as precursors for the formation of permanent shear bands or strong flow localization (Barrat and Lemaitre, 2011; Falk and Langer, 2011; Falk *et al.*, 2004; Maloney and Lemaitre, 2006; Shi *et al.*, 2007).

This general discussion of theoretical approaches to the rheology of yield stress materials suggests that several layers of theoretical descriptions coexist in the literature. It is perhaps important to realize that different theories may be useful to answer different types of questions. Therefore, it is perhaps not a very constructive attitude to use computer simulations or experimental work to “compare” or “discriminate” distinct theoretical models based on a specific set of measurements, since each model may actually serve a very different purpose or address a different question, each one being equally relevant in a given context.

Some theoretical models are primarily devised to address the question of the existence and the emergence

of a fluid-to-solid transition. Numerous theoretical approaches to the glass transition in dense fluids have been extended to account for the mechanical properties in the vicinity of the transition (Berthier and Biroli, 2011), such as for instance mode-coupling theories (Götze, 2008) and Bouchaud’s trap model (Bouchaud, 1992). Even in this restricted context, these two approaches differ widely in their scope and in their spirit. Mode-coupling theories were developed as truly microscopic or “first-principle” approaches to understand the dynamics of simple liquids near a glass transition (Bengtzelius *et al.*, 1984; Götze, 2008). Note that mode-coupling theory is itself only a subsection of a larger theoretical construction called “random first order transition theory” (Lubchenko and Wolynes, 2007), which has been extended in several different ways to treat the rheology of glassy materials (Berthier *et al.*, 2000; Fuchs and Cates, 2002; Lubchenko, 2009; Miyazaki and Reichman, 2002; Yoshino and Mézard, 2010). On the other hand, trap models correspond to more phenomenological descriptions of the glass phenomenon, and have attracted attention in particular in the context of aging phenomena inside glassy phases. The rheological trap model is called the “soft glassy rheology model” and has been studied extensively (Sollich, 1998; Sollich *et al.*, 1997), both in steady state conditions, in the context of rheological aging, and in even more complicated time-dependent situations, with interesting connections to the physics of thixotropic materials (Fielding *et al.*, 2009, 2000).

A second family of theoretical models actually postulates from the start that a solid amorphous state exists, which is characterized by a finite yield stress. These models are then able to explore in more detail how such a solid system might flow under an applied shear stress larger than the yield stress. This is for instance the intent of shear transformation zone model, first initiated by Falk and Langer (Falk and Langer, 1998, 2011). More recently, a broad family of coarse-grained elasto-plastic models has been developed, of the kind put forward for instance in (Baret *et al.*, 2002; Picard *et al.*, 2002). Obviously here, no information can be gained for instance about the dependence of the yield stress on external control parameters, but these models can more efficiently explore the consequences of nonlinear flow curves, and might be able to describe in a relevant manner more complex situations such as shear bands, kinetic heterogeneities under flow, fractures, time-dependent phenomena, or flow in confined geometries, as discussed in more detail in Sec. IV.

2. Flow curves from theories

Given the impressive number of theoretical models dealing with the rheology of amorphous solids, one may wonder whether some theoretical insights can be gained

into the analytic form of the flow curves of yield stress materials beyond the popular Herschel-Bulkley model described in Sec. II.A, which provides an efficient fitting model but is essentially empirical.

In the following we describe quantitatively and compare the outcomes of three families of theoretical approaches, which represent different paradigms to analyze flow curves in yield stress materials. It should be noted that flow curves in steady state simple shear flows only represent one the many aspects of the rheology of yield stress materials, and some models also make detailed predictions for, e.g., time-dependent flows or more complex geometries. Reviewing model predictions for all these phenomena would however require a review article on its own (Voigtman, 2014).

a. Soft glassy rheology. The soft glassy rheology (SGR) model is a direct extension of Bouchaud’s trap model that incorporates mechanical degrees of freedom in a minimal manner to describe the interplay between glassy dynamics and shear deformation (Sollich *et al.*, 1997). The original trap model was mainly devised to study the physics of the glass transition and the aging dynamics in systems quenched suddenly into a glassy phase (Bouchaud, 1992; Bouchaud and Dean, 1995). The SGR model provides an evolution equation for the probability distribution of the system in terms of energy and stress variables. In the presence of a constant shear stress, steady state flow curves can be predicted, with a behavior that is ruled by the only control parameter of the model, namely the “temperature” T . Whereas the initial trap model explicitly refers to T as the temperature of a thermal bath coupled to the system, the SGR model differs somewhat on the precise interpretation of the temperature and uses the words “effective temperature”, in order to include athermal materials such as foams or emulsions in the same framework. The temperature T is then thought as quantifying the strength of mechanical “noise” triggered by the flow itself. For more detailed discussion of effective temperatures in driven materials, we refer the reader to the following references: (Berthier *et al.*, 2000; Bouchbinder and Langer, 2009a,b,c; Cugliandolo *et al.*, 1997a; Sollich and Cates, 2012). Despite its simplicity, the SGR model offers a rich variety of possible flow curves, depending on the temperature regime (Sollich, 1998).

In the absence of a flow, the system undergoes a glass transition at some critical temperature T_c , below which ergodicity breaking occurs. With an imposed shear flow, three temperature regimes are observed. First, when $T > 2T_c$ the system exhibits a Newtonian flow, as expected for a simple fluid state. A second, somewhat unexpected, regime occurs when $T_c < T < 2T_c$ where the system displays a pure power-law rheology of the form $\sigma \approx \dot{\gamma}^n$, with a “shear-thinning” exponent $0 < n = T/T_c - 1 < 1$. This regime is peculiar as it corresponds to a “solid” system

with an infinite viscosity at rest when $\dot{\gamma} \rightarrow 0$, but without a finite yield stress. If the shear-thinning exponent n is small, it might be very difficult to distinguish this behavior from a Herschel-Bulkley functional form. Another peculiarity of this regime is that the viscosity is infinite despite the fact that the temperature is strictly above the glass transition temperature and the system actually reaches thermal equilibrium (see (Lequeux and Ajdari, 2001) for a detailed discussion of this issue).

The third regime is for temperatures below the critical temperature of the model, $T < T_c$, where the rheology is found to be described exactly by the Herschel-Bulkley model, $\sigma \approx \sigma_y(T) + \dot{\gamma}^n$ and the shear-thinning exponent is now $0 < n = 1 - T/T_c < 1$; a temperature dependent yield stress $\sigma_y(T)$ emerges continuously at the glass temperature, with a linear onset $\sigma_y(T \lesssim T_c) \approx 1 - T/T_c$ and a smooth approach to a finite zero temperature limit $\sigma_y(T \rightarrow 0) > 0$.

Note that the behaviour of the flow curves is smooth at the transition temperature, $T = T_c$, where the system has no yield stress but the shear-thinning exponent vanishes, a situation that can easily be confused with a finite yield stress. It is interesting to remark also that all exponents are temperature dependent quantities, and as such they carry no deep physical meaning but simply reflect the complex interplay between the broad distribution of relaxation times in the equilibrium model and the external mechanical forcing. This implies, in particular, that no particular scaling form of the flow curves is obtained in this approach in any temperature regime, or even in the immediate vicinity of the critical temperatures of the model.

b. Mode-coupling theories. Mode-coupling theory appears as a subset of the theoretical approach to the glass transition called random first order transition theory, which aims at describing many different aspects of the statistical mechanics of materials undergoing a fluid to glass transition (Berthier and Biroli, 2011; Lubchenko and Wolynes, 2007). The “mode-coupling approach” is itself not a unique theory, and several related lines of research coexist; a few of them have been developed to include also mechanical degrees of freedom, much in the spirit of the SGR model. It is interesting to also contrast the outcome of the various models.

A first approach (Berthier *et al.*, 2000; Cugliandolo *et al.*, 1997b) consists of solving without approximation the driven dynamics of simple, but rather abstract, glass models that are known to exhibit an equilibrium dynamics that is in the same universality class as other mode-coupling approaches, such as p -spin glass models or other disordered models (Kirkpatrick and Thirumalai, 1987). A second line of work starts from microscopic equations of motion for a fluid, and develops “mode-coupling” approximations to derive closed but approximate dynamical

equations for microscopic correlation functions. Both approaches might then be extended to include shear flows and study the interplay between glassy dynamics and rheology.

In all of these mode-coupling approaches, the equilibrium dynamics is well understood and is characterized by a well-defined critical temperature T_c where the relaxation time, often called the alpha-relaxation time $\tau_\alpha(T)$, diverges algebraically. Near the glass transition, time correlation functions develop a well-known two-step decay, with an intermediate plateau reflecting the transient caging of the particles in dense fluids. In rheological terms, this simply signals that very viscous fluids near a glass transition are viscoelastic and behave as solids at intermediate timescales. The approach and departure from this plateau regime involve non-trivial power-law regimes, which are the hallmark of mode-coupling theories (Götze, 2008).

In all mode-coupling approaches, the glass transition is destroyed by the imposed shear flow, and the microscopic relaxation timescale does not diverge at the glass transition anymore, but rather becomes dependent on the imposed shear rate $\dot{\gamma}$. However, the resulting flow curves differ somewhat in their details.

In schematic mean-field models, the rheology exhibits Newtonian behavior at temperatures above T_c at very low shear rates, but the dynamics become strongly dependent on $\dot{\gamma}$ when the “dressed” Péclet number, $P_e \equiv \tau_\alpha \dot{\gamma}$, becomes larger than unity. This results in the following scaling form for the flow curves,

$$\eta(\dot{\gamma}, T) = \eta_0(T) [1 + \dot{\gamma}/\dot{\gamma}_0]^{n-1}, \quad (7)$$

where $\eta_0(T) \sim \tau_\alpha(T)$ is the Newtonian viscosity, $\dot{\gamma}_0$ a microscopic frequency, and n a shear-thinning exponent whose value is $n = 1/3$ in the specific family of models studied in (Berthier *et al.*, 2000). The physical interpretation of Eq. (7) is quite transparent, as it implies that equilibrium dynamics is unaffected by the shear flow when the shear rate is slower than the spontaneous structural relaxation of the material, whereas the mechanical deformation accelerates the dynamics in the opposite limit, which automatically yields a smaller viscosity.

At the glass transition, a pure power-law rheology is thus obtained, $\sigma(\dot{\gamma}, T = T_c) \sim \dot{\gamma}^n$, whereas a temperature dependent power-law rheology is obtained in the glass phase: $\sigma(\dot{\gamma}, T < T_c) \sim \dot{\gamma}^{n(T)}$ with a shear-thinning exponent decreasing from $n(T = T_c) = 1/3$ to $n(T \rightarrow 0) = 0$, but with no finite yield stress. Therefore the rheology of the glass phase bears strong similarities to the intermediate temperature regime of the SGR model. The absence of a yield stress is perhaps physically unexpected, but is actually quite natural in the context of mean-field approaches whose aging dynamics in the glass phase is very well understood (Cugliandolo and Kurchan, 1993). In the absence of external flow, the system slowly relaxes along the flat or “marginal” regions of its free en-

ergy landscape, but does not penetrate deeper free energy minima. This is a general feature of mean-field glassy dynamics. The power-law rheology found in the glass phase is believed to result directly from this marginal dynamics, and non-mean-field effects are believed to manifest themselves by the emergence of a finite yield stress, as explored in (Berthier, 2003).

Using the liquid theory path to derive mode-coupling equations for glassy fluids under flow results in a set of dynamical equations that reduce to the usual mode-coupling phenomenology described above for the equilibrium dynamics. However, the driven dynamics under shear flow provides a set of predictions that differ somewhat from the schematic mean-field models, for reasons that are physically not very transparent. Mode-coupling equations have been derived in a number of ways that are technically quite involved, but the different derivations essentially provide similar predictions for the flow curves (Fuchs and Cates, 2002, 2009; Miyazaki and Reichman, 2002). The predicted flow curves in the vicinity of the glass transition closely reflect the complexity of the time regimes observed for time correlation functions. A distinctive feature of these mode-coupling approaches is that a finite yield stress is obtained in the glass phase. In detail, the critical flow curve at $T = T_c$ obeys a Herschel-Bulkley functional form with a finite yield stress, $\sigma_y(T = T_c) > 0$, and a shear-thinning exponent with a non-universal value [specific approximations give $n \approx 0.15$ (Fuchs and Cates, 2003)]. The power-law approach to a finite yield stress closely mimics the power-law approach to a finite plateau found for time correlations functions.

Just below the glass transition, the yield stress increases algebraically with decreasing the temperature, $\sigma_y(T \lesssim T_c) - \sigma_y(T_c) \approx \sqrt{T_c - T}$, which again mimics the temperature behaviour of the plateau in time correlation functions (indeed the two are intimately connected within the theory). In this regime, the flow curves are again well described by a Herschel-Bulkley functional form. The limit of low temperatures is, however, problematic within the theory which makes the unphysical prediction that the yield stress eventually vanishes in the $T \rightarrow 0$ limit (Ikeda and Berthier, 2013). This implies that the theory is actually not well suited to describe the yield stress of glassy systems deep in the glass phase. This is perhaps not surprising, as the starting point of the theory is actually an equation of motion for the fluid. It should thus be kept in mind that mode-coupling theories should be used to describe the interplay of glassy dynamics and shear flow in the vicinity of kinetic arrest. This theoretical limitation is in fact fully understood in the context of random first order transition theory, where the structure and dynamics of the glass phase is actually treated analytically using a completely different approach based on an approximate treatment (involved replica techniques) of the complex free energy

landscape characterizing glassy materials (Yoshino and Mézard, 2010). Recent progress in this direction have been substantial (Charbonneau, 2014; Parisi and Zamponi, 2010), and the theory is now being developed to treat mechanical properties, such as the shear modulus (Yoshino and Zamponi, 2014). Very recently, stress-strain curves in quasi-static deformation protocols have been obtained analytically (Rainone *et al.*, 2015). Reconciling these thermodynamic replica calculations to dynamic equations derived within mode-coupling theories represents a clear challenge for future research, which remains to be tackled (Szamel, 2010).

c. Jamming rheology. We have described qualitatively the flow curves obtained in simple models undergoing an ideal jamming transition in Sec. II.B.2, in connection with the experimental results displayed in Fig. 3. We simply recap the main findings here, in order to contrast the obtained flow curves from the previous schemes.

In the vicinity of the jamming transition, flow curves display a number of scaling features. The system exhibits upon compression across ϕ_J a diverging Newtonian viscosity and an emerging yield stress. An approximate scaling form as in Eq. (7) is obtained below the jamming transition in the non-Brownian suspension regime, where the Newtonian viscosity diverges as $\eta_0(\phi) \sim (\phi_J - \phi)^{-\beta}$, with β a critical exponent frequently reported in the range $\beta \approx 1.5 - 2.5$ (Andreotti *et al.*, 2012; Boyer *et al.*, 2011). A very recent large-scale numerical study for ideal (non-frictional) hard particles reports $\beta \approx 2.55$ (Kawasaki *et al.*, 2015). Exactly at the jamming transition, a pure power-law rheology is obtained with a non-trivial shear-thinning exponent $n \approx 0.38$, again with strong preasymptotic corrections (Olsson and Teitel, 2012). Finally, above jamming, a Herschel-Bulkley functional form describes the data very well, with a yield stress increasing continuously (but algebraically) from zero at the transition. These flow curves have been characterized numerically in great detail (Hatano, 2010; Ikeda *et al.*, 2012; Olsson and Teitel, 2007, 2012), and have also received experimental support (Paredes *et al.*, 2013). There is currently a large theoretical activity to better understand the physical origin of these exponents and to relate them to more microscopic quantities characterizing the structure of athermal packings in the vicinity of the jamming transition (DeGiuli *et al.*, 2014; Lerner *et al.*, 2012; Tighe *et al.*, 2010; Yoshino and Zamponi, 2014). This is again a very active and promising research avenue.

III. HOW THE YIELD STRESS IS DETERMINED CLASSICALLY: MEASUREMENT TECHNIQUES

Over the years, two categories of methods have been proposed for measuring a characteristic stress associated with the solid-fluid transition that has been generically labeled as “the” yield stress. The first category concerns means that do not involve the use of a rheometer, such as squeeze flows (Rabideau and Coussot, 2009), penetrometry (Boujlel and Coussot, 2012), stop flows on inclined planes (Coussot and Boyer, 1995; de Kee *et al.*, 1990). We do not detail these methods and we refer the reader to a recent exhaustive review on such techniques (Coussot, 2014). Here we rather focus on a second category that involves the use of a rheometer and on basic protocols that include shear start-up experiments, creep experiments and stress- or strain-controlled oscillatory sweep. In this section, we revisit these different protocols in light of recent experiments coupled with local investigation techniques that provide, for each protocol, a mesoscopic scenario and a physical meaning for the estimates of the yield stress. Except for a few simple yield stress materials for which different methods leads to comparable values, for most of yield stress materials the yield stress estimate is method-dependent and strongly related to the state of the sample prior to the measurement. This is why we first review yield stress measurements that start from the solid state (shear start-up, strain or stress sweep) and then turn towards the measurements that start from the liquid state (flow curve extrapolation, flow cessation experiments). We finally compare these different methods.

A. General overview of yield stress determination under drag flow

In rotational shear rheometry a shear stress is imposed and the corresponding shear rate (or strain) is recorded, or vice-versa. Typical geometries used for performing this type of measurement include concentric cylinders, plate-plate and cone-plate geometries (Barnes *et al.*, 1989; Larson, 1999). A large variety of techniques based on the use of a rheometer has been introduced to estimate the yield stress. Before describing in detail the various methods, we provide here a general overview of the ways and means of measuring σ_y under drag flow.

The yield stress can be determined from *steady shear measurements* by extrapolating flow curves (σ vs. $\dot{\gamma}$) to the limit $\dot{\gamma} \rightarrow 0$ or by fitting the curves to a rheological model, like Bingham, Herschel-Bulkley or Casson [see Fig. 10(a)]. In practice, the accuracy of this way of determining the yield stress is highly influenced by the minimum $\dot{\gamma}$ that is measured with the rheometer (Barnes and Walters, 1985). Both the imposed variable ($\dot{\gamma}$ or σ) and the sweep direction and rate used for constructing the flow curve can impact the yield stress estimates, es-

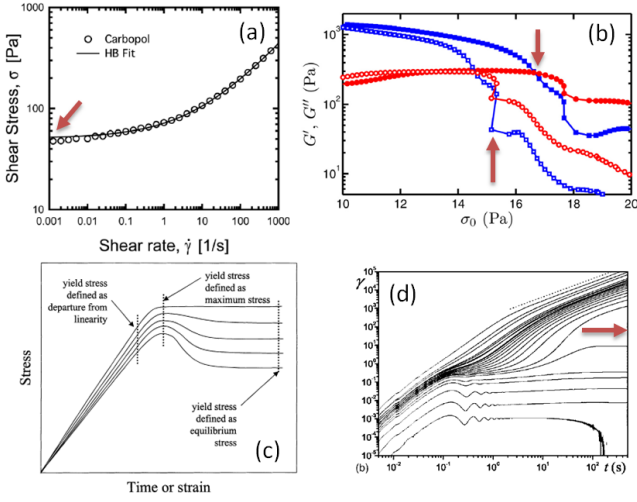


FIG. 10 Various methods to determine the yield stress in experiments. (a) Extrapolation of the flow curve in the limit of vanishing shear rates. Experiments performed on a carbopol microgel using roughened cone and plate fixtures. The black line is the best Herschel-Bulkley fit. Extracted from (Dimitriou *et al.*, 2013). (b) Oscillatory stress sweep experiment performed on a 6% wt. carbon black gel at two different sweep rates: 7 (open) and 34 (filled) $\text{mPa}\cdot\text{s}^{-1}$, respectively. Here, the yield stress defined as the intersection of G' (blue) and G'' (red) depends on the sweep rate. Extracted from (Perge *et al.*, 2014). (c) Sketch of the stress response to a shear start-up experiment. The yield stress can be defined as the stress corresponding to the end of the linear regime, as the stress maximum, or as the equilibrium stress. Extracted from (Barnes and Nguyen, 2001). (d) Strain response to a step stress experiments for various stresses ranging from 0.22 to 220 Pa. Extracted from (Coussot *et al.*, 2006).

pecially in the case of thixotropic systems (Cruz *et al.*, 2002; Divoux *et al.*, 2013; Fall *et al.*, 2010b).

The yield stress can also be determined from *large amplitude oscillatory shear (LAOS) tests* by performing strain sweeps at a low frequency. These measurements consist in imposing a sinusoidal shear strain of amplitude γ_0 and frequency ω , given by $\gamma(t) = \gamma_0 \sin(\omega t)$. By analyzing the stress signal, it is possible to determine the storage (G') and loss (G'') moduli. At low amplitudes, i.e. within the linear viscoelastic regime, G' is determined from the component of the stress in phase with $\gamma(t)$ and G'' from the component of the stress in phase with $\dot{\gamma}(t)$ (Ferry, 1980). By plotting G' and G'' as functions of either the strain amplitude γ_0 or the shear stress amplitude σ_0 , the yield stress may be given by: (i) the point at which $G' = G''$, which has been called “characteristic modulus” by (Larson, 1999), or by (ii) the intersection of the power-law equations representing the behaviors well above and well below the yielding point (Rouyer *et al.*, 2005). Alternatively, by plotting σ_0 vs γ_0 , σ_y is determined from the intersection of a line with slope equal to G' at low strains with a power law at high strains (Mason *et al.*, 1996; Saint-Jalmes and Durian, 1999). However,

this definition of σ_y from power-law equations representing the behavior at low and at high strains remains empirical. Moreover, under LAOS, the response becomes nonlinear and needs to be analyzed considering the full spectrum of strain or stress harmonics (Ewoldt *et al.*, 2008; Hyun *et al.*, 2011; Rogers *et al.*, 2011b). In the case of strongly time-dependent materials, the estimate of σ_y may also depend on the details of the LAOS ramp protocol, as illustrated in Fig. 10(b).

Stress relaxation experiments also allow for the determination of the stress that remains in equilibrium after a constant σ or $\dot{\gamma}$ has been imposed in a rotational rheometer and once the material has been brought to rest (Nguyen and Boger, 1983). However, such residual stress does not generally provide a reliable estimate of the yield stress σ_y , as relaxation might allow the stress to decay to value smaller than the real yield stress. Finally *transient stress measurements* during shear start-up experiments allow the determination of σ_y by imposing $\dot{\gamma}$ and recording the resulting σ as a function of time t or of strain γ . The yield stress can then be defined in (at least) three different ways: (i) as the stress at the end of the linear elastic region, (ii) the maximum stress, and (iii) the minimum stress at equilibrium for which the system flows, as shown in Fig. 10(c). Under an imposed shear stress (*creep experiments*), the yield stress is commonly estimated as the stress separating steady-state flow states from arrested states [see Fig. 10(d)]. Given the variety of empirical methods used to defined “the” yield stress, it should appear as no surprise that no single number can account for the outcome of all experimental results. In fact, these measurements should be seen as capturing a similar phenomenon using distinct tools, and “the” best measure of a yield stress may very well depend on the precise objective of the measurement.

In the rest of this section, we describe in more detail the various above-mentioned techniques by identifying two separate categories: (i) methods that involve a solid-to-liquid transition and (ii) methods that involve a liquid-to-solid transition to determine the yield stress. Such a separation allows us to emphasize the physical processes involved in the various protocols used for probing the yielding transition. We then briefly comment on the comparisons made in the literature between the different techniques.

B. Yield stress measured starting from the solid state

1. Shear-start up experiments

Under a constant external shear rate, the stress increases linearly with the strain. It departs from the elastic regime at intermediate strains, e.g. $\gamma \sim 0.1$ for bentonite suspensions (Nagase and Okada, 1986), 0.2 for microgels (Divoux *et al.*, 2011a), etc. and goes through

a maximum before decreasing toward its steady-state value. This general behavior is sketched in Fig. 10(c). Observed in numerous yield stress fluids such as foams (Khan *et al.*, 1988), emulsions (Batista *et al.*, 2006; Papenhuijzen, 1972), microgels (Divoux *et al.*, 2011a), clays (Nagase and Okada, 1986), mud (Nguyen and Boger, 1983), or attractive gels (Koumakis and Petekidis, 2011; Lidell and Boger, 1996), this stress overshoot has been widely used to estimate the yield stress as the maximum stress reached during shear start-up. Interestingly, the stress corresponding to the strain at which the material departs from the linear regime has been barely studied (Lin and Brodkey, 1985; Nagase and Okada, 1986), although it corresponds quite naturally to the definition of the *yield stress*, i.e., the stress above which the material stop behaving as an elastic solid and starts flowing like a liquid. Of course, for such a measure to be meaningful, one should also consider more precisely whether a genuine “purely elastic” regime might hold in a realistic macroscopic sample. Most authors have rather chosen to focus on the stress maximum, which is now referred to as the *static yield stress* in the literature (Varnik *et al.*, 2004), although it was first coined dynamic yield stress (Lidell and Boger, 1996) as the material has already left the linear regime at this point.

The determination of the stress maximum is actually sensitive to numerous artifacts. Wall slip (discussed in more detail in Sect. IV.C) leads to measuring the stress at which the material starts experiencing slippage at the wall, which occurs at stresses lower than the stress required for the bulk material to yield. A less reported, yet critical, practical issue is the effect of the response time of the rheometer. Indeed, experiments performed on stress-controlled rheometers involve a feedback loop that is used to impose the specified shear rate. This shear rate is reached after a lag time that may be longer than the timescale over which the stress overshoot takes place. Very few papers mention this technical issue (Nagase and Okada, 1986) or actually provide direct evidence that the experiment is truly performed under *constant* shear rate (Divoux *et al.*, 2011b).

Let us now review the various control parameters impacting the value of the stress maximum. First, the stress overshoot strongly depends on the value of the applied shear rate (Nguyen and Boger, 1983) and on the preshear history through the waiting time between the preshear used to reset the fluid memory and the start of the experiment. Systematic experiments performed on stabilized suspensions of silica particles (Derec *et al.*, 2003), carbopol microgels (Divoux *et al.*, 2011a) and attractive gels (Koumakis and Petekidis, 2011) report a power-law increase of the stress maximum with the external shear, with an exponent ν such as $0.1 \leq \nu \leq 0.5$. This power-law scaling is captured by fluidity models (Derec *et al.*, 2003), Stokesian simulations (West *et al.*, 1994) and Brownian dynamics simulations of particle gels

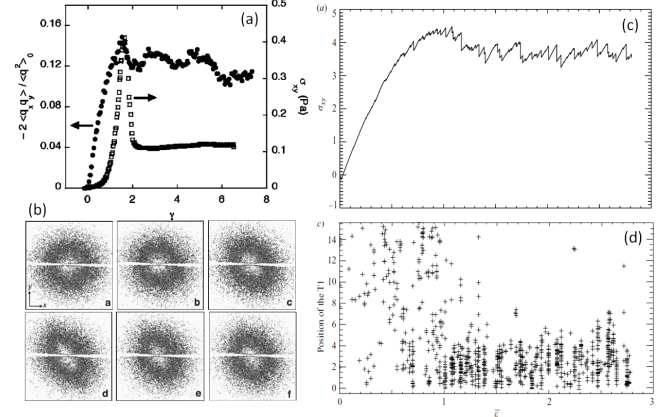


FIG. 11 (a) Normalized off-diagonal component of $\langle \hat{q}\hat{q} \rangle$ and the shear stress σ_{xy} vs. strain γ during a shear start-up experiment ($\dot{\gamma} = 0.17 \text{ s}^{-1}$) for a DLCA polystyrene gel ($\phi = 10^{-3}$). (b) Contour plots of a representative cascade of scattering patterns collected during a start-up experiment ($\dot{\gamma} = 0.56 \text{ s}^{-1}$) with $t = 0.1$ -a, 1.1 -b, 2.2 -c, 3.5 -d, 6.3 -e, 8.3 s-f. Maximum anisotropy is observed at $t \simeq 3.5$ s. (a) and (b) Extracted from (Mohraz and Solomon, 2005). Evolutions of the shear stress (c) and positions of the T1 events in a foam sheared in a 2D Couette cell (d) as a function of the applied strain during a shear start-up experiment. Data from numerical simulations, extracted from (Kabla *et al.*, 2007).

(Park and Ahn, 2013; Whittle and Dickinson, 1997), although the microscopic parameters controlling the exponent ν stand out as open questions. This power-law scaling also contrasts with the logarithmic increase reported for bidisperse Lennard-Jones mixtures for which the increase of the stress maximum can be interpreted in the framework of the Ree-Eyring viscosity theory (Rottler and Robbins, 2005; Varnik *et al.*, 2004) and appears quite natural in the context of aging studies of glassy materials. For a given applied shear rate, the stress maximum increases with the sample age, i.e. with the waiting time t_w between the preshear and the shear start-up, and the overshoot disappears for waiting times shorter than $1/\dot{\gamma}$ (Derec *et al.*, 2003; Divoux *et al.*, 2011b; Letwimolnun *et al.*, 2007). Such a behavior is well captured by the Soft Glassy Rheology model (Fielding *et al.*, 2000) and by the fluidity model (Moorcroft *et al.*, 2011), although both models predict a logarithmic increase of the stress maximum with t_w , whereas experimental results rather lean towards a weak power-law dependence. Finally, an internal key parameter impacting the stress maximum is the packing fraction ϕ . Although the stress maximum has been reported to increase qualitatively with ϕ for foams (Khan *et al.*, 1988), the influence of ϕ remains poorly studied in dense assemblies of soft particles. In the case of dense colloidal suspensions, the amplitude of the stress overshoot vanishes as random close packing is approached, emphasizing the key role of the available free volume for the particles to rearrange in this transient

process (Koumakis *et al.*, 2012).

Regarding the local behavior of the fluid during shear start-up, recent experimental and numerical works have shed new light on the nature of the stress maximum. In Brownian colloidal systems the stress maximum coincides with the maximum structural anisotropy (Koumakis *et al.*, 2012; Mohraz and Solomon, 2005) [see Fig. 11(a,b)]. For attractive gels the stress maximum corresponds to the rupture of the gel network, while for dense hard-sphere-like systems, individual colloids experience an apparent superdiffusive motions as they are being pushed out of their cage by shear (Koumakis *et al.*, 2012; Zausch *et al.*, 2008). In the case of a jammed assembly of soft particles, the deformation is almost elastic – only a few rearrangements that are uniformly spatially distributed have been reported in foams (Kabla *et al.*, 2007) [see Fig. 11(c,d)], while linear velocity profiles have been observed in microgels up to the stress maximum (Divoux *et al.*, 2011b).

To summarize, the stress maximum observed during shear start-up experiments is a complex quantity that depends on both the preshear history and on the applied shear rate. This is perhaps not too surprising, as this “transient” measurement invokes no relaxation towards a well-defined steady-state dynamical behaviour and is moreover performed at a finite strain rate, which introduces an additional timescale into the set-up. The complex dependencies reported experimentally then reflect different local scenarios depending on the nature of the interactions between the constituents. Although the stress maximum obtained for an arbitrary value of the applied shear rate can be used to define for instance the strength of a drilling fluid (Speers *et al.*, 1987), one should keep in mind that shear start-up does not give access to a single quantity but rather to a rate-dependent static yield stress. In particular, the stress maximum appears to be an increasing function of the applied shear rate, as well as on the waiting time when aging is involved.

2. Creep experiments

For stresses applied above the yield stress, the material eventually flows, whereas for stresses lower than the yield stress, the material behaves as a solid and the deformation tends toward a constant strain. Equivalently, the shear rate reaches a non-zero steady-state value in the former case, while it vanishes in the latter case. This “bifurcation” between a finite steady-state viscosity and an apparently infinite viscosity in principle provides a well-defined estimation of the yield stress as the critical stress separating these two regimes (Coussot *et al.*, 2002a,b, 2006; Cruz *et al.*, 2002; Møller *et al.*, 2006) [see Fig. 10(d)]. This method is a little cumbersome, however, as the yield stress is obtained by dichotomy, while

for each experiment the time for the material to flow increases as the applied shear stress gets closer to the yield stress (Møller *et al.*, 2009a). The question of deciding whether a steady state (constant strain) is reached and whether the system eventually flows or not becomes even more crucial in the case of very long transients and of “delayed yielding,” where no apparent flow can be detected for long times before the material finally yields (Chaudhuri and Horbach, 2013; Gibaud *et al.*, 2010; Magda *et al.*, 2009; Uhlherr *et al.*, 2005). This issue will be addressed in detail in Section IV.D.3. Note that only a handful of spatially resolved experimental data associated with stress-controlled experiments are available, and the local scenario from the early moment of the creep up to the abrupt fluidization remains mostly an open issue. Linear velocity profiles have been reported for microgels (Divoux *et al.*, 2011b) although flow inhomogeneities may also be triggered by the mechanical and chemical properties of the boundary conditions (Chan and Mohraz, 2013), as discussed at length in section IV.C. Even more recently, confocal microscopy has been used to estimate the characteristic size of dynamically cooperative clusters in colloidal gels under creep flow (Chan and Mohraz, 2014). Finally, creep experiments have also been studied in elongational flows. Depending on the applied shear stress, the material either tends toward a constant strain at low stresses or flows at larger stress values, which allows one to measure a static yield stress (Husband *et al.*, 1993). The case of elongational flows of yield stress fluids will be addressed in more details in Sect. V.

3. Large-amplitude oscillatory shear (LAOS) experiments

Under oscillatory shear, one classically estimates the yield point by progressively increasing the amplitude γ_0 of the oscillatory strain. At low strain amplitudes the solidlike material is elastically deformed and the storage modulus G' remains constant and much larger than the loss modulus G'' . At larger strain amplitudes G' typically decreases and crosses G'' at a strain value γ_{0c} that can be used to infer the yield stress. For oscillation amplitudes larger than γ_{0c} , G'' gets much larger than G' , indicating a fluidlike behavior, see Fig. 12. This experimental situation is therefore characterized by the introduction of a measurement timescale (given by the inverse of the frequency at which the system is sheared), but in contrast to shear start-up experiments, this methodology requires that a well-defined non-equilibrium steady state is achieved during the measurement.

Surprisingly, very few systematic, quantitative comparisons with the above estimations of the yield stress have been performed (Rouyer *et al.*, 2005). The possible dependence of γ_{0c} on the oscillation frequency has not been discussed either. Another estimate of the yield stress can be inferred from oscillatory measurements by

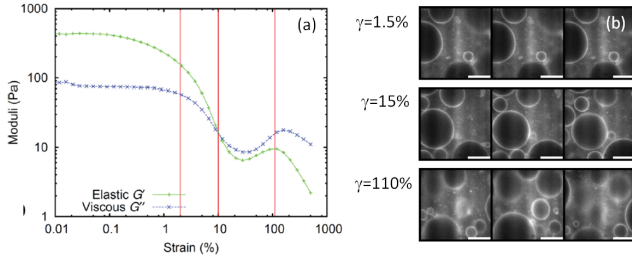


FIG. 12 (a) Evolution of the shear moduli of a Pickering emulsion stabilized by silica colloids during a strain sweep. The volume fraction of the oil is 65%. (b) Confocal images of the emulsion during shear taken 40 nm into the sample to avoid wall effects and obtained at different strains during the strain sweep. Scale bars correspond to 20 μm . For $\gamma < 0.10$ the droplets slide along each other but remain trapped in the cages formed by their neighbors. For $\gamma \geq 0.10$ the moduli intersect and the droplets can be seen to move irreversibly, although their displacement over a period is much less than their diameter. For $\gamma > 0.30$, G' and G'' increase due to jamming, which results in apparent shear-thickening, and the droplets move rapidly during each period, over distances larger than their own diameter. Extracted from (Hermes and Clegg, 2013).

plotting the stress amplitude σ_0 vs the strain amplitude γ_0 . Under small deformation, the stress amplitude grows linearly with the strain amplitude. This linear dependence markedly changes upon yielding and generally becomes a sublinear power-law. The intersection between the extrapolations of both power-law behaviors in σ_0 vs γ_0 allows one to define a yield stress and yield strain (Mason *et al.*, 1996). This latter definition was shown to be in quantitative agreement with the yield stress inferred from the flow curve in the case of concentrated emulsions (Mason *et al.*, 1996) and microgels (Mohan *et al.*, 2013b), and in good agreement in the case of colloidal gels (Walls *et al.*, 2003). However the change of power-law behavior in σ_0 vs γ_0 a priori reflects the onset of the nonlinear regime rather than the solid–fluid transition itself so that the link between the two different estimates of σ_y from oscillatory measurements remains to be clarified.

Estimates of the yield stress (or of the associated characteristic yield strain) based on measurements of G' and G'' vs γ_0 (or σ_0) under large amplitude oscillatory shear (LAOS) have been widely used on a variety of yield stress materials in the past, e.g. concentrated emulsions (Mason *et al.*, 1996), colloidal suspensions (Pham *et al.*, 2006; Puertas *et al.*, 2005), soft colloid–polymer mixtures (Truzzolillo *et al.*, 2013), soft thermoresponsive microgel and core-shell particles (Carrier and Petekidis, 2009; Le Grand and Petekidis, 2008; Siebenbürger *et al.*, 2012), Laponite suspensions (Negi and Osuji, 2010c) and alumina and fumed silica suspensions (Kumar *et al.*, 2012; Marunaka and Kawaguchi, 2014), among many others, and a classification of the most frequent evolutions of viscoelastic moduli with oscillation amplitude has been

proposed (Hyun *et al.*, 2002, 2011).

As an interesting recent advance, this approach has been used to unveil a striking difference between attractive and repulsive colloidal glasses. Whereas the elastic modulus decreases monotonically in dense hard-sphere-like systems, attractive glasses display a two-step yielding, which results from the existence of two distinct microscopic lengthscales in the system: the adhesion range (responsible for initiating phase separation) and the cage size in the glassy dense phase (responsible for the dynamic arrest). (Chan and Mohraz, 2012; Koumakis *et al.*, 2013; Laurati *et al.*, 2011; Pham *et al.*, 2006). Such a two-step scenario has been observed through strain-step experiments (Koumakis and Petekidis, 2011), but its interpretation still requires full confirmation from direct local investigations. A general framework coined “strain-rate frequency superposition” has been proposed to account for the evolution of the viscoelastic moduli with stress or strain amplitude in terms of the strain-rate dependence of a single characteristic structural relaxation time (Wyss *et al.*, 2007). Although appealing due to simple scalings and physical interpretation, the validity of this approach outside the strictly linear regime has later been questioned (Erwin *et al.*, 2010; Hess and Aksel, 2011).

More generally, the connection between the evolution of G' and G'' and a detailed microscopic scenario for yielding remains elusive in the absence of complementary measurements. First, this is because macroscopic viscoelastic moduli G' and G'' alone measured in the nonlinear regime do not correctly reflect the sample behavior under LAOS, and higher harmonic content must be taken into account to fully understand the nonlinear response of a yield stress material under LAOS. This is reflected in the complex shapes of the Lissajous-Bowditch (strain vs stress) curves that are classically plotted as a function of frequency in so-called “Pipkin diagrams” to allow for a qualitative fingerprinting of the nonlinear effects of LAOS (Ewoldt *et al.*, 2010; Pipkin, 1972). The issue of nonlinearity has been quantitatively addressed during the last three decades through the development of Fourier transform (FT) rheology (Ganeriwala and Rotz, 1987; Wilhelm, 2002; Wilhelm *et al.*, 2012). Since the harmonic content lacks a clear physical interpretation, various alternative approaches based on other decompositions of the nonlinear signal have been proposed that provide valuable physical information on the material behavior during one oscillation cycle (Cho, 2005; Ewoldt, 2013; Ewoldt *et al.*, 2008; Klein *et al.*, 2007; Rogers *et al.*, 2011b). Among them, the orthogonal decomposition in Chebyshev polynomials proposed by (Ewoldt *et al.*, 2008) has the advantages of being unique and directly connected to Fourier coefficients, and of providing measures with a simple physical interpretation in terms of strain hardening, strain softening, etc. (Hyun *et al.*, 2011). Such approaches have recently been used to characterize the physical processes involved in yielding un-

der LAOS in colloidal glasses formed by multiarm star polymers (Rogers *et al.*, 2011a,b) and block copolymer micelles (Poulos *et al.*, 2013; Renou *et al.*, 2010), as well as in a commercial hair gel (Hess and Aksel, 2011) and both a carbopol microgel and model waxy crude oils for which a constitutive model based on the concept of “kinematic hardening” has been devised (Dimitriou *et al.*, 2013; Dimitriou and McKinley, 2014).

Second, more microscopic insights can be gained by coupling oscillatory shear to other characterization techniques, such as structural measurements or local tracking of particle motion. For example, the “light scattering (LS) echo” technique, whereby the amount of irreversible rearrangements can be monitored during yielding under LAOS, has been used in concentrated emulsions (Hébraud *et al.*, 1997), hard-sphere glasses (Petekidis *et al.*, 2002, 2003, 2004) and colloidal gels (Laurati *et al.*, 2014). Very recently, direct tracking of particle-stabilized droplets in Pickering emulsions through confocal imaging has provided support for the concepts of cage breaking in repulsive systems and of bond breaking and rearrangement in attractive systems (Hermes and Clegg, 2013) [see Fig. 12]. Direct observations of the microstructure were also reported for various experimental systems, such as microgel suspensions (Nagamanasa *et al.*, 2014), and emulsions (Keim and Arratia, 2014; Knowlton *et al.*, 2014). Along the same lines, time-resolved neutron and x-ray scattering now allows one to follow the evolution of shear-induced anisotropy in the microstructure of colloidal gels during one single LAOS cycle (Kim *et al.*, 2014; Min Kim *et al.*, 2014; Rogers *et al.*, 2014).

From a more theoretical point of view, recent advances in modeling and simulation of LAOS flows have also led to significant progress in unveiling the physical importance of caging effects in the yielding of both hard-sphere glasses (Brader *et al.*, 2010; Koumakis *et al.*, 2013) and dense assemblies of soft particles (Mohan *et al.*, 2013b). The idea has also emerged that the yielding transition corresponds to a change in the dynamics at the microscopic scale between reversible particle trajectories at small applied stress, and a chaotic dynamics beyond the yielding point (Fiocco *et al.*, 2013; Regev *et al.*, 2013). At present, theoretical analysis seem to predict a smooth transition between the two regimes (Brader *et al.*, 2010; Perchikov and Bouchbinder, 2014), whereas experiments seem to present contrasting evidences on this point (Hermes and Clegg, 2013; Knowlton *et al.*, 2014). Therefore, the nature of the yielding transition under oscillatory shear remains to be fully elucidated.

Finally, wall slip, time-dependence and heterogeneous flows may seriously complicate the picture of yielding under oscillatory shear (Gibaud *et al.*, 2010; Perge *et al.*, 2014; Walls *et al.*, 2003). These various issues will be addressed in Section IV, mainly in the context of steady flow, but one should keep in mind that they may also raise important questions during LAOS experiments.

C. Yield stress measured starting from the liquid state

1. Extrapolation of the flow curve in the limit of vanishing shear rates

The experiment consists in ramping down the shear rate from high to low values. The material, liquid-like at first, is progressively brought into a solid-like state, ideally through a series of steady states. The extrapolation of the stress in the limit of vanishing shear rates points towards a stress value that is now often referred to as the *dynamic yield stress*. This method is conceptually more elegant, as it involves a well-defined steady state for the system under shear, whereas the extrapolation to zero-shear rate implies that the external flow does not introduce an additional timescale into the definition of the yield stress. Of course, the method is practically quite involved as it requires the establishment of steady flow at (in principle) arbitrarily low shear rates, which might of course be problematic.

In the 1970’s and early 1980’s, scientists used this method on experimental data of σ vs $\dot{\gamma}$ plotted in linear coordinates. As the data were often recorded in the presence of wall slip at low shear rates, the extrapolation was usually performed over an arbitrary window at quite high shear rate values (Lang and Rha, 1981; Nguyen and Boger, 1983). The estimated yield stress was therefore extremely sensitive to the extrapolation method which led to a long-lasting debate in the literature on the pros and cons of different fitting models, such as the Bingham, Casson or Herschel-Bulkley models, as briefly summarized in (Nguyen and Boger, 1992). The use of a logarithmic representation for the shear rate axis, typically from $\dot{\gamma} \sim 10^{-3} \text{ s}^{-1}$ to 10^3 s^{-1} , made it possible to give equal importance to the high and low shear rates. In a log-log plot and in the absence of wall slip, the flow curve displays a plateau at low shear-rate values [see Fig. 10(a)] by which extrapolation to vanishing shear rates points towards a better-defined dynamic yield stress. The Herschel-Bulkley model is observed to fit the experimental data properly over several decades in the case of dense assemblies of soft particles, such as emulsions, microgels and foams among others (Ovarlez *et al.*, 2013a), and to provide a robust yield stress value. Note that a proper and convincing extrapolation should result in a pure power-law behavior of the *viscous* stress, namely the difference $\sigma - \sigma_y$ between the stress and the yield stress, vs. the shear rate $\dot{\gamma}$, i.e. in a straight line in a log-log plot, as reported for instance by (Fall *et al.*, 2010b; Katgert *et al.*, 2009; Möbius *et al.*, 2010; Shaukat *et al.*, 2012b; Tighe *et al.*, 2010).

The above methodology suffers however from several important limitations and should be used with care. First, wall slip can affect the flow at low shear rates. The stress may then present a kink toward lower values, as classically observed in emulsions, microgels or colloidal

gels (Ballesta *et al.*, 2012; Meeker *et al.*, 2004b; Seth *et al.*, 2008). Wall slip will be discussed in more details in Section IV.C below. Second, time-dependent phenomena such as thixotropy may also strongly impact the estimation of the yield stress. Indeed the shape of the flow curve and therefore its extrapolation in the limit of vanishing shear rates may also depend on the rate at which the shear rate is swept (Divoux *et al.*, 2013), and for some materials, e.g. some attractive colloidal gels (Ovarlez *et al.*, 2013b), may even be a subtle function of the previous flow history. The dynamic yield stress obtained for a time-dependent material should thus be associated with a given protocol and used with caution whenever quantitative comparisons are made between several materials.

2. Flow cessation experiments

In this method, the sample loaded in the rheometer is sheared at a given shear rate long enough to reach the steady state. The shear rate is then set to zero and the initially liquid-like material turns into a solid while the stress decreases towards a constant *residual* or *internal* stress σ_r that has also been coined *yield stress* by several authors (Magnin and Piau, 1990; Michaels and Bolger, 1962; Nguyen and Boger, 1983; Tiu and Boger, 1974), although some authors early noticed that this residual stress was always smaller than the yield stress provided by other measurement methods (Keentok, 1982). In fact, just like the stress maximum measured in shear start-up experiments, the residual stress is not a material constant but decreases for increasing values of the shear rate applied prior to flow cessation, as reported for colloidal glasses and attractive gels (Ballauff *et al.*, 2013; Fritschi *et al.*, 2014; Negi and Osuji, 2010b; Osuji *et al.*, 2008; Ovarlez and Chateau, 2008) as well as for dense suspensions of soft particles (Mohan *et al.*, 2013a) [see Fig. 13(a)]. Nonetheless, the measurement of a well-defined residual stress often remains a critical issue, as after flow cessation the stress is observed to relax over long timescales and does not reach a steady-state value (Ballauff *et al.*, 2013; Osuji *et al.*, 2008) [see Fig. 13(a,c)]. σ_r is thus computed after an arbitrary relaxation duration that is limited by the patience of the experimentalist and/or evaporation. Therefore flow cessation experiments do not lead to the measurement of the yield stress, but rather give access to a history-dependent frozen-in quantity that depends on several parameters.

Not suffering from the above mentioned issues, the dynamics of the stress upon flow cessation is as important as the stress final value as it provides tests for theoretical description of flow cessation. For thermal glasses, the stress relaxes as a power-law as predicted by the Soft Glassy Rheology model (Cates *et al.*, 2004), and is associated with subdiffusive motions of the particles (Ballauff

et al., 2013; Fritschi *et al.*, 2014) [see Fig. 13(d)]. For intermediate times, relaxation curves remarkably scale with the pseudo-deformation $\dot{\gamma}t$ defined as the product of the shear rate applied prior to flow cessation and the time elapsed since flow cessation (Ballauff *et al.*, 2013) [see Fig. 13(c)]. In the case of a dense assembly of soft particles, the stress relaxes through two distinct steps. A rapid relaxation, interpreted as the ballistic motion of the particles in the framework of a micromechanical model (Seth *et al.*, 2011) is followed by a slow relaxation of the elastic contact forces between the jammed particles (Mohan *et al.*, 2013a) [see Fig. 13(b)]. Finally, flow cessation experiments performed on laponite suspensions with varying quench durations reveal that the stress follows a sigmoidal relaxation, and that slower quenches lead to smaller residual stresses at short times that relax at long time over a characteristic duration that scales inversely with the quench rate (Negi and Osuji, 2010b). Overall, experimental observables inferred from stress relaxation still raise a number of open questions that could be of interest for future studies.

D. Comparison between the different methods

Only a handful of papers offer a detailed comparison between the yield stresses obtained on the same system using different methods. Reasonable if not quantitative agreement was found between yield stresses determined by LAOS and steady shear experiments for emulsions (Mason *et al.*, 1996), microgels (Mohan *et al.*, 2013b) and colloidal silica gels (Walls *et al.*, 2003), while discrepancies were observed in foams and attributed to shear localization or strain history effect (Rouyer *et al.*, 2005) [see Fig. 14]. The *static* yield stress obtained from shear start-up experiments is in general larger than the one obtained under LAOS or by steady shear (Derec *et al.*, 2003; Divoux *et al.*, 2011b; James *et al.*, 1987; Laurati *et al.*, 2011), although these three yield stresses have recently been reported to coincide in some cases for dense assemblies of microgels (Mohan *et al.*, 2013a) and emulsions (Paredes *et al.*, 2015), at least within a factor of two, which suggests that the yield stresses determined by these methods could coincide for simple yield stress fluids.

Finally, for time-dependent materials, the different methods lead to distinct stress values. For instance, the yield stress determined from steady shear is larger than the one obtained by LAOS (Grenard *et al.*, 2014), while the yield stress determined by creep experiments is larger than the one determined by steady shear (James *et al.*, 1987). However, as time appears here as a key parameter, it becomes difficult –if still relevant– to compare a yield stress measured on a material initially in a solid state with a yield stress measured on the same material in a liquid state. Indeed, the yielding transition may take

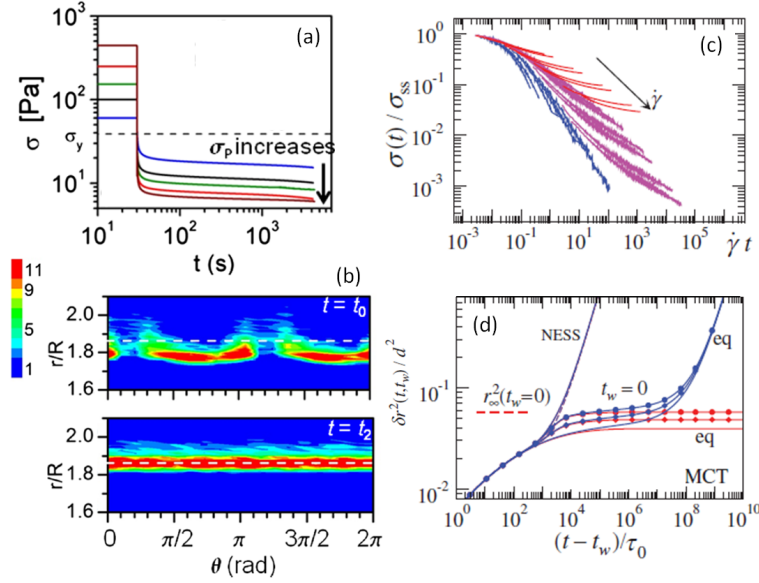


FIG. 13 (a) Stress relaxation upon flow cessation: experiments with microgels for different preshear stresses (from 60 to 443 Pa). The internal stress σ_r , defined by linear extrapolation of the stress measured over a short time interval (< 50 s) after flow cessation, is larger for smaller preshear stress and becomes quite significant for preshear stresses approaching the yield stress. (b) Pair distribution function in polar coordinates in the flow gradient plane at two different times during flow relaxation: during preshear ($t = t_0$), the angular distortion of the microstructure illustrates accumulation of neighboring particles in the compressive upstream quadrant ($\pi/2 < \theta < \pi$) and depletion in the extensional quadrant ($0 < \theta < \pi/2$). At the beginning of the internal stress plateau ($t = t_2$), the mean center-to-center distance has relaxed to its equilibrated value indicated by the dashed white line (equilibrium mean center-to-center distance). (a) and (b) extracted from (Mohan *et al.*, 2013a). (c) Evolution of the stress after flow cessation normalized by the stress prior to flow cessation σ_{ss} as a function of $\dot{\gamma}$ for a hard sphere colloidal suspension. The curves correspond to various imposed shear rates $\dot{\gamma}$ prior to flow cessation, and different packing fractions. Glass states are shown in red, liquid states in blue. (d) Mean-squared displacement $\delta r^2(t; t_w)$ starting at a waiting time t_w after cessation of steady shear, in units of particle diameters obtained by MCT for both a glassy and a liquid state. The MSD exhibits an intermediate-time plateau indicating transient caging of particles in their nearest-neighbor shells. (c) and (d) extracted from (Ballauff *et al.*, 2013).

place over long timescales and may strongly depend on the shear history, as early emphasized by (Cheng, 1986) and detailed below in Sect. IV.

E. Yield stress or yield strain?

A *yield strain* can a priori be associated with each of the yield stresses inferred from the different techniques discussed above, as the ratio of the stress σ_y to the elastic modulus G_0 of the solidlike material at rest. However, another approach is to directly define –and measure– a yield strain as the strain separating solidlike from fluidlike behavior, from which a yield stress can then be inferred simply through the elastic modulus (Mewis and Spaull, 1976). Whether or not these two approaches actually coincide is an interesting and most often open issue. In particular, it raises the question of whether yielding is related to stress-controlled or strain-controlled processes. Recent measurements on carbopol microgels and emulsions shows that the yield strain strongly depends on the method that is employed [Fig. 15]. In particular, the yield strain determined from oscillatory sweep is much

larger than the yield strain obtained with other methods. This last result suggests that for these systems at least, the natural variable associated with the yielding process may rather be the stress than the strain (Paredes *et al.*, 2015).

IV. FLOW DYNAMICS OF YIELD STRESS FLUIDS

This section is devoted to the dynamics of yield stress fluids in the case where a stress above the yield stress is applied. We first address in detail the broad distinction introduced in Sect. II.D between simple yield stress materials and thixotropic ones. After reviewing methods to experimentally distinguish between both categories, we examine the current interpretations and models for the steady-state shear-banding flows generally observed in thixotropic fluids. Second we raise the important question of the effects of boundary conditions on the flow of yield stress fluids. We emphasize the most recent findings on wall slip phenomena, their origin depending on the system microstructure, and the ways to deal with slippage in practice. We close this section by listing a

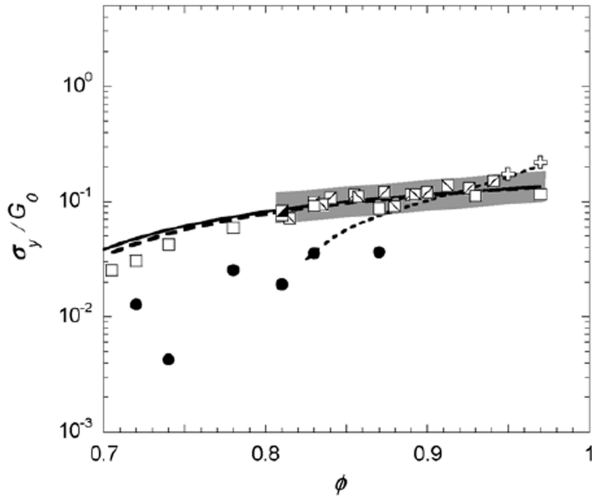


FIG. 14 Yield stress normalized by elastic shear modulus vs. volume fraction for foams and emulsions. Experimental data extracted from various publications: (Princen and Kiss, 1987, 1989) (dotted line), (Saint-Jalmes and Durian, 1999) oscillatory (continuous black line), (Khan *et al.*, 1988) (crosses), (Mason *et al.*, 1996): oscillatory (\square), steady shear (\bullet) experiments, and (Rouyer *et al.*, 2005) Gillette foam for oscillatory and inclined plane (half-filled box) measurements, TTAB foam (oscillatory). The dashed line corresponds to the curve: $\sigma_y/G_0 = 0.39(\Phi - \Phi_c)/\Phi$. Note the discrepancy between the steady shear and the oscillatory measurements. Extracted from (Rouyer *et al.*, 2005).

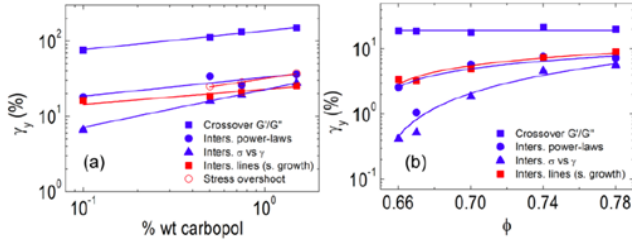


FIG. 15 Yield strain as a function of (a) the mass fraction for carbopol microgels and (b) the volume fraction ϕ for emulsions obtained with different methods. Blue symbols correspond to yield strains obtained from oscillatory measurements. Red symbols correspond to yield strains obtained from stress growth experiments. Extracted from (Paredes *et al.*, 2015).

few “hot topics” that have emerged within the last few years, namely the creep behavior of yield stress fluids prior to yielding, their dynamics under confinement, and the origin of the timescales involved in transient regimes.

A. Distinction between simple and thixotropic yield stress fluids

1. From flow curve measurements

Steady-state flow curves $\sigma = \sigma(\dot{\gamma})$ can be used to distinguish between two types of yield stress materials (Møller *et al.*, 2009b). The first category, coined “simple” yield stress fluids, exhibits a *continuous* and monotonic constitutive equation, which is well fitted by the phenomenological Herschel-Bulkley law $\sigma = \sigma_y + A\dot{\gamma}^n$ [Fig. 16(a)]. As a consequence, whatever the applied shear rate, even in the limit of vanishing values, there is always a finite shear stress above σ_y at which the material flows. Conversely, whatever the applied shear stress above σ_y , there is always a finite shear rate reached by the material. Therefore, such materials may flow at arbitrarily small velocities as long as they experience $\sigma \geq \sigma_y$. This behavior has been reported mainly for dense suspensions of soft particles, i.e. microgels (Cloitre *et al.*, 2003; Coussot *et al.*, 2009), dense emulsions (Mason *et al.*, 1996; Princen and Kiss, 1989) and foams (Denkov *et al.*, 2005; Katgert *et al.*, 2009; Khan *et al.*, 1988; Marze *et al.*, 2008).

The second category of yield stress fluids which includes for instance clays, fiber suspensions and colloidal gels, is characterized by a *discontinuous* flow curve [Fig. 16(b)]. These materials generally show pronounced time-dependence and are therefore coined “thixotropic” yield stress fluids. Indeed, in addition to a yield stress σ_y , these materials are also characterized by a critical shear rate, $\dot{\gamma}_c$, below which they cannot flow steadily in homogeneous conditions (Coussot *et al.*, 2002c). The constitutive equation appears as truncated compared to the case of a simple yield stress fluid. Above $\dot{\gamma}_c$ it is generally well fit by a power-law behavior. The Herschel-Bulkley description is thus replaced by the discontinuous constitutive equation:

$$\sigma = A\dot{\gamma}^n, \quad \text{for } \sigma > \sigma_y, \quad (8)$$

$$\dot{\gamma} = 0, \quad \text{for } \sigma < \sigma_y. \quad (9)$$

In summary, based on the flow curve, two categories of yield stress fluids may be broadly distinguished: those with a continuous flow curve (“simple” yield stress fluids) and those with a discontinuous flow curve (“thixotropic” yield stress fluids). At this stage, it is tempting to draw an analogy with equilibrium phase transitions, where a continuous flow curve would correspond to a second-order solid–fluid transition while a discontinuous flow curve would correspond to a first-order solid–fluid transition. One should note, however, that in practice it may be difficult to discriminate between these two categories on the sole basis of the steady-state flow curve (Dennin, 2008), especially when the flow curve is obtained under controlled shear rate. This is because the flow may become unstable and heterogeneous at low imposed shear rates

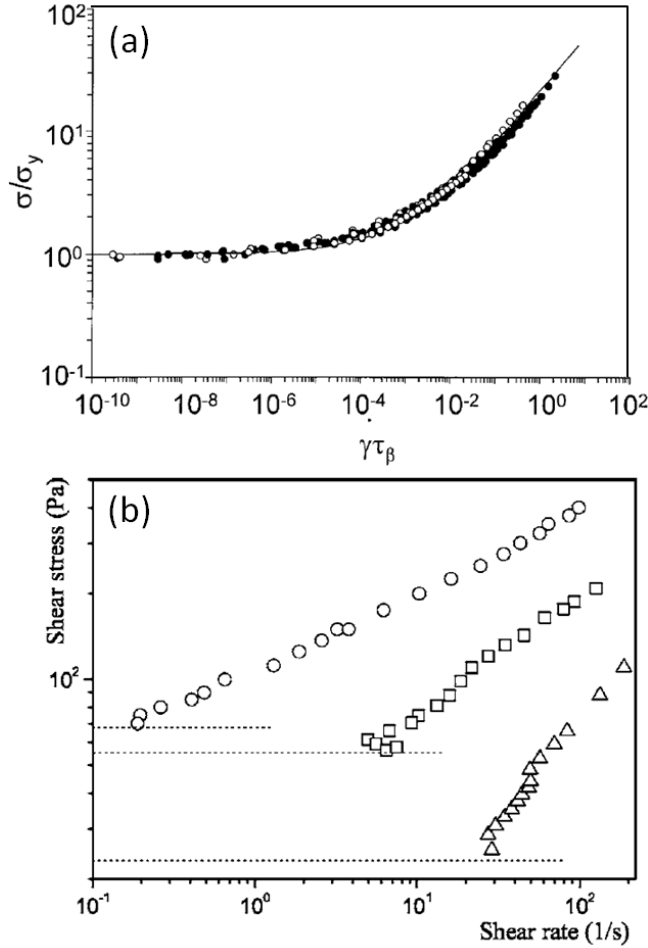


FIG. 16 Representative flow curves for (a) a simple yield stress fluid, here microgels of different cross-link density and different concentrations. The continuous line is the equation $\sigma/\sigma_y = 1 + (\dot{\gamma}\tau_\beta/\gamma_0)^{0.45}$, where τ_β is the fluid relaxation time [extracted from (Cloitre *et al.*, 2003)]. (b) Three different thixotropic materials: a hair gel, a commercial mustard, and a bentonite suspension, from top to bottom. Note that each of these materials displays a minimum shear rate $\dot{\gamma}_c$ below which no steady flow is possible. The horizontal dotted lines indicate the yield stresses of the different materials [extracted from (Coussot *et al.*, 2006)].

($\dot{\gamma} < \dot{\gamma}_c$), leading to an *apparent* flow curve that does not necessarily reflect the unstable constitutive behavior of the material. Wall slip may also seriously complicate the interpretation of rheological data, as detailed below in Sect. IV.C. Finally, ensuring that the flow curve is truly measured in “steady state” may be difficult as the flow curve has to be swept over finite time windows, which may interfere with the material intrinsic timescales (Divoux *et al.*, 2013; Ragouilliaux *et al.*, 2006; Rogers *et al.*, 2008). The development of techniques that allow to locally measure the velocity profiles and/or the volume fraction has helped to classify the yield stress materials not only based on global rheological measurements but

also on local information (Bonn *et al.*, 2008; Chan and Mohraz, 2013; Manneville, 2008). This is discussed below in section IV.A.3.

2. From “viscosity bifurcation”

A practical consequence of the existence of a critical shear-rate $\dot{\gamma}_c$ is the striking avalanche-like behavior of thixotropic yield stress fluids under an applied shear stress in the vicinity of the yield stress (Coussot *et al.*, 2002a,b; Cruz *et al.*, 2002). Within a narrow range of stresses of a few pascals around the yield stress, one may observe two very different macroscopic responses: for $\sigma < \sigma_y$, the material deforms and progressively stops flowing, whereas for $\sigma > \sigma_y$ the material experiences an abrupt fluidization, characterized by an increase of the shear rate up to a finite steady-state value, which recalls avalanche behavior. Figure 17 shows such a behavior observed in a drilling mud (Ragouilliaux *et al.*, 2006). Depending on the applied shear stress, two regimes can be distinguished where the apparent steady-state viscosity $\eta \equiv \sigma/\dot{\gamma}$ differs by several orders of magnitude. In the specific case of Fig. 17, for $\sigma \leq 2.80$ Pa the viscosity apparently diverges towards infinity, pointing to a non-flowing final state, while for $\sigma \geq 2.85$ Pa, η reaches a finite steady-state value indicating a flowing state. The fact that the two regimes are separated by at least 5 orders of magnitude in the steady-state viscosity allows one to precisely estimate the yield stress of this particular system as $2.80 < \sigma_y < 2.85$ Pa. Moreover the fact that no steady-state value for η is found above a given $\eta_c \simeq 5$ Pa.s points to a critical shear rate $\dot{\gamma}_c = \sigma_y/\eta_c \simeq 0.57$ s⁻¹.

The above behavior has been coined a “viscosity bifurcation” in the sense that the yield stress separates two regimes characterized by widely different values of the steady-state viscosity. It is characteristic of yield stress fluids with a critical shear rate, namely thixotropic yield stress fluids. This terminology is, however, somewhat unfortunate since a divergence of the viscosity is also expected for $\sigma \rightarrow \sigma_y^+$ or $\dot{\gamma} \rightarrow 0$ in simple yield stress fluids. In this latter case, the divergence is continuous and any (arbitrarily large) value of the final viscosity can be reached close to the yield stress without any forbidden shear rate range. In the language of bifurcations, yielding in simple yield stress fluids would therefore be analogous to a *supercritical* bifurcation while in thixotropic yield stress fluids it would correspond to a *subcritical* bifurcation.

3. From local measurements

Local velocity profiles allow one to deepen the distinction between simple and thixotropic yield stress materials. Indeed, on the one hand, simple yield stress fluids

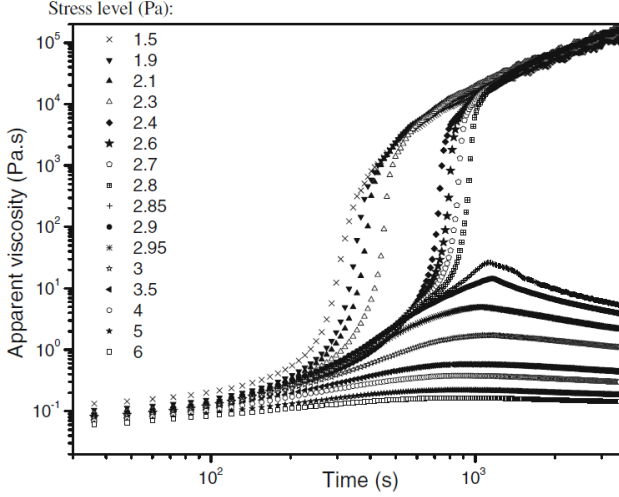


FIG. 17 Temporal evolution of the apparent viscosity $\eta = \sigma/\dot{\gamma}$ of a drilling mud for various applied shear stresses below and above the yield stress $\sigma_y \simeq 2.82$ Pa. The drastic change of behavior within a range of less than 0.1 Pa that encompasses the yield stress illustrates the viscosity bifurcation scenario. Extracted from (Ragouilliaux *et al.*, 2006).

are expected to display homogeneous velocity profiles in steady state, at least in experimental geometries with small enough stress heterogeneity. This results from the fact that simple yield stress fluids are characterized by a one-to-one relationship between shear rate and shear stress. On the other hand, the situation is more complex for thixotropic yield stress materials due to the “forbidden” range of shear rate between 0 and $\dot{\gamma}_c$. We shall show below that even when the stress field is perfectly homogeneous, these materials are expected to exhibit steady-state heterogeneous velocity profiles when the global shear rate is applied in the “forbidden” range, a phenomenon referred to as *shear-banding*.

Within the last two decades a number of different tools to measure the local velocity field within standard rheological geometries have emerged, including particle tracking, dynamic light scattering, magnetic resonance or ultrasonic imaging (Besseling *et al.*, 2009; Bonn *et al.*, 2008; Callaghan, 2008; Gallot *et al.*, 2013; Manneville, 2008; Manneville *et al.*, 2004; Salmon *et al.*, 2003b). Thanks to these techniques it has been confirmed experimentally that simple yield stress fluids generally display homogeneous steady-state velocity profiles that are in agreement with their monotonic macroscopic rheology. The macroscopic flow curve recorded by a conventional rheometer is also referred to as the *global* or *engineering* flow curve (Barnes *et al.*, 1989). In practice, the *local* rheology is compared to the global rheology by plotting the local shear stress $\sigma(\mathbf{r})$ as a function of the local shear rate $\dot{\gamma}(\mathbf{r})$, where \mathbf{r} denotes the spatial position inside the rheometer. The stress distribution within the sample $\sigma(\mathbf{r})$ is known from the momentum equation with negligible in-

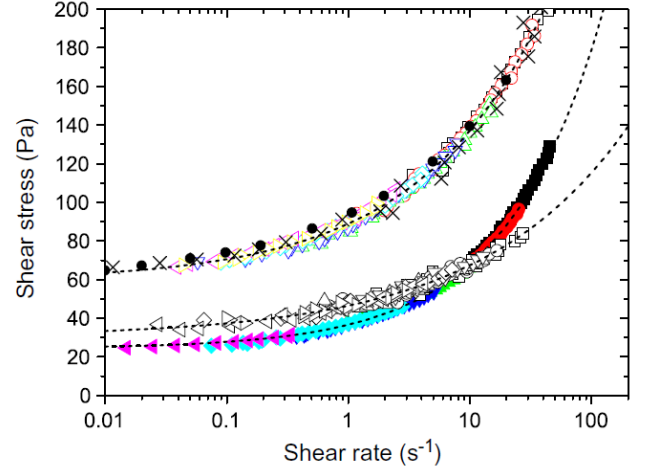


FIG. 18 Flow curves of (from bottom to top) a concentrated emulsion, a foam and a microgel measured locally in a wide gap Couette cell using magnetic resonance imaging. Macroscopic data for the microgel measured in the Couette geometry (\times) and in a cone-and-plate geometry (\bullet) are also shown. The emulsion is composed of silicone oil droplets ($6.5 \mu\text{m}$ diameter) dispersed at a 75% volume fraction in a mixture of 50% wt. glycerine and 50% wt. water stabilized by Brij and trimethyl tetradecyl ammonium bromide at a 1% wt. concentration (Ovarlez *et al.*, 2008). The foam is composed of bubbles of $45 \mu\text{m}$ diameter at a 92% volume fraction in a SLES foaming solution described in (Ovarlez *et al.*, 2010). The microgel is a hair gel (Vivelle Dop, France), which is mainly composed of carbopol in water (Coussot *et al.*, 2009). Extracted from (Ovarlez *et al.*, 2013a).

ertia while $\dot{\gamma}(\mathbf{r})$ is inferred from the local velocity field $\mathbf{v}(\mathbf{r})$. In the specific case of a Couette geometry (concentric cylinders of radii $R_1 < R_2$), one gets, regardless of the fluid rheology:

$$\sigma(r) = \sigma_0 \frac{R_1^2}{r^2}, \quad (10)$$

where r is the radial distance to the rotation axis. The local shear rate is derived from the azimuthal velocity profile $v(r)$ according to:

$$\dot{\gamma}(r) = -r \frac{\partial}{\partial r} \left(\frac{v}{r} \right). \quad (11)$$

Similar relationships can be derived for cone-and-plate and plate-plate geometries or for pipe flow.

The superposition of macroscopic rheological data and local flow curves is shown in Fig. 18 in the case of a concentrated emulsion, a microgel and a foam. This specific case illustrates the excellent agreement obtained between local and global rheological behavior in that both fall on a single curve. Such consistency has been successfully tested for different boundary conditions and different geometries (Divoux *et al.*, 2012), including Couette cells with wide gaps that display large stress gradients (Coussot *et al.*, 2009; Ovarlez *et al.*, 2010, 2008). In

the latter case of a wide-gap Couette geometry, depending on the applied stress, the local stress $\sigma(r)$ may fall below the yield stress. This leads to a heterogeneous flow where a solid region characterized by a pluglike flow (where $\sigma(r) < \sigma_y$) coexists with a flowing region (where $\sigma(r) > \sigma_y$). Similar pluglike flow is observed in the case of the channel flow of simple yield stress fluids due to the wide spatial variations of the shear stress, which necessarily vanishes in the center of the channel (Pérez-González *et al.*, 2012; Poumaere *et al.*, 2014). Such a shear localization therefore results solely from large stress heterogeneity and should be clearly distinguished from the intrinsic shear localization seen in thixotropic yield stress fluids and referred to as “shear-banding” to avoid any confusion (Ovarlez *et al.*, 2013a, 2009). Although it may have important practical consequences for application, shear localization due to the flow geometry merely appears as an experimental artifact which does not contradict the continuous solid–fluid transition of simple yield stress fluids.

It is also worth noting that local and global measurements in simple yield stress fluids may differ in the case of *confined* geometries, i.e. when the gap size becomes comparable to the mesoscopic scale characteristic of the fluid microstructure. In such a case, the effect of a local rearrangement due to shear spans over a range larger than the single grain/drop/bubble scale and may reach the gap size. This modifies the local rheology of the fluid while the global rheology remains unchanged. This issue is further emphasized as a “hot topic” in Sect. IV.D.2.

Another key issue lies in the fact that experiments are always performed over a finite duration while transient regimes may become extremely long-lived in the vicinity of the yield stress (Divoux *et al.*, 2011a, 2010). This leads to the question of whether or not the data reported in the literature are always truly at steady state. This point, recently raised in (Ovarlez *et al.*, 2013a) to explain an apparent mismatch between local and global rheology reported in emulsions (Bécu *et al.*, 2006; Salmon *et al.*, 2003a), is also addressed in a “hot topic” in Sect. IV.D.3. A simple methodology to characterize the transient character and determine the associated timescale (or, equivalently, strain scale) of the flow inhomogeneities has been introduced in computer simulations (Chaudhuri *et al.*, 2012a), but this has not fully explored in experiments yet.

Finally, depending on the value of the applied shear

origin of shear localization	simple YSF	thixotropic YSF
critical shear rate	not present	present
stress heterogeneity	present	present
wall slip	possible	possible

TABLE I Different types of shear localization in simple and thixotropic yield stress fluids (YSF).

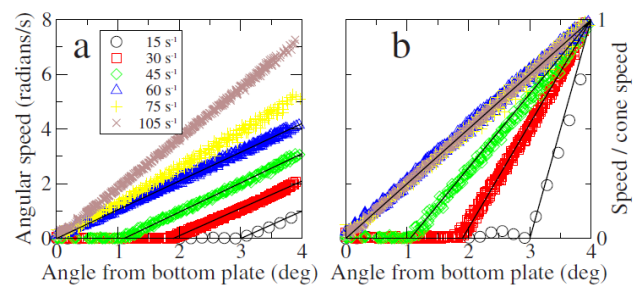


FIG. 19 Example of shear-banded flows. (a) Velocity profiles in a 4° cone and plate geometry of a colloidal silica suspension (Ludox TM-40) for shear-rates ranging from 15 to 105 s^{-1} . (b) Velocity profiles normalized by the cone velocity. Extracted from (Møller *et al.*, 2008).

rate, thixotropic yield stress materials have been shown to flow either homogeneously (for $\dot{\gamma} > \dot{\gamma}_c$) or to display heterogeneous velocity profiles (for $\dot{\gamma} < \dot{\gamma}_c$). In the latter case, a solid-like region coexists with a liquid-like band sheared at $\dot{\gamma} = \dot{\gamma}_c$ (Møller *et al.*, 2008) and the relative extent of both bands ensures that the average shear rate coincides with the macroscopic applied shear rate (Cousot *et al.*, 2002c; Ovarlez *et al.*, 2009). This solid–fluid coexistence therefore corresponds to a *true* shear localization (i.e. to shear banding) in the sense that it is observed independently of any geometry-dependent stress heterogeneity. A way to distinguish between simple and thixotropic yield stress behaviors from local velocity measurements in a wide-gap Couette geometry is to look at the slope of the velocity profile close to the interface separating flowing and solid regions: if the slope is finite (and equal to $\dot{\gamma}_c$), the material is a thixotropic yield stress fluid, while for a simple yield stress fluid the local shear rate (and hence the slope of the velocity profile) goes continuously to zero (Ovarlez *et al.*, 2009). Of course such a distinction may be technically difficult depending on the experimental uncertainty of the velocity measurements. Therefore it is more advisable to test for true shear localization in geometries such as the cone-and-plate geometry or small-gap Couette geometry, where spatial variations of the shear stress are minimized.

Representative velocity profiles in a colloidal gel obtained in a cone-and-plate geometry are displayed in Fig. 19. In this case the amount of fluidlike material is seen to increase proportionally to the global applied shear rate for $0 < \dot{\gamma} < \dot{\gamma}_c$. This points to an equivalent of a “lever rule” for solid–fluid coexistence and once again emphasizes the analogy between yielding in thixotropic materials and a first-order phase transition. Table I summarizes the distinction between shear banding due to the existence of a critical shear rate and shear localization due to stress heterogeneity. It also points out the possibility of apparent slippage at the walls, which can be seen as another form of (extreme) shear localization and

will be addressed in details in Sect. IV.C.

B. What causes steady-state shear banding?

In this section, we examine the possible mechanisms invoked in the literature to explain the steady-state shear-banded velocity profiles reported in thixotropic yield stress fluids. We shall first see that in the case of Brownian suspensions, steady-state shear banding can be related to an unstable branch of the flow curve (Møller *et al.*, 2008), often interpreted and modeled as the result of a competition between spontaneous aging and shear-induced rejuvenation, although only indirect evidence for such a competition has been reported up to now. Aging processes arise from attractive interactions at the level of the microstructure, and attractive interactions have been shown to be a sufficient ingredient to induce steady-state shear banding. However it remains unclear precisely what type of microstructure and interactions are required for steady-state shear banding to occur. In the case of dense suspensions of non-Brownian particles, shear banding has been related to the competition between sedimentation and shear, and more generally to volume fraction heterogeneities. Recent observations in colloidal glasses suggest that such a flow–concentration coupling scenario may be more generic.

1. Competition between aging and shear rejuvenation

The existence of a critical shear rate $\dot{\gamma}_c$ in thixotropic yield stress materials is often explained in terms of an underlying decreasing branch of the flow curve at low shear rates (Olmsted, 2008) as first discussed for viscoelastic “wormlike micelle” surfactant solutions (Spenley *et al.*, 1993). In such a scenario, the constitutive relation of the material is actually a decreasing function for shear rates ranging from 0 to $\dot{\gamma}_c$. In this shear rate range, the flow is therefore mechanically unstable, which leads to some sort of phase separation between an arrested region and a flowing band sheared at $\dot{\gamma}_c$ (Picard *et al.*, 2002). The size of the flowing band is expected to follow the “lever rule” already mentioned above in Sect. IV.A.3. In practice, the decreasing branch of the flow curve cannot be accessed through steady-state measurements, since once shear bands have developed, the shear stress reaches a constant value independent of the applied shear rate $0 < \dot{\gamma} < \dot{\gamma}_c$. This is equivalent to the Maxwell plateau in first-order phase transitions and results in an apparently flat flow curve for low shear rates. Still, transient measurements in the unstable shear rate range can be used to unveil the underlying decreasing flow curve as reported by (Møller *et al.*, 2008) on a colloidal gel.

Experimentally, a fair amount of recent work has shown that one can turn a simple yield stress fluid into

a thixotropic material by tuning attractive interactions between the individual constituents. So far, such work has been limited to emulsions in which attractive interactions have been induced either through depletion forces (Bécu *et al.*, 2006) controlled by the addition of surfactants (Bibette *et al.*, 1992), or by the addition of minute amounts of clay particles (Fall *et al.*, 2010b; Paredes *et al.*, 2011; Ragouilliaux *et al.*, 2007). In the latter case, clay particles are expected to create reversible links between the droplets, although the exact nature of such links is not well understood. Without attractive interactions, sheared emulsions display homogeneous velocity profiles in steady state, whereas once some attraction is introduced, one observes the emergence of a critical shear rate $\dot{\gamma}_c$ and steady-state shear banding for applied rates lower than $\dot{\gamma}_c$.

However, the minimal amount of attraction necessary to permanently form banded profiles is still an open issue. Also, the exact influence on the rheological behavior of the way attraction is induced in the system remains to be assessed. A better understanding of the role of microscopic interactions should be gained from experiments where the attraction between microscopic constituents is continuously tuned, e.g. in a model system of colloids or deformable droplets (Saunders and Vincent, 1999). Full characterization of such model systems in terms of relaxation and restructuration timescales would help to confirm quantitatively the simple physical picture mentioned above (Coussot and Ovarlez, 2010). Such a path is being explored numerically, see (Chaudhuri *et al.*, 2012a; Irani *et al.*, 2014). Although supported by recent experiments on rheological hysteresis (Divoux *et al.*, 2013), the idea that the two distinct categories of yield stress fluids discussed in Sect. IV.A may actually cover the same kind of materials, but whose restructuration dynamics occur over very different timescales, remains to be fully explored.

2. Simple theoretical models

Perhaps the simplest model based on the idea of a competition between aging and shear rejuvenation is the toy-model known in the literature as the “ λ -model” (Coussot *et al.*, 2002a; Mujumdar *et al.*, 2002). The basic assumptions of this model are: (i) there exists a structural parameter, λ (hence the name of the model) that describes the local degree of interconnection of the microstructure, (ii) the viscosity η increases with increasing λ , and (iii) for an aging system at low (or zero) shear rate λ increases, while at sufficiently high shear rates the flow breaks down the structure so that λ decreases to a low steady-state value. These assumptions can be simply

quantified through the following dynamic equations:

$$\frac{d\lambda}{dt} = \frac{1}{\tau_{\text{age}}} - \alpha\dot{\gamma}\lambda \quad (12)$$

$$\eta = \eta_0(1 + \beta\lambda^n), \quad (13)$$

where τ_{age} is the characteristic aging time for microstructure build-up, α determines the rate with which the microstructure is being broken down under shear, η_0 is the limiting viscosity at high shear rates, and β and n are parameters quantifying how strongly the microstructure influences the viscosity. The steady-state flow curve is easily found to be:

$$\sigma = \eta_0\dot{\gamma} + \frac{\eta_0\beta}{(\alpha\tau_{\text{age}})^n\dot{\gamma}^{n-1}}. \quad (14)$$

Three physically different situations can therefore be distinguished depending on the value of n :

- $0 < n < 1$: the material is a shear-thinning (power law) fluid with no yield stress.
- $n = 1$: the material behaves as a simple yield stress fluid with Bingham rheology and a yield stress $\sigma_y = \eta_0\beta/(\alpha\tau_{\text{age}})$. In this case, the viscosity diverges continuously when the stress is lowered towards σ_y .
- $n > 1$: the shear stress diverges both at zero and infinite shear rates so there exists a finite shear rate $\dot{\gamma}_c = [\beta(n-1)]^{1/n}/(\alpha\tau_{\text{age}})$ at which the shear stress has a minimum $\sigma_y = n\eta_0\dot{\gamma}_c$. Once the stress is dropped below this minimum the steady-state shear rate drops abruptly from the value corresponding to the minimum in the flow curve to zero, so the steady-state viscosity jumps discontinuously from some low value to infinity. This situation corresponds qualitatively to the case of a thixotropic yield stress material showing a viscosity bifurcation and steady-state shear banding associated with an underlying nonmonotonic flow curve. More refined versions of the λ -model have been proposed in the literature, e.g. in the case of a colloidal gel made of fractal particulate aggregates (Møller *et al.*, 2008), leading to similar results.

In the λ -model, the critical shear rate is directly related to the only timescale of the problem, namely the characteristic aging time through $\dot{\gamma}_c \propto 1/\tau_{\text{age}}$. However, for real materials, other timescales may also come into play, such as viscoelastic relaxation times, as already mentioned in Sect. II.D. To account for additional intrinsic relaxation timescales, a simplified mean-field argument has been recently proposed based on two timescales (Coussot and Ovarlez, 2010): a macroscopic relaxation time τ_{rel} , equivalent to the viscoelastic time which can easily be measured through stress relaxation experiments, and a microscopic restructuring time τ_{age}

associated with the fluid spontaneous aging. Such an aging phenomenon may occur over very different timescales, since it is driven either by particle aggregation in systems displaying microscopic attractive interactions, e.g. clays and attractive colloidal gels, or by the thermally activated reorganization towards minimal energy in dense systems, such as dense emulsions or microgels (Cloitre *et al.*, 2000; Coussot, 2007; Sollich *et al.*, 1997; Viasnoff and Lequeux, 2002). Note that this *physical* aging is different in nature from the *chemical* aging due to chemical reactions over very long timescales, such as the slow release of Na^+ ions in laponite clay, which cannot be reversed by shear (Shahin and Joshi, 2010, 2012). Accounting for the fact that the total stress applied on a sample serves either to fluidize the sample or to make it flow, the model produces a simple expression of the flow curve

$$\frac{\sigma}{G\gamma_c} = \tau_{\text{rel}}\frac{\dot{\gamma}}{\gamma_c} + \frac{1}{1 + \tau_{\text{age}}\dot{\gamma}/\gamma_c}, \quad (15)$$

where G is the characteristic elastic modulus of elements that break above a critical strain γ_c . The behavior of the material is then governed by the ratio $\Theta = \tau_{\text{rel}}/\tau_{\text{age}}$. In particular the material presents a critical shear rate for $\Theta < 1$, i.e. for a sufficiently long restructuring time. In this case $\dot{\gamma}_c = \gamma_c(1/\sqrt{\Theta} - 1)/\tau_{\text{age}}$ is related not only to the value of the restructuring timescale τ_{age} but also to the relaxation timescale through Θ . Interestingly, simple yield stress behavior corresponds to the point where restructuring becomes faster than viscoelastic relaxation ($\Theta \geq 1$). Therefore the key point of this toy-model is to show that one can continuously go from a monotonic flow curve to a non-monotonic flow curve, i.e. from a simple to a thixotropic yield stress fluid, by increasing the duration of the restructuring time, as illustrated in Fig. 20.

The idea of a competition between a restructuring timescale and shear flow, which is at the core of the mean-field model of Coussot and Ovarlez, has recently been implemented in the elasto-plastic coarse-grained modeling initiated by (Picard *et al.*, 2004). The influence of the timescale competition between structural rearrangement and elastic recovery has been explored in full detail (Martens *et al.*, 2012). This study not only confirms the non-monotonic character of the global flow curves for a certain set of control parameters, but can also explore the spatial consequences of the non-monotonicity in a realistic geometry. In particular, the emergence of a “phase separation” between flowing and non-flowing regions in the system, i.e. permanent shear bands, was clearly observed, thus putting the ideas of (Coussot and Ovarlez, 2010) on firmer grounds. Similar ideas involving a self-consistent dynamics following structural reorganization have been explored in various modeling contexts, see for instance (Cheddadi *et al.*, 2012; Fielding *et al.*, 2009; Jagla, 2007). Although these models all give a consis-

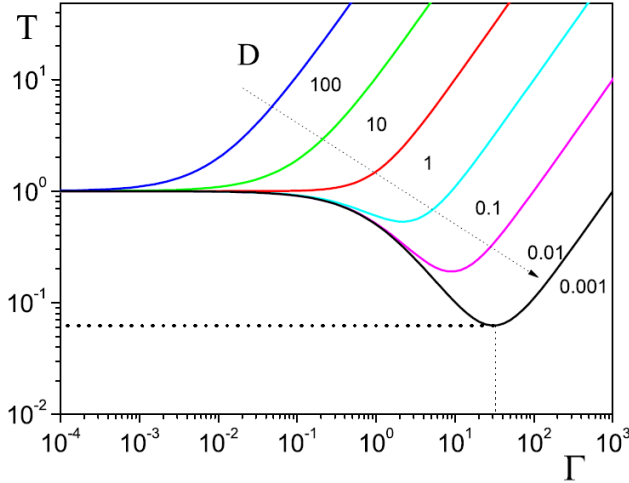


FIG. 20 Dimensionless flow curves stress T vs. the shear rate Γ for different values of the ratio D of the fluid relaxation time η_0/G'_0 where η_0 denotes the zero shear viscosity, over the restructuring time θ , i.e. a time for a microscopic link to reform after being broken. Extracted from (Coussot and Ovarlez, 2010).

tent picture of a timescale competition leading to non-monotonic flow curves in some well-chosen regimes, and thus may give rise to shear bands and viscosity bifurcation, very little progress has been made to understand at a more microscopic level both the physical origin of these timescales and how to control their evolution by tuning, for instance, the interaction between colloidal particles. This clearly stands as an important open problem for future research in this area.

Whereas non-monotonic flow curves necessarily give rise to shear bands (Olmsted, 2008), as observed in a variety of complex fluids, a simpler scenario can also hold in the specific context of yield stress materials. Because the shear bands observed in a yield stress material delimit a flowing phase from an arrested phase (and not two different fluids as in more traditional complex fluids), shear banding can be explained by a simple picture where a monotonic global flow curve of the Herschel-Bulkley type with a finite *dynamic yield stress* σ_y , as in Eq. (3), coexists with a static branch at $\dot{\gamma} = 0$ existing for $\sigma < \sigma_y^s$, where σ_y^s is a *static yield stress*. The strict inequality $\sigma_y^s > \sigma_y$ ensures the existence of a finite stress regime, $\sigma \in [\sigma_y, \sigma_y^s]$ where the shear rate is bi-valued, and can be either zero or finite, see Fig. 21.

This scenario was explored theoretically in (Berthier, 2003), where the two phases were shown to correspond to two different families of dynamical solutions under the same external stress values in the context of a specific driven glassy model. These solutions respectively correspond to a fluid and an arrested phase. A similar explanation was shown to explain the presence of permanent (or at least very long-lived) shear bands in the com-

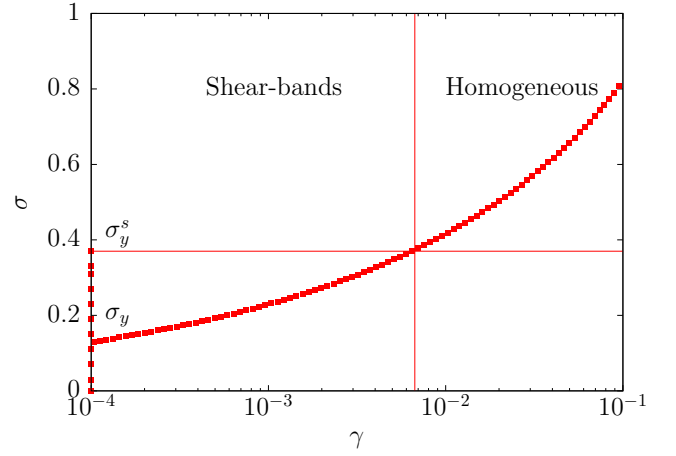


FIG. 21 Scenario for shear banding in yield stress materials. A monotonic flow curve with a finite dynamic yield stress σ_y coexists with a static branch at $\dot{\gamma} = 0$ and $\sigma < \sigma_y^s$, where σ_y^s is the static yield stress. The shear rate is bi-valued for a range of shear stress $\sigma \in [\sigma_y, \sigma_y^s]$, which may lead to shear bands. Adapted from (Berthier, 2003).

puter simulation of a glass-forming liquid in the glassy region below the glass transition temperature (Varnik *et al.*, 2003). There again, a clear separation was observed between the dynamic extrapolation of the homogeneous flow curve and the direct determination of the static yield stress value. Detailed numerical studies have shown, however, that carefully measuring these two yield stress values is not an easy task (Peyneau and Roux, 2008; Xu and O'Hern, 2006). Finally, the validity of this scenario was also demonstrated in a numerical study of concentrated assemblies of soft particles where the degree of particle adhesion was tuned (Chaudhuri *et al.*, 2012a), in analogy with the experimental investigations described above (Bécu *et al.*, 2006; Fall *et al.*, 2010b; Ovarlez *et al.*, 2008; Ragouilliaux *et al.*, 2006). In this numerical study, the emergence of flow inhomogeneity was again directly connected to a discontinuity of the flow curve at $\dot{\gamma} = 0$, which was moreover observed to be strongly enhanced by adhesive forces, thus establishing a direct link between increasing the adhesion and promoting the shear banding behaviour (Chaudhuri *et al.*, 2012a).

3. Flow-concentration coupling

In the case of suspensions of dense and rigid non-colloidal particles, shear banding may also result from volume fraction heterogeneities. Particles being denser than the surrounding fluid, there is a competition between sedimentation and shear-induced resuspension (Fall *et al.*, 2009; Ovarlez *et al.*, 2006). If shear-induced resuspension is not efficient enough, contacts between particles trigger the formation of a percolated network and of heterogeneous volume fraction profiles, leading to

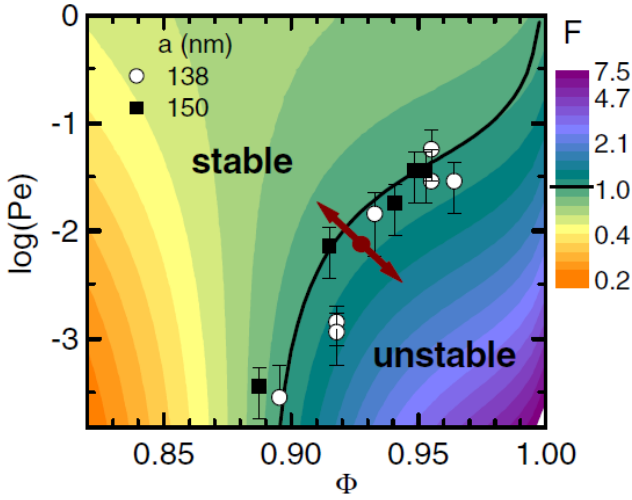


FIG. 22 Critical flow rate (written as a Péclet number P_e) below which the flow becomes unstable and the material experiences shear localization. Colors mark the value of F , which compares the concentration of particles and shear to the diffusive spreading of both particles and shear. Symbols: experimental values for P_e for two different sizes of colloidal particles. Red arrows: possible evolution of an unstable state. Extracted from (Besseling *et al.*, 2010).

shear banding. Interestingly, such a flow-concentration coupling argument has also been invoked recently to account for shear banding in colloidal glasses (Besseling *et al.*, 2010). The underlying key idea is that despite a homogeneous stress field, minute local variations of the volume fraction ϕ may result in significant changes in the yield stress value, which strongly depends on ϕ . At low applied shear rates in sufficiently dense packings [Fig. 22], the flow may become unstable (Schmitt *et al.*, 1995): fluctuations trigger the jamming of a region of the material, which further turns into steady-state shear banding. This type of localization could therefore be interpreted as a precursor to shear-induced thickening (Fall *et al.*, 2010a), although more experimental work is needed to draw an overall conclusion.

C. Wall slip related effects

As already briefly mentioned in Table I, in the vicinity of a *smooth* solid boundary, the velocity (v_{sample}) of a yield stress fluid may differ from the velocity (v_{wall}) of the boundary. One may either observe $v_{\text{sample}} < v_{\text{wall}}$, e.g. in the case of a shearing device driven at constant velocity v_{wall} , or $v_{\text{sample}} > v_{\text{wall}} = 0$ close to a fixed surface or in capillary or channel flows. In both cases, this apparent discontinuity in velocity at the wall is caused by a thin and highly sheared region adjacent to the wall of lower viscosity than the bulk material. This phenomenon, referred to as *apparent wall slip* or more often simply as

wall slip in the literature, has been first described as an artifact that experimentalists should get rid of in order to avoid improper interpretations of rheological measurements. Indeed, wall slip affects steady-state flow curves and thus constitutes a hindrance to properly determine constitutive equations, and estimate yield stresses. Experimentalists have therefore developed practical solutions, either to determine the true deformation experienced by the bulk of the sample so as to correct for wall slip, or to eliminate wall slip by using surfaces of well-chosen roughness (Barnes, 1995). Although elucidating the exact microscopic structure of the lubrication layer remains an experimental challenge due to its small width (typically smaller than $1 \mu\text{m}$), to its very high local shear rate, and to its proximity with a solid boundary, it is reasonably thought of as being composed of pure solvent in the case of colloidal gels or suspensions (Hartman Kok *et al.*, 2004, 2002) or as a film of continuous phase in emulsions (Princen, 1985). The emergence of local techniques such as velocimetry to quantify slip velocities have brought about a better understanding of the behavior of yield stress materials near boundaries, allowing one to develop successful microscopic models in the case of dense assemblies of soft particles (Seth *et al.*, 2011). In the case of attractive gels, a recent body of evidence strongly suggests that the dynamics close to a wall may not be easily decoupled from the bulk dynamics and that wall slip is not merely a rheometric complication, as recently pointed out with a delightfully provocative tone by (Buscall, 2010). Wall slip may indeed have more subtle effects on the yielding scenario and on the transient behavior of yield stress fluids, with sometimes dramatic effects on the nature of the stationary state (Gibaud *et al.*, 2008, 2009). This section addresses the various issues related to wall slip in yield stress fluids in light of such recent developments.

1. Impact on flow curve measurements

Let us start by examining the effect of wall slip on the flow curve. In the presence of wall slip, the measured *apparent* shear rate overestimates the *true* shear rate within the material (or correspondingly the strain indicated by a rheometer overestimates the true deformation experienced by the bulk of the material). Consequently, the apparent flow curve is shifted to high shear rates compared to the actual constitutive equation of the bulk material. In general, at low shear rates—where wall slip effects are the most pronounced—the apparent flow curve displays a kink and/or a plateau at a stress lower than the yield stress estimated in the absence of wall slip [see Fig. 23(a) for examples in a microgel and an emulsion]. This signature was reported in the literature as early as 1975 in the pioneering work of (Vinogradov *et al.*, 1975) and, since then, on a broad range of yield

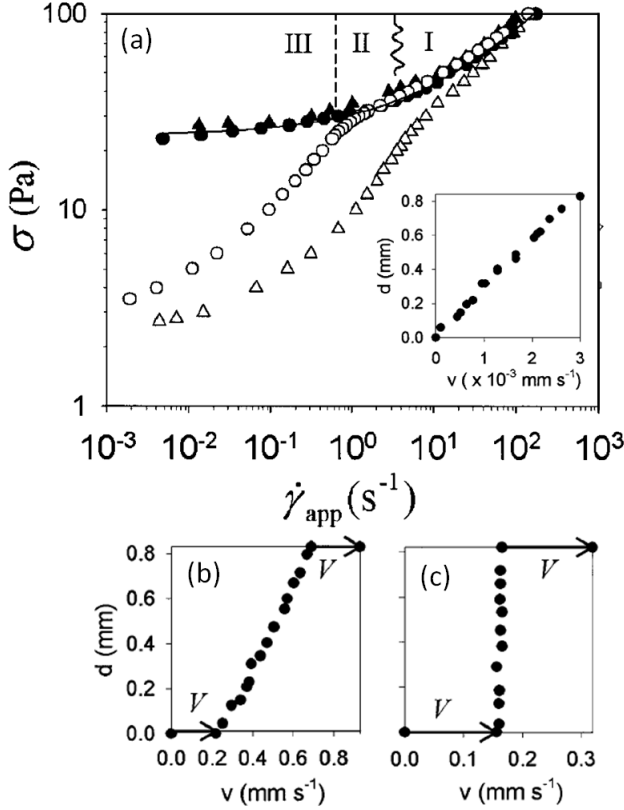


FIG. 23 Stress σ vs. the apparent shear rate $\dot{\gamma}_{app}$ for a microgel paste (○) [resp. (●)] and an emulsion (△) [resp. (▲)] of packing fraction $\phi \simeq 0.77$ obtained in a cone-and-plate device for smooth (resp. rough) surfaces. Regimes I to III refer to microgel slip behavior discussed in the text. The inset shows the velocity profile measured with rough surfaces for $\sigma/\sigma_y = 1.05 \pm 0.1$. Velocity profiles measured with smooth surfaces for (b) $\sigma/\sigma_y = 1.3 \pm 0.1$ and (c) $\sigma/\sigma_y = 0.9 \pm 0.1$. Adapted from (Meeker *et al.*, 2004b).

stress materials including colloidal gels (Buscall *et al.*, 1993; Mas and Magnin, 1994), dense Brownian suspensions (Ballesta *et al.*, 2008, 2012), emulsions and microgels (Meeker *et al.*, 2004a,b) as well as foams (Marze *et al.*, 2008). In particular, wall slip leads to significant deviations from the Herschel-Bulkley behavior at low shear rates, and the apparent flow curve is strongly surface-dependent in this limit (Seth *et al.*, 2008).

2. Physical origin of wall slip in yield stress fluids

Direct flow visualization coupled to rheology has made it possible to go one step further in interpreting the apparent lower stress plateau in the presence of wall slip. The seminal work of (Magnin and Piau, 1990) on carbopol microgels, coupling rheology to direct observations of the strain field, has inspired numerous subsequent studies coupling flow visualization to standard rheology (Aral and Kalyon, 1994; Kalyon *et al.*, 1993;

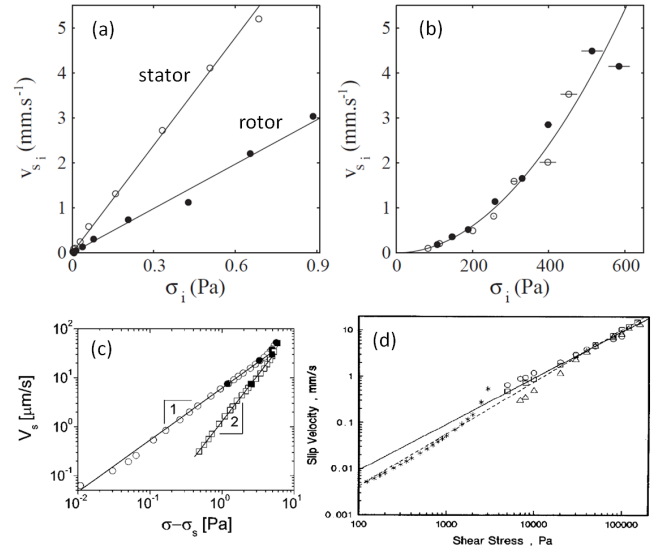


FIG. 24 Slip velocity vs. shear stress at the rotor (●) and at the stator (○) for (a) a dilute emulsion $\phi = 0.2$ and (b) a dense emulsion $\phi = 0.75$. The slip velocity is linear in the dilute regime and quadratic for dense packing for stresses above the yield stress. Extracted from (Salmon *et al.*, 2003a). (c) Slip velocity vs. the excess stress in a dense emulsion for stresses below the yield stress in a plate-plate geometry. The top plate is either coated with a weakly adhering polymer surface (□, ■) or a non-adhering glass surface (○, ●). The wetting properties of the boundary conditions strongly impact the scaling of the slip velocity. Extracted from (Seth *et al.*, 2012). (d) Slip velocity vs. shear stress in a suspension of ammonium sulfate particles in PBAN. Data obtained in capillary flows with dies of various aspect ratio (○, □, △) and a plate-plate geometry (*). The solid line corresponds to a linear behavior. Extracted from (Yilmazer and Kalyon, 1989).

Persello *et al.*, 1994). Subsequently, the combination of rheology and other local measurement techniques such as light scattering velocimetry in Couette geometry (Salmon *et al.*, 2003a) and particle tracking velocimetry in cone-and-plate (Ballesta *et al.*, 2008, 2012; Meeker *et al.*, 2004a,b; Paredes *et al.*, 2011) and plate-plate geometries (Seth *et al.*, 2012) has provided quantitative measurements of slip velocities and a scenario for the different yield stress materials. Let us first discuss the case of yield stress fluids composed of soft deformable particles before turning to rigid particles.

In yield stress fluids made of soft components, the solid behavior results from the tightly packed structure of deformable objects, and the lubrication layers that develop at smooth walls are intimately related to the particles' deformability. For shear rates such that $\sigma \leq \sigma_y$ [see regime III in Fig. 23(a)], there is no flow within the bulk and the apparent motion is entirely due to wall slip [see Fig. 23(c)]. This regime generally correlates with a stress drop or "kink" clearly visible on steady-state macroscopic measurements. For intermediate shear rates, typically $\dot{\gamma} \sim 1\text{--}10\text{ s}^{-1}$, the material is sheared but wall slip is still

significant and steady-state velocity profiles are a combination of bulk shear and wall slip (Meeker *et al.*, 2004b; Salmon *et al.*, 2003a). Finally, for low shear rates that correspond to $\sigma \gg \sigma_y$ [see regime I in Fig. 23(a)], wall slip depends strongly on the geometry and on the gap width, e.g. it is negligible in cone-and-plate geometry (Meeker *et al.*, 2004b; Seth *et al.*, 2008), while it may reach up to roughly 10% in a Couette cell with a 3 mm gap (Divoix *et al.*, 2012; Salmon *et al.*, 2003a). More quantitatively, the slip velocity, defined as $v_s = |v_{\text{sample}} - v_{\text{wall}}|$ increases as a power-law of the slip stress (i.e. stress at the wall): $v_s \propto \sigma^p$, where the exponent p depends on the geometry and on the chemical nature of the boundaries. For small applied shear rates such that $\sigma \leq \sigma_y$, the slip velocity does not depend significantly on the packing fraction but is strongly influenced by the chemical nature of the walls. Indeed, v_s displays a nearly quadratic scaling, i.e. $p \simeq 2$ in the case of attractive/non-wetting surfaces, whereas $p = 1$ for repulsive and/or wetting walls (Seth *et al.*, 2008, 2012) [see Fig. 24(c)]. Both exponents have been successfully described at the scale of a single drop/grain/bubble by the elastohydrodynamic lubrication theory as the result of a balance between the bulk osmotic pressure and the viscous dissipation taking place in the thin lubrication layer that separates the squeezed particles from the wall (Meeker *et al.*, 2004a; Seth *et al.*, 2008). For larger shear-rates such that $\sigma \gtrsim \sigma_y$, the exponent p is geometry-dependent, as mentioned above. Although the slip velocity was first reported to be constant for experiments performed in cone-and-plate geometries on microgels and emulsions (Meeker *et al.*, 2004a,b), experiments performed in a plate-plate geometry reveals a linear scaling (Seth *et al.*, 2012), whereas emulsions sheared in a smooth Couette cell (Salmon *et al.*, 2003a) [see Fig. 24(b)] and microgels flowing in rough microchannels (Geraud *et al.*, 2013) display a quadratic increase with the slip stress (i.e. the stress at the wall). This strong dependence of v_s with the geometry remains to our knowledge unaccounted for and could be related to the stress heterogeneity and/or to the chemical nature of the boundaries. Note that in this range of large stresses, the influence of the packing fraction in the glassy state has not been explored.

However, in the liquid regime, i.e. for low or intermediate packing fractions, soft particles are no longer pressed against each other nor elastically deformed. The material neither presents a yield stress nor exhibits any solid-like feature, and the quadratic scaling of the slip velocity with the slip stress is replaced by a linear dependence, as reported in a Couette geometry (Salmon *et al.*, 2003a) [see Fig. 24(a)] in agreement with what is observed for liquid suspensions of rigid particles, discussed in the following paragraph. This last result strongly suggests that particle deformability does not play a significant role in the dilute regime.

The slip of yield stress fluids composed of rigid parti-

cles has been studied in the case of both Brownian and non-Brownian systems, but its understanding remains much sparser. For dense Brownian suspensions, slip is dominant at low shear-rates. Below $\dot{\gamma} \sim 1\text{--}5 \text{ s}^{-1}$, the steady-state stress displays a “kink” towards lower values in a qualitatively similar fashion to what is discussed in the previous paragraph. The slip velocity increases linearly with the slip stress while a sub-colloidal solvent layer, whose thickness is velocity independent is located at the wall (Ballesta *et al.*, 2012). In the case of non-brownian suspensions the stress-kink at low shear rate is observed for attractive particles but barely visible for suspensions which components display repulsive interactions. Regardless of the interparticle interactions, the slip velocity increases as a power-law of the slip stress: $v_s \propto \sigma^p$, with an exponent $p \simeq 1$ (Aral and Kalyon, 1994; Grenard *et al.*, 2014; Jana *et al.*, 1995; Soltani and Yilmazer, 1998; Yilmazer and Kalyon, 1989) [see Fig. 24(d)]. The thickness of the slip layer is a function of the particle size and decreases roughly linearly with increasing bulk packing fraction, as observed for various types of concentrated suspensions studied in different geometries (Kalyon, 2005) – although this result may not hold for polydisperse samples (Soltani and Yilmazer, 1998). The chemical properties of both the particle surfaces and of the boundary conditions seem to affect wall slip, but the quantitative impact on $v_s(\sigma)$ remains to be determined (van Kao *et al.*, 1975). Furthermore, the detailed mechanism for slip in non-Brownian suspensions remains unclear and may originate from various effects. Indeed, contrary to the case of dense assemblies of soft particles, inhomogeneous velocity fields and/or stress gradients induce particle migration from high shear rate regions towards low shear rate regions, leading to gradients in the local volume fraction. This phenomenon, which was first studied in pressure driven flows (Nott and Brady, 1994; Segré and Silberberg, 1961), also favors a depletion near the wall that fosters wall slip. Furthermore, particle migration is more likely to play a crucial role in the rheology of attractive gels whose packing fractions are low, easily initiating gradients in packing fraction once fluidized. Thus one can expect that wall slip in such attractive suspensions is strongly dependent on the shape of the velocity profiles and therefore on the shear geometry. This point certainly deserves more work in a near future.

To summarize, wall slip results from a subtle combination of the effects of the microstructure (rigid vs soft particles), of the chemical nature of the walls and of the geometry. The classical picture in terms of particle migration and wall depletion (Barnes, 1995), although relevant in more dilute suspensions, is challenged in jammed assemblies of deformable particles where lubrication effects becomes paramount. A full understanding of mixed cases and of the various scalings observed experimentally for slip velocities is yet to be reached.

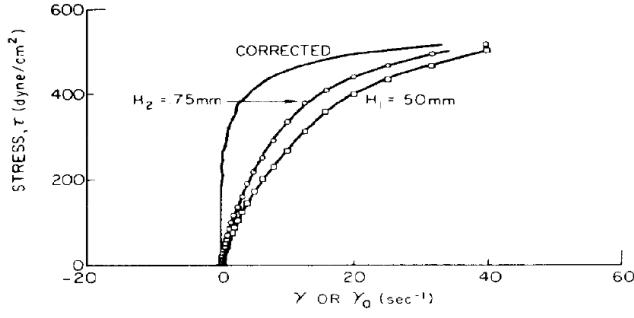


FIG. 25 Shear stress vs. shear rate for a dense emulsion ($\phi = 0.923$) measured in a plate-plate geometry with smooth boundary conditions for two different gap sizes (500 and 750 μm respectively). The stress vs. the shear rate computed from the method developed by Mooney and extended by Yoshimura and Prud'homme displays a yield stress, while this is not obvious from the raw measurements. Extracted from (Yoshimura and Prud'homme, 1988).

3. How to deal with wall slip in practice?

Two types of solutions have been proposed in the literature, either to quantify the effect of wall slip from the determination of the constitutive equation, or to eliminate it. An elegant solution due to Mooney (Mooney, 1931) and further extended by (Yoshimura and Prud'homme, 1988), (Kiljański, 1989) and (Wein and Tovchigrechko, 1992) consists of determining the relationship between the apparent shear stress and rate for gaps of different sizes. Combining at least two measurements and assuming that (i) the slip velocity is a function of stress only and (ii) slippage is the same at both the rotor and the stator, one can recover the constitutive relationship $\sigma(\dot{\gamma})$ corrected for wall slip (see Fig. 25). This method has been successfully applied to various yield stress fluids, including emulsions (Yoshimura and Prud'homme, 1988), microgels (Meeker *et al.*, 2004a), and dense suspensions (Hartman Kok *et al.*, 2004, 2002; Kalyon, 2005; Kalyon *et al.*, 1993; Yilmazer and Kalyon, 1989), while the two assumptions on which it relies have been verified by local measurements of slip velocities (Salmon *et al.*, 2003a). However, this time-consuming method only allows one to extract the true constitutive equation but does not modify wall slip.

To prevent wall slip one needs to modify the nature of the wall. The use of rough boundary conditions allows one to properly determine constitutive equations without wall slip (Vinogradov *et al.*, 1975). The roughness of the wall has been tuned from a few microns to hundreds of microns by using sandblasted surfaces (Buscall *et al.*, 1993), grooved surfaces (Magnin and Piau, 1990), serrated tools (Nickerson and Kornfield, 2005), or by gluing waterproof sand-paper (Seth *et al.*, 2008, 2012) or a monolayer of particles on the cell walls (Isa *et al.*, 2007). As a more exotic solution, some authors have even glued

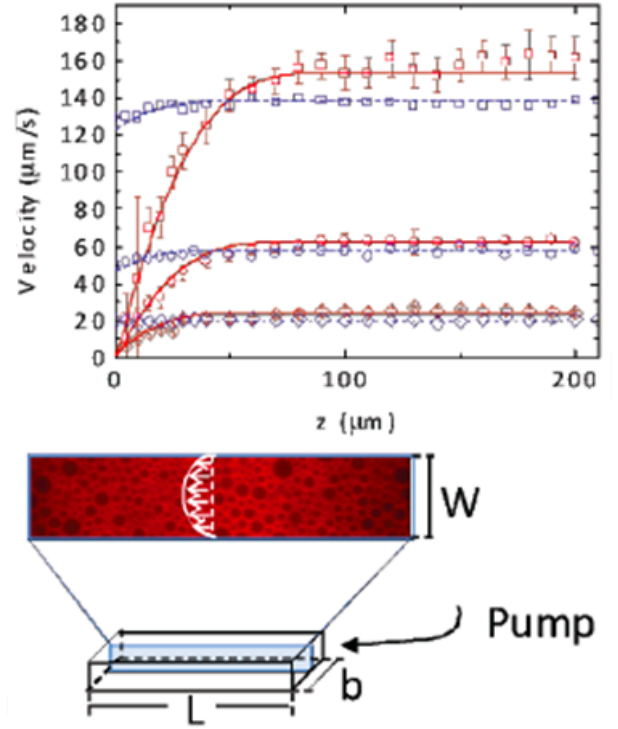


FIG. 26 Velocity profiles of a dense emulsion flowing in a rectangular microchannel (gap $w = 400 \mu\text{m}$). Images obtained by confocal microscopy. Velocity profiles in blue correspond to smooth boundary conditions treated with a piranha solution. The oil droplets experience wall slip. Velocity profiles in red correspond to smooth but silanized boundary conditions. The oil droplets stick to the surface, creating an effectively rough boundary condition. Flow rates: 0.2, 0.5 and 1.2 10^{-2} mL/min. Extracted from (Paredes, 2013).

the sample to the plate of the rheometer (Navickis and Bagley, 1983). The accepted paradigm is that the roughness of the surface should be comparable to the size of the microstructure, since a low roughness would not be efficient, while a very large roughness, including vane cup geometries, may trigger secondary flows (Ovarlez *et al.*, 2011). Nonetheless, to the best of our knowledge the available data remain empirical and there has not been any extensive study that would systematically explore the effect of the ratio between the roughness scale and the particle size.

Last but not least, the chemical nature and wetting properties of the walls can be also tuned to force the adhesion of the material even for smooth interfaces. This has been successfully achieved on colloidal silica gels at low deformations using hydrophobic boundaries (Walls *et al.*, 2003), and on aqueous microgels and oil-in-water emulsions using silicon boundaries (Seth *et al.*, 2008, 2012) and glass walls with different chemical treatment, as illustrated in Fig. 26. Wettability and chemical matching will certainly receive more attention in the upcoming

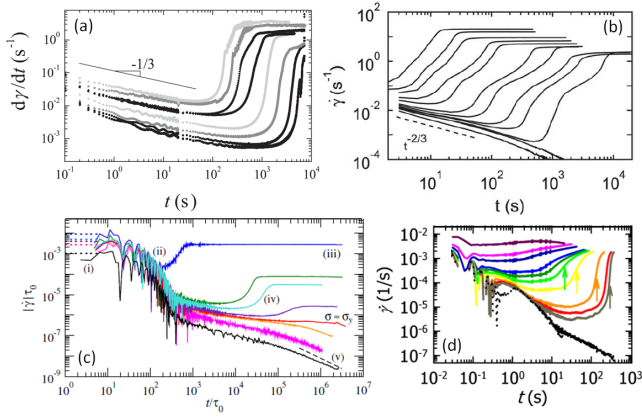


FIG. 27 Shear rate responses vs. time for creep experiments at different imposed shear stresses in various materials: (a) a polycrystalline hexagonal columnar phase, extracted from (Bauer *et al.*, 2006), (b) a carbopol microgel, extracted from (Divoux *et al.*, 2011a), (c) a core-shell PS-PNIPAM particle glass, extracted from (Siebenbürger *et al.*, 2012) and (d) a carbon black gel at 8 % wt. Extracted from (Sprakel *et al.*, 2011).

years.

D. “Hot topics”

In the following we focus on three questions that have recently attracted increasingly large interest. These “hot topics” aim at emphasizing current burning issues on the dynamics of yield stress fluids that should give rise to even more research effort in the coming years.

1. How do yield stress materials creep prior to fluidization?

A robust feature of creep experiments in yield stress fluids prior to fluidization is a power-law decrease of the shear-rate [see Fig. 27] that strongly resembles the “Andrade creep” reported for hard solids (da C. Andrade, 1910), which has been attributed to collective dislocation dynamics (Csikor *et al.*, 2011; Miguel *et al.*, 2008, 2002). Such power-law creep has also been reported for cellulose gels (Plazek, 1960) and more recently for various amorphous soft solids such as polycrystalline surfactant hexagonal phases (Bauer *et al.*, 2006), carbopol microgels (Divoux *et al.*, 2011a), core-shell p-NIPAM colloidal particles (Siebenbürger *et al.*, 2012) and thermo-reversible protein gels (Brenner *et al.*, 2013). Yet Andrade-like creep remains mostly unexplored in soft materials such as yield stress fluids. Local velocimetry suggests that the strain field is macroscopically homogeneous during this first regime (Divoux *et al.*, 2011a; Grenard *et al.*, 2014). Characterizations at finer, ideally microscopic, scales are in line in order to unveil the presence of plasticity or microcracks during the initial loading phase and to make a

clear link between the physical mechanisms at play in the creep of ordered solids and of disordered soft materials. New insights should also be gained by adapting recent numerical models to creep situations (Colombo and Gado, 2014; Fusco *et al.*, 2014). For stresses applied below the yield stress, the interplay between creep deformation and aging leads to long-time strain responses that are more complex than power-laws and that strongly depend on the sample age, as reported in laponite clay suspensions (Baldewa and Joshi, 2012; Negi and Osuji, 2010a) and in star glassy polymers (Christopoulou *et al.*, 2009). Such dynamics under the yield stress also deserve specific attention in future work.

2. How do yield stress materials behave in confined geometries?

a. Cooperative effects in simple yield stress fluids. Rheological properties and in particular constitutive equations have been discussed up to now in the context of “large” geometries, i.e. with gaps much larger than the granularity of the fluid microstructure, typically at least by two orders of magnitude. In this limit, the constitutive equation does not depend on the gap size. However, when determined in confined geometries, constitutive equations have been reported to depend on the exact value of the gap width (Clasen and McKinley, 2004; Davies and Stokes, 2008; Yan *et al.*, 2010). Accordingly, the local constitutive equation is modified in confined geometries and does not follow the Herschel-Bulkley model valid for large gaps [see Fig. 28], as clearly demonstrated in microchannels of small size on emulsions (Goyon *et al.*, 2010, 2008) and carbopol microgels (Geraud *et al.*, 2013). A nonlocal modeling that relies on the idea that the flow occurs through successive and partially correlated plastic events over a certain area quantified by a cooperativity length ξ has been invoked to describe the local velocity profiles (Bocquet *et al.*, 2009). The key ingredient is the number of plastic events per unit time (or fluidity) defined as $f = \dot{\gamma}/\sigma$, which is influenced both by the local contribution of the flow and by plastic events taking place at a distance smaller than ξ . This leads to the following simple differential equation for f :

$$\xi^2 \frac{\partial^2 f}{\partial x^2} + (f_{\text{bulk}} - f) = 0, \quad (16)$$

where x is the direction of the stress gradient and f_{bulk} denotes the “bulk” fluidity value i.e. the fluidity expected in a large-gap geometry where no nonlocal effects take place. The solution to this equation successfully accounts for flow profiles [see inset of Fig. 28] and dynamical arrest in confined geometries (Chaudhuri *et al.*, 2012b).

Recently the local fluidity has been related to the local shear rate fluctuations $\delta\dot{\gamma}(x)$ (Jop. *et al.*, 2012), which strongly suggests that the nonlocal rheology originates in the mechanical noise induced by the flow. It is also worth

mentioning that such a modification of the rheology due to confinement is not specific to yield stress materials since it affects for instance the flow of wormlike micellar systems in microchannels (Masselon *et al.*, 2008). For more details on the current issues raised by confinement of yield stress fluids we refer the reader to the recent review by (Mansard and Colin, 2012).

We shall only emphasize two open issues here. First, the question of whether similar cooperative effects may be at play during start-up flows stands should be addressed. Indeed, in a partially fluidized material undergoing a transient regime, the fluid at rest is also confined between the wall and the flowing band. This point, which raises the question of the –possibly slow– dynamics of cooperative effects might be related to the diverging duration of transient regimes discussed below in the next “hot topic.” Second, long-range effects have also been reported in granular materials (Nichol and van Hecke, 2012; Nichol *et al.*, 2010; Reddy *et al.*, 2011) where the solidlike behavior of grains located next to a flowing band vanishes and gives way to fluidlike response even far away from the main flow. Whether this effect is simply due to an alteration of the force network or whether it is related to the aforementioned nonlocal rheology remains to be investigated.

b. Shear-induced structuration of attractive yield stress fluids. Another striking effect of confinement on yield stress fluids is the spectacular shear-induced structuration observed in the case of attractive particulate systems at moderate shear rates, typically $0.1 < \dot{\gamma} < 10 \text{ s}^{-1}$. Examples include colloid polymer mixtures (DeGroot *et al.*, 1994), flocculated magnetic suspensions (Navarrete *et al.*, 1996), carbon nanotubes (Lin-Gibson *et al.*, 2004), attractive emulsions (Montesi *et al.*, 2004), carbon black and alumina dispersions (Grenard *et al.*, 2011; Negi and Osuji, 2009; Osuji *et al.*, 2008), and microfibrillated cellulose (Karppinen *et al.*, 2012) [see Fig. 29]. In all these thixotropic yield stress fluids, the microstructure was shown to rearrange into a striped pattern of log-rolling flocs aligned along the vorticity direction, either indirectly through light scattering measurements (DeGroot *et al.*, 1994) or through scanning electron microscopy (Navarrete *et al.*, 1996) and optical microscopy (Grenard *et al.*, 2011; Karppinen *et al.*, 2012; Lin-Gibson *et al.*, 2004; Montesi *et al.*, 2004; Negi and Osuji, 2009; Osuji *et al.*, 2008). In the fully-developed state of the shear-induced pattern, the system completely separates into concentrated shear-induced flocs and regions of pure solvent, so that any global rheological measurement on such a macroscopically phase-separated system becomes hard to interpret.

In some of the above attractive systems, shear-induced structuration has been linked to the emergence of negative normal stresses (Lin-Gibson *et al.*, 2004; Montesi

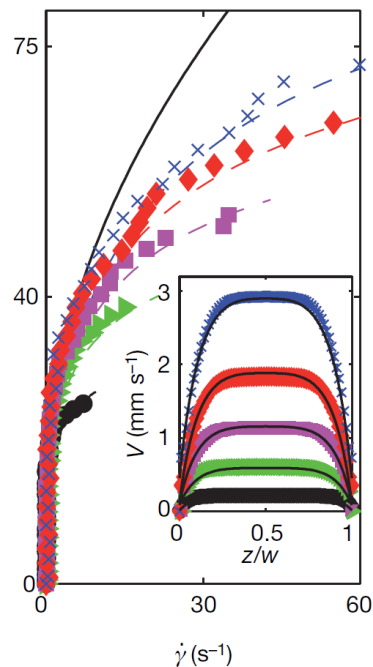


FIG. 28 Global and local flow curves (black solid line and color symbols respectively) for a dense emulsion ($\phi = 0.75$ and 20% polydispersity). Global data are obtained in a wide gap Taylor-Couette cell, while local flow curves are deduced from velocity profiles measured in a $w = 250 \mu\text{m}$ thick microchannel with rough surfaces, for various pressure drops ranging from 300 to 900 mbar (inset). No overlap of the local flow curves is observed. Dashed lines are predictions for the local flow curves at the given pressure drop, as obtained from the nonlocal rheological model [see Eq. 16] with a flow cooperativity length $\xi = 22.3 \mu\text{m}$. Inset: solid lines are the velocity profiles predicted by the nonlocal rheological model. Extracted from (Goyon *et al.*, 2008).

et al., 2004; Negi and Osuji, 2009) and it was proposed to interpret vorticity alignment as the consequence of an elastic instability of the elastic flocs, akin to a Weissenberg effect that would occur locally within individual flocs (Lin-Gibson *et al.*, 2004; Montesi *et al.*, 2004). However clear experimental evidence for such an interpretation and a detailed theory that would prove the link between an elastic instability and shear-induced structuration are still lacking.

Moreover, shear-induced structuration only occurs within a given range of shear rates. On the one hand, for very low shear, wall slip may become predominant and generally prevents the system from being sheared in the bulk (see also Sect. IV.C) so that it remains in a homogeneous solidlike state. On the other hand, structuration does not occur above some critical shear rate, most probably due to the predominance of viscous forces and particle resuspension by shear. Coming up with a theory that would provide a complete physical mechanism for the present shear-induced pattern formation and that could predict both their characteristics and the shear rate lim-

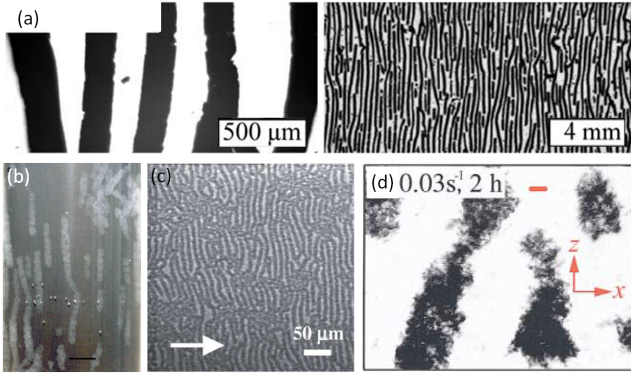


FIG. 29 Shear-induced patterns observed in various yield stress fluids under shear in confined geometries. (a) Carbon black gel under simple shear with a gap thickness of $173 \mu\text{m}$ as seen with optical microscopy with large and low magnifications (left and right respectively). Extracted from (Grenard *et al.*, 2011). (b) Suspension of micro fibrillated cellulose at 0.1% wt. after shearing 10 min at 0.5 s^{-1} in a Taylor Couette cell. Extracted from (Karppinen *et al.*, 2012). (c) Emulsions under simple shear for a gap thickness of $12 \mu\text{m}$. The arrow indicates the direction of shear. Extracted from (Montesi *et al.*, 2004). (d) Optical micrograph of a quiescent semidilute non-Brownian colloidal nanotube suspension at 0.5% wt. The red scale bar is $10 \mu\text{m}$ and the gap thickness is $50 \mu\text{m}$ (Lin-Gibson *et al.*, 2004).

its where they appear is an important future challenge. Indeed, this striking effect of confinement not only affects the interpretation of rheological measurements but may also be of prime importance in applications involving confined flows of attractive particulate systems. Finally, one may also wonder whether the strong cooperative effects observed here in attractive, thixotropic yield stress materials are related in any way to those mentioned in the previous paragraph for simple yield stress fluids.

3. What is the origin and scaling of the yielding timescales?

So far, emphasis has been put on the steady state achieved by yield stress materials under a given shear rate or shear stress. However it is quite obvious that such a steady state is not reached instantaneously and that transient regimes, e.g. from solidlike behavior at rest to liquidlike behavior above yielding, convey tremendous physical information on the yielding process.

In particular it can be expected that upon approaching the yield stress the time needed to reach a flowing steady state can grow longer and longer, possibly pointing to a divergence of some characteristic timescale. If this timescale can be reliably estimated as a function of the various control parameters (applied stress or shear rate, packing fraction, temperature), then the question is whether physically-relevant information can be inferred on the yielding transition from such scalings. The aim of

this “hot topic” is to review recent work focusing on the timescales associated with yielding, to raise open questions and draw future research directions on time dependence in yielding.

a. Power-law scalings of the fluidization time and transient shear banding. It has been reported that transient regimes may become surprisingly long-lived in the vicinity of the yield stress. As mentioned above, that the dynamics becomes increasingly slow upon approaching the yield stress is not surprising and has been reported in a large number of papers (Aral and Kalyon, 1994; Caton and Baravian, 2008; Gopalakrishnan and Zukoski, 2007; Rogers *et al.*, 2008). More quantitative and local insights have been gained from recent velocimetry experiments during shear start-up and creep experiments on simple yield stress fluids, namely carbopol microgels (Divoux *et al.*, 2011b, 2010, 2012) and, to a lesser extent, emulsions (Bécu *et al.*, 2005; Perge, 2014). These experiments have revealed that the expected homogeneous velocity profiles are reached after a transient regime that involves shear banded velocity profiles [see Fig. 30]. In carbopol microgels, the fluidization time τ_f , i.e. the duration of the transient shear banding regime, was shown to follow power-law scalings $\tau_f \sim A/\dot{\gamma}^\alpha$ and $\tau_f \sim B/(\sigma - \sigma_y)^\beta$ with $\alpha \simeq 2-3$ and $\beta \simeq 4-6$ under imposed shear rate and under imposed shear stress respectively (Divoux *et al.*, 2011a, 2010, 2012). In all cases, the final homogeneous flow is consistent with the global steady-state rheology indicating simple yield stress behavior [see Fig. 30(e)].

Interestingly, these scalings naturally lead to a constitutive equation $\sigma(\dot{\gamma})$ that coincides with the Herschel-Bulkley equation [see Eq. (3)] in which the phenomenological exponent n appears as the ratio of the above-mentioned exponents $n = \alpha/\beta \simeq 1/2$ (Divoux *et al.*, 2011a): power-law scalings of τ_f provide a direct link between the transient and the steady-state behaviors of a simple yield stress material, and have recently been interpreted in terms of a critical-like phenomenon (Chaudhuri and Horbach, 2013; Divoux *et al.*, 2012).

It is important to clearly distinguish the transient shear banding phenomenology from the time-dependent behavior of thixotropic materials. Here, rather than a competition between aging and shear rejuvenation, the transition from a solid-like state to a liquid-like state seems to involve plastic events and damage accumulation in a way that resembles hard solids. Indeed, one can observe that the flowing band slowly “erodes” the material at rest before the whole material experiences a rather sudden fluidization. Such an induction phase suggests that erosion by the fluidized band somehow fragilizes the bulk arrested microgel, bringing it to a critical state before complete sudden fluidization occurs. Such a critical state could be analogous to the one reached right before its collapse by a colloidal gel experiencing “delayed

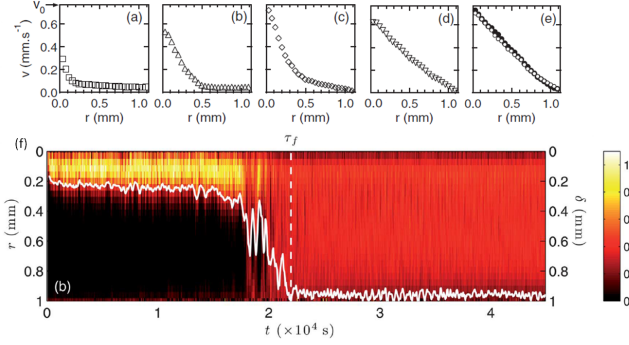


FIG. 30 Transient shear banding in a carbopol microgel in the Taylor-Couette geometry. (a)–(e) Velocity profiles $v(r)$, where r is the distance to the rotor, in a rough geometry at different times during the stress relaxation for an applied shear rate of 0.7 s^{-1} . The arrow indicates the rotor velocity v_0 . Extracted from (Divoux *et al.*, 2010). (f) Spatiotemporal diagram of the local shear rate $\dot{\gamma}(r, t)$ in a smooth geometry for an applied shear rate of 0.5 s^{-1} . The white line shows the position $\delta(t)$ of the interface between the fluidized band and the solid-like region. The vertical dashed line indicates the fluidization time τ_f , i.e. the time at which the shear rate field becomes homogeneous. Extracted from (Divoux *et al.*, 2012).

sedimentation” (Barlett *et al.*, 2012; Buscall *et al.*, 2009; Teece *et al.*, 2011). However more experiments that provide access to the structure of the band at rest will be needed in the future to confirm such a picture. Moreover, a systematic comparison with recent molecular dynamic simulations of disordered systems could help to bridge the gap between yield stress fluids and amorphous solids (Fusco *et al.*, 2014).

From a theoretical point of view, a general criterion for the formation of transient shear bands has been proposed by (Moorcroft *et al.*, 2011; Moorcroft and Fielding, 2013) that provides a connection with either the stress overshoot under an imposed shear rate or the delayed yielding under creep in yield stress fluids or viscoelastic fluids. In this approach the power-law scaling for the fluidization time under creep is recovered, but with a smaller exponent $\beta \simeq 1$ (Moorcroft and Fielding, 2013). Another recent promising work consists in a structural model of colloidal aggregates that incorporates viscoelasticity (Illa *et al.*, 2013; Lehtinen *et al.*, 2013; Mohtaschemi *et al.*, 2014). Such a phenomenological model recovers power-law scalings but only predicts trivial exponents $\alpha = \beta = 1$ and thus fails to capture the link between both transients and the steady-state rheology observed in microgels. Theories at a more microscopic level, such as the Shear Transformation Zone (STZ) theory, may shed deeper light on the physical processes at play.

b. Exponential scalings: activated processes and brittle-like failure. Whereas rather few papers have focused on transient fluidization under an applied shear rate, ex-

periments under a constant external shear stress, i.e. *creep* experiments, have unraveled long-lived transients in numerous yield stress fluids, including attractive gels such as carbon black gels (Gibaud *et al.*, 2010; Grenard *et al.*, 2014), coated silica particles (Gopalakrishnan and Zukoski, 2007; Sprakel *et al.*, 2011) and colloidal glasses (Siebenbürger *et al.*, 2012). The creep response typically displays three regimes: (i) the Andrade-like primary creep regime already discussed above in the first “hot topic”, followed by (ii) a gradual acceleration up to an abrupt fluidization of the material that later (iii) reaches a steady state [see Fig. 27]. The time at which the strain rate increases by several orders of magnitude defines a fluidization time τ_f which coincides with the establishment of homogeneous velocity profiles (Gibaud *et al.*, 2010; Grenard *et al.*, 2014). Interestingly, in attractive colloidal systems, τ_f generally decreases exponentially with the applied shear stress (Gibaud *et al.*, 2010; Gopalakrishnan and Zukoski, 2007; Grenard *et al.*, 2014; Sprakel *et al.*, 2011). Such a scaling $\tau_f \sim \exp(-\sigma/\sigma_0)$ involves a characteristic stress σ_0 which has been interpreted and modeled in the framework of bond breaking through thermally activated processes (Gopalakrishnan and Zukoski, 2007; Lindström *et al.*, 2012).

Alternative exponential scalings, such as the Griffith-like scalings $\tau_f \sim e^{(\sigma_0/\sigma)^p}$ with $p = 1, 2$ or 4 (Griffith, 1921; Lawn, 1993; Pomeau, 1992; Vanel *et al.*, 2009), have been proposed in the context of yield stress fluids (Caton and Baravian, 2008) and of transient networks (Mora, 2011; Tabuteau *et al.*, 2009). Such scalings hint to fracture-like dynamics, although it may be difficult to discriminate between various exponential –or even power-law– scalings due to the experimentally limited range of accessible shear stresses. This raises the question of the “brittleness” of yield stress fluids: while the physics of yielding in concentrated, jammed assemblies of soft particles such as microgels or emulsions appear to rely on (microscale) plasticity associated with (macroscale) shear banding, early studies based on direct visualization of the sample edges have shown some colloidal systems, e.g. Laponite suspensions (Magnin and Piau, 1990; Pignon *et al.*, 1996) and concentrated suspensions (Aral and Kalyon, 1994; Persello *et al.*, 1994), to be prone to fracture-like behaviour. Revisiting these pioneering works with modern temporally and spatially resolved techniques appears to be a necessary step to classify such strain localization in terms of fracture, wall slip or shear banding and to sort out the possible effects of the experimental geometry on the flow dynamics.

c. Dynamics induced by wall slip in transient and steady-state flows. In Sect. IV.C we have considered wall slip only through its effect on steady-state flow curves and velocity profiles. However, it has long been known, most prominently in the context of polymers, that wall slip often

goes along with instability and complex time-dependence (Denn, 2008, 2001; Graham, 1995). In light of the above discussion on fluidization timescales, it also seems natural to ask whether slippage at the walls shows interesting variations, both during transient regimes and at steady state. Surprisingly only a handful of papers have dealt with the dynamics of wall slip in yield stress fluids. Various start-up experiments in smooth geometries, e.g. on emulsions (Bécu *et al.*, 2005), carbopol microgels (Divoux *et al.*, 2010) and laponite clay suspensions (Gibaud *et al.*, 2009), have reported slip velocities that are strongly correlated to the fluidization dynamics and to the temporal evolution of the shear stress as well as stick-slip oscillations in the steady state (Divoux *et al.*, 2011a; Ianni *et al.*, 2008; Pignon *et al.*, 1996). Very recent unsteady experiments in pipe flows report similar coupling between the solid–fluid transition and wall slip, including strongly fluctuating behaviors (Poumaere *et al.*, 2014).

Fluctuations of slip velocities have also been reported in a Langmuir monolayer with a yield stress but were not correlated to the global stress response (Majumdar *et al.*, 2011). To open the discussion we wish to emphasize the work by (Gibaud *et al.*, 2008, 2009) on laponite suspensions which illustrates that boundary conditions not only strongly affect the transient fluidization process but may also lead to totally different steady states, in this case shear banded flows vs homogeneous flows. Recent numerical results also suggest that the internal stress distribution prior to shear start-up affects the steady state (Cheddadi *et al.*, 2012). These results clearly question the existence of a well-defined, unique flow curve for a yield stress fluid and reveal the influence of both the boundary conditions and the initial conditions on the steady state reached after yielding.

In order to summarize the three above-mentioned “hot topics,” we close this section by listing a few open questions that remain on the dynamics of yield stress materials:

- Is there any plasticity occurring during Andrade-like creep? If yes, where is it localized?
- How does nonlocality due to confinement sets in during transient material response?
- What is the physical mechanism responsible for shear-induced vorticity alignment in confined attractive yield stress fluids?
- What are the differences (if any) between the material microstructure in the transient shear band and in the rest of the sample?
- What is the nature of the wall-fluid interactions that drive slip phenomena and how can they affect bulk flow?

V. TOWARDS A CONTINUUM TREATMENT OF YIELD STRESS MATERIALS

A. Rheology

1. Properly invariant 3-D models

The focus thus far has been on the response of yield stress materials in a shearing deformation, for which a one-dimensional mechanical constitutive equation the Bingham, Herschel-Bulkley, or Casson model, for example is adequate to describe the post-yield deformation and flow when combined with the momentum balance. Many applications involve flow in more complex geometries, however, so a properly invariant three-dimensional constitutive equation is required. Invariant three-dimensional constitutive equations for the Bingham fluid were introduced by (Hohenemser and Prager, 1932; Oldroyd, 1947a; Prager, 1961). Oldroyd’s formulation assumes that the material is a linearly elastic solid at stresses below the yield criterion, where the yield surface is defined by a von Mises criterion. The full constitutive equation is then as follows:

$$\sigma = \left[\eta_p + \frac{\sigma_y}{\sqrt{\frac{1}{2}\Pi_\Delta}} \right] \Delta, \quad \frac{1}{2}\Pi_\sigma \geq \sigma_y^2 \quad (17)$$

$$\sigma = G\gamma, \quad \frac{1}{2}\Pi_\sigma < \sigma_y^2 \quad (18)$$

Here, $\Pi_A \equiv A : A$ is the second invariant of the tensor A , $\Delta \equiv \nabla \mathbf{v} + \nabla \mathbf{v}^T$ is the rate of deformation tensor, and γ is the strain tensor; $\sqrt{\frac{1}{2}\Pi_\Delta}$ reduces to the shear rate in a simple shear flow. The applicability of the von Mises criterion has been established for a variety of yield stress materials by (Shaukat *et al.*, 2012a), as shown in Fig. 31, and by (Ovarlez *et al.*, 2010).

Equation (18) is rarely employed in applications; it is conventional to assume that the modulus G is infinite, in which case there can be no deformation. The condition in the unyielded region then becomes

$$G \rightarrow \infty : \Delta = 0, \quad \frac{1}{2}\Pi_\sigma < \sigma_y^2. \quad (19)$$

The equivalent three-dimensional generalizations of the Herschel-Bulkley and Casson equations are straightforward. For the Herschel-Bulkley fluid, which is commonly used, the constant plastic viscosity η_p in Eq. (17) is simply replaced by a power-law, $K \left(\frac{1}{2}\Pi_\Delta \right)^{n-1}$. In fact, it is well established that some yield stress fluids exhibit non-linear elasticity prior to yielding; foams exhibit normal stresses that are qualitatively different from those described by Eq. (18) but can be described by the Mooney-Rivlin elastic equation, for example (Habibi *et al.*, 2015). Apparent viscoelasticity is also observed prior to yielding, as in colloidal “red mud” suspensions (Denn and Bonn,

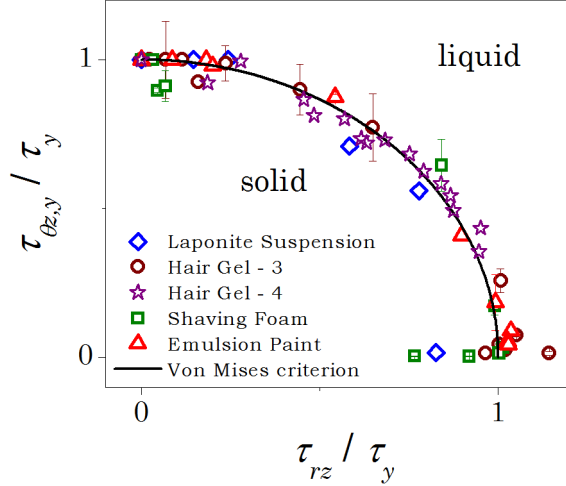


FIG. 31 Validation of the von Mises criterion for a variety of yield-stress materials subjected to combined rotation and compression between parallel plates. Extracted from (Shaukat *et al.*, 2012a)

2011). Some yield stress liquids appear to be viscoelastic following yielding, and a properly invariant generalization of the Bingham model to account for viscoelasticity was first introduced by White (White, 1979). We will return to the issue of viscoelasticity subsequently.

2. Extensional flow

Rheometry is a study of stresses in flow fields that are well defined and controllable, so no constitutive equations are required in order to extract the stresses. Most rheometry is done in shear, but uniform uniaxial extension is also widely practiced, and the *elongational viscosity* η_E is defined, in analogy to the shear viscosity, as the ratio of the tensile stress in uniform uniaxial extension to the extension rate. For Newtonian fluids, simple geometrical arguments show that the ratio of elongational to shear viscosity should equal 3; the ratio is often referred to as the Trouton ratio Tr . Shear and elongational viscosities can be very different in complex fluids, however, and this difference may lead to a complex fluid response that constitutive laws derived solely from shear data are unable to describe. For instance, there is a large body of work on dilute polymer solutions that shows that the Trouton ratio can be as large as 10^5 (Amarouchene *et al.*, 2001; Anna *et al.*, 2001). There has been little attention in the literature to the elongational flow of yield-stress fluids. Uniform uniaxial extension for an incompressible fluid is defined in cylindrical coordinates by:

$$v_z = \dot{\gamma}_E z, \quad v_r = -\frac{1}{2}\dot{\gamma}_E r, \quad v_\theta = 0 \quad (20)$$

The total axial stress is given $-p + \tau_{zz}$, where p is the isotropic pressure and τ_{zz} is the axial (stretch) component of the extra stress. The isotropic pressure is determined by balancing the radial stress against atmospheric pressure at the filament radius R , leading ultimately to the result

$$\sigma_{zz} = \tau_{zz} - \frac{1}{2}(\tau_{rr} + \tau_{\theta\theta}) - \frac{\gamma}{R} \quad (21)$$

where γ is the interfacial tension. It follows from Eq. 17 that

$$\begin{aligned} \tau_{zz} &= \frac{2\sigma_y}{\sqrt{3}} + 2\eta_p \dot{\gamma}_E \\ \tau_{rr} = \tau_{\theta\theta} &= -\frac{\sigma_y}{\sqrt{3}} - \eta_p \dot{\gamma}_E \end{aligned} \quad (22)$$

The deformation-dependent part of the tensile stress can then be calculated as:

$$\tau_{zz} - \frac{1}{2}(\tau_{rr} + \tau_{\theta\theta}) = \sqrt{3}\sigma_y + 3\eta_p \dot{\gamma}_E \quad (23)$$

This relation generalizes in a straightforward way to the Herschel-Bulkley fluid. Taking the limit $\dot{\gamma}_E \rightarrow 0$, the material yields in the absence of surface tension effects when the tensile stress equals $\sqrt{3}\sigma_y$.

For calculating the Trouton ratio, we compare the shear viscosity η_s to the elongational viscosity η_E at equal values of $\sqrt{\frac{1}{2}\Delta} : \Delta$, so we set $\dot{\gamma} = \sqrt{3}\dot{\gamma}_E$; we then find

$$\eta_s = \frac{\tau_y}{\sqrt{3}\dot{\gamma}_E} + \eta_p, \quad \eta_E = \frac{\sqrt{3}\tau_y}{\dot{\gamma}_E} + 3\eta_p \quad (24)$$

from which it immediately follows that $Tr = \frac{\eta_E}{\eta_s} = 3$. The important conclusion here is that the yield stress does not appear explicitly in the result for the Trouton ratio, which is identical to that for any generalized Newtonian fluid.

We now consider the actual measurement of the elongational yield stress and viscosity. In practice it is not straightforward to have a steady uniform uniaxial elongational (= stretching) flow in the laboratory, so most of the experiments are done in unsteady situations. The measurement is usually done by looking at the thinning rate of fluid filaments in either a filament thinning (Chellamuthu *et al.*, 2009) or a drop detachment experiment (Amarouchene *et al.*, 2001); from the thinning rate one directly obtains the strain rate, and one then has to evaluate the stresses in the filament. For Newtonian fluids the connection between the thinning dynamics of the neck and the fluid properties is well established (Eggers, 1997). For complex fluids, a number of studies have been carried out, and for instance for the dilute polymer case, a direct connection between the shear and elongation properties has been established, validating constitutive equations for dilute polymer solutions (Wagner *et al.*, 2005).

For yield stress materials, on the other hand, the situation appears to be more complicated. There are only a few experimental studies of the elongational yield stress and the flow behavior beyond the yield stress; i.e., the elongational viscosity. As for the former, very recently a detailed study was done by (Martinie *et al.*, 2013), who conclude that for a number of investigated materials, the ratio of this elongational yield stress to the shear yield stress is $\sqrt{3}$, in agreement with the Bingham and Herschel-Bulkley predictions and the von Mises criterion. They also show that this holds for both thixotropic and simple yield stress materials, and conclude that the three dimensional Herschel-Bulkley model can consequently be used to calculate the behavior of yield stress materials in complex flow situations. The few existing measurements of the post-yield elongational viscosity cast some doubt on this strong statement, however. Several authors have, in agreement with the ideas of Martinie *et al.*, postulated the same rheological response for the extensional flow as the thinning behavior in shear flow. (Balmforth *et al.*, 2010a,b; Doshi and Basaran, 2004; German and Bertola, 2010; Renardy and Renardy, 2004) and (Yildirim and Basaran, 2006). Although some experiments seem to concur with the idea that shear thinning implies elongational thinning (Huisman *et al.*, 2012), recent experiments in which the yield stress was varied over a large range suggest that the post-yield elongational viscosity is constant, while the shear rheology is strongly thinning (Aytouna *et al.*, 2013).

It is known that particle segregation may occur in the stretching of thin filaments of suspensions (Denn and Morris, 2014). (Luvet *et al.*, 2014) recently suggested that the observed discrepancies may be caused by subtle differences between filament thinning and drop detachment experiments due in part to non-local rheology effects similar to those observed in the stretching experiments for suspensions and in microchannels (Goyon *et al.*, 2008).

3. Normal Stresses

One common manifestation of nonlinearity is the presence of non-zero normal stress differences in steady shear, whereby a deformation in one plane causes a stress in the transverse direction (the Poynting effect in solid mechanics). If we define the flow direction as “1”, the transverse direction in which there is a velocity gradient as “2”, and the neutral or vorticity direction as “3”, then two normal stress differences can be defined for an incompressible material: $N_1 = \sigma_{11} - \sigma_{22}$ (the first normal stress difference) and $N_2 = \sigma_{22} - \sigma_{33}$ (the second normal stress difference). In flexible polymeric systems, where most rheological studies have been carried out, N_1 is positive and much larger in magnitude than N_2 , which is negative. Data are far more limited in suspensions, but it is gen-

erally accepted that N_2 is negative and larger than N_1 ; there is no general agreement regarding the algebraic sign of N_1 (Denn and Morris, 2014). The signs and relative magnitudes of the normal stress differences for polymers are the driving force for the Weissenberg effect, whereby the polymer climbs up a rotating rod; conversely, suspensions exhibit a negative Weissenberg effect because of the very different normal stress behavior. Measurements for particulate systems are frequently made for flow between rotating parallel plates, where the normal force on the plate gives the difference $N_1 - N_2$; N_1 is obtained from the normal force from shearing in a cone-and-plate geometry, which has limited applicability in a particulate system.

The invariant three-dimensional versions of the Bingham, Herschel-Bulkley, and related equations defined by Eq. (17) and the accompanying text predict strictly zero normal stress differences in shear flow. Early work by (Frölich and Sack, 1946) on dilute dispersions of elastic spheres in a Newtonian liquid and by (Oldroyd, 1953) on dilute emulsions led to linear equations that, when made properly invariant, may exhibit positive first normal stresses and are in fact identical to the “Oldroyd-B” equation often used to describe the rheology of dilute polymer solutions, so normal stresses are to be expected. (Schowalter *et al.*, 1968) showed theoretically that drop distortion in flowing foams and emulsions leads to finite normal-stress functions for which analytical forms can be obtained as functions of the shear rate, drop (bubble) size and volume fraction of the dispersed phase. Viscoelastic models for yield-stress fluids discussed subsequently do predict non-zero normal stress differences in simple shear.

There are very limited data on normal stresses in yield-stress fluids. In a comprehensive review, (Kraynik, 1988) describes the dominant normal stress in steady shear flow of foams and emulsions to be large and positive, and he concludes that the signs and relative magnitudes of the normal stress functions are in accord with those for polymer melts and solutions, i.e., N_1 is positive, with an absolute value that is larger than N_2 , which is negative (Edwards, 1987). This is also what is found in simulations of concentrated emulsions (Loewenberg and Hinch, 1996), where both the normal stress and shear thinning were attributed to the alignment of drops in the flow direction. The same conclusion is reached by Larson for the normal stresses as functions of the deformation measured, e.g., in oscillation or through stress-strain curves (Larson, 1999). However, as also emphasized by Larson, experiments are scarce. Habbibi *et al.* (JOR, submitted) have recently reported positive N_1 and negative N_2 for a foam and an emulsion following yielding, with N_1 and N_2 of comparable magnitude.

N_1 has been reported to be positive in steady shear flow of Carbopol (Ahonguio *et al.*, 2014) and for foams in large-amplitude oscillatory experiments (Labiaussie *et al.*,

2007). No clear consensus has yet emerged even on the sign of the normal stress differences, however, there are for instance reports of a negative first normal stress difference in flowing “attractive” emulsions in which the droplets attract each other (Montesi *et al.*, 2004).

The experimental procedure is very important. (Labiausse *et al.*, 2007) point out that trapped stresses or strains due to the loading of the sample in the rheometer can add an offset to the normal stress difference measured in the transverse direction (N_1 or $N_1 - N_2$, depending on the geometry). Such phenomena have indeed been encountered in previous unsuccessful attempts to measure the normal stress response of foams reported in the literature. Labiausse *et al.* argue that the problems are less serious than in their oscillatory shear experiments and conclude that N_1 for their foam is positive (Labiausse *et al.*, 2007). Free-surface curvature effects have been cited as the cause of negative normal stresses in a foam and emulsion at low shear rates by (Habibi *et al.*, 2015), who subtracted these values from the measured normal stresses in order to obtain the rheological data. Overall, there is still a paucity of normal stress data for yield stress materials in flow. It is clear from the available data, however, that the standard constitutive equations are lacking an essential non-linear coupling that may be important in flows other than those used for rheometry.

B. Fluid Mechanics

1. Analytical approaches

Flows of Bingham fluids are frequently characterized by the dimensionless Bingham number, $Bn = \sigma_y R / \eta_p V$, where R and V are a characteristic length and velocity, respectively. (For the Herschel-Bulkley fluid the equivalent dimensionless group is sometimes called the Oldroyd number, $Od = \sigma_y R^n / K V^n$, which reduces to the Bingham number for $n = 1$.) σ_y characterizes the stress at low deformation rates, just beyond yielding, while $\eta_p V / R$ characterizes the viscous stress at very high rates, where the yield stress is irrelevant; hence, this dimensionless group has obvious applicability only in the limits of zero or infinity. It is important to keep in mind that this type of scaling is the sole determinant of the flow only when there is a single characteristic length scale.

Yield-stress fluids tend to be highly viscous when flowing, and turbulence is rarely encountered. The body of knowledge of non-turbulent flows in classical fluid mechanics is built around a small number of exact solutions to the Navier-Stokes and (inertialess) Stokes equations for incompressible Newtonian fluids, from which the insight into approximations such as boundary layer theory and the lubrication approximation is derived. The early insight into the flow of viscoelastic fluids was gained by considering perturbations to known solutions for New-

tonian fluids. There is no body of exact non-trivial solutions for yield-stress fluids, nor is there a straightforward way to incorporate perturbations about Newtonian fluid behavior. The location of the yield surface is unknown in general flows, save a single example by (Burgos *et al.*, 1999). (Oldroyd, 1947b) introduced a plastic boundary-layer approximation for yield-stress fluids, and this idea was implemented for flow about a sphere by (Beris *et al.*, 1985). Lubrication analyses are contained, for example, in (Covey and Stanmore, 1981) and (Dai and Bird, 1981), but it is straightforward to demonstrate from strictly kinematical arguments that continuity of the velocity and stress at the yield surface cannot be satisfied within the context of conventional asymptotic approaches (Lipscomb and Denn, 1984). In Oldroyd’s analysis (Oldroyd, 1947b; Prager, 1961), for example, matching is carried out only to order $Bn^{-2/3}$, and such methods must be used with delicacy. Asymptotic methods typically lead to “pseudo-plugs” that do not rigorously satisfy all matching or yield conditions, a concept that is implicit in Oldroyd’s work but introduced formally in (Walton and Bittleston, 1991) and (Balmforth and Craster, 1999). The issue of asymptotics is addressed in recent work by (Putz *et al.*, 2009) and a review by (Balmforth *et al.*, 2014).

2. Computational issues

There is now an extensive numerical literature on the flow of yield-stress fluids. The most common approach is to remove the discontinuity in Eqs. (17) and (18) by regularization, which transforms the computational problem into a conventional one for a purely viscous liquid, and then to vary the regularization parameter to try to obtain convergence to the solution of the discontinuous problem. Three regularizations are in common use for the Bingham model, with the obvious modification for the Herschel-Bulkley model.

(i) Bercovier and Engelman (Bercovier and Engelman, 1980):

$$\sigma = \left[\eta_p + \frac{\sigma_y}{\sqrt{\frac{1}{2}\Pi_\Delta + \epsilon^2}} \right] \Delta \quad (25)$$

(ii) Two-viscosity (Gartling and Phan-Thien, 1984; Lipscomb and Denn, 1984):

$$\sigma = \frac{\eta_p}{\epsilon} \Delta, \quad \sqrt{\frac{1}{2}\Pi_\Delta} < \epsilon \sigma_y / \eta_p$$

$$\sigma = \left[\eta_p + \frac{(1 - \epsilon)\sigma_y}{\sqrt{\frac{1}{2}\Pi_\Delta}} \right] \Delta, \quad \sqrt{\frac{1}{2}\Pi_\Delta} \geq \epsilon \sigma_y / \eta_p \quad (26)$$

(iii) Papanastasiou (Papanastasiou, 1987):

$$\sigma = \left[\eta_p + \frac{\sigma_y \{1 - \exp(-\frac{1}{2}\Pi_\Delta/\epsilon)\}}{\sqrt{\frac{1}{2}\Pi_\Delta}} \right] \Delta \quad (27)$$

The Bingham model should be approached in all three formulations in the limit as $\epsilon \rightarrow 0$. There are no universal convergence proofs, and numerical issues usually become important in numerical solutions before ϵ can become sufficiently small to establish convergence of the stress field and obtain precise yield surfaces. Thus, whenever regularization is employed there must be a small amount of flow (apparent creep) in what is interpreted as the unyielded region, since ϵ must always be non-zero; i.e., the regularization method essentially computes pseudo-plugs. Convergence of the smooth regularizations is discussed in (Liu *et al.*, 2002) and (Frigaard and Nouar, 2005). The regularization approach requires no modification to a computational fluid dynamics (CFD) code that can employ a purely viscous non-Newtonian constitutive equation, and regularization is incorporated into commercial CFD codes.

An alternative approach to computation is based on the fact that the velocity field of a yield stress fluid in creeping (inertialess) flow satisfies a variational inequality, as first shown by (Oldroyd, 1947a). This notion was subsequently developed into a computational scheme that can be quite effective for flow in ducts of various shapes, as well as flows with free surfaces. The variational integral is formulated in Lagrangian form through the introduction of a Lagrange multiplier that multiplies the incompressibility constraint; this Lagrangian is augmented by a quadratic penalty function that drives the overall solution to one in which the yield surfaces are obtained as part of the solution. The essential features of the augmented Lagrangian (AL) method are developed in several books published separately and together by Lions and Glowinski between 1973 and 1985, including (Fortin and Glowinski, 1983), but the approach was not widely applied for another two decades. There are detailed discussions of the application to yield-stress fluids in (Moyers-Gonzalez and Frigaard, 2004) and (Huigol and You, 2005) for duct flows, and in (Dimakopoulos *et al.*, 2013) for two-phase flows with bubbles. These studies indicate the AL method is generally more robust than regularization, although it is more complex to implement.

The first significant numerical solution for a three-dimensional (albeit axi-symmetric) flow of a yield-stress fluid appears to be by (Beris *et al.*, 1985), who employed the Bercovier and Engleman regularization to study creeping flow past a sphere, which is a problem for which an analytical solution is known for Newtonian liquids. It is readily established that there must be unyielded regions near the stagnation points at the

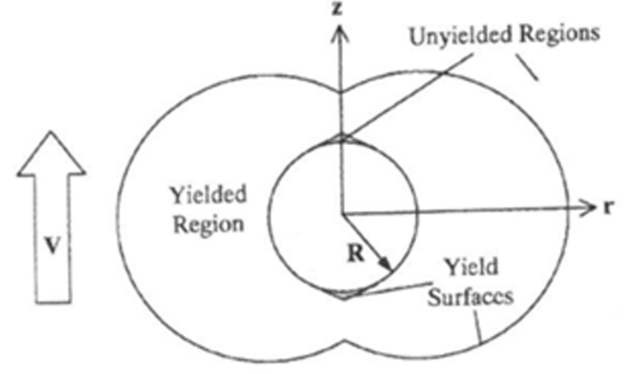


FIG. 32 Schematic of unyielded regions around a sphere in creeping flow in a Bingham fluid

polar caps, as well as a yield surface at a finite distance from the moving sphere, as shown schematically in Fig. 32. The presence of the outer yield surface requires a circulating flow in the neighborhood of the equatorial plane in order to satisfy overall mass conservation. Figure 33 shows a calculation of the attached yield surface at the polar cap for different values of the dimensionless group $Y_g = 2\pi\sigma_y R^2/F$, where F is the buoyant force. This study is unusual among regularization calculations in that the presence of the yield surface was confirmed by an independent calculation in which the yield surface was taken as a fixed boundary at which the velocity and stress conditions were satisfied, and it represents the “gold standard” for such calculations. (Putz and Frigaard, 2010) have employed the AL method to compute the two-dimensional flow of a Bingham Fluid past oblate and prolate ellipses, where the flow is qualitatively similar to the flow past the sphere. The corresponding problem of bubble and droplet flow in a Bingham liquid shows unusual unyielded “ears” centered on the equatorial plane, which must precess along the bubble or droplet surface (Dimakopoulos *et al.*, 2013; Singh and Denn, 2008); an example is given in Fig. 34. There is an extensive treatment of bubble flow in yield-stress fluids in (Dimakopoulos *et al.*, 2013); see also (Lavrenteva and Nir, 2010) for a general survey of free-surface flows.

What is notable about all the calculations is that fore-and-aft symmetry is preserved in the creeping flow limit for solids and non-deformable bubbles, and it is straightforward to demonstrate that a Bingham or similar fluid model will always satisfy fore-aft symmetry in a geometry that has fore-aft symmetry. We return to this point subsequently.

Most published solutions of the flow of yield-stress fluids have been for flows in channels of various cross-sections. A large number of solutions using the Papanastasiou regularization to compute flows with changing cross-sections can be found in (Mitsoulis, 2007), and these are typical of the genre. (Moyers-Gonzalez and

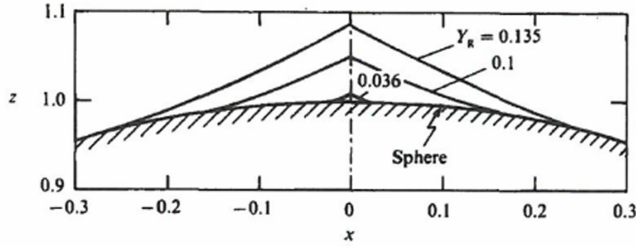


FIG. 33 Unyielded regions at the polar cap for creeping flow of a Bingham fluid around a sphere for various values of $Y_g = 2\pi\sigma_y R^2/F$ (Beris *et al.*, 1985), reproduced with the permission of Cambridge University Press.

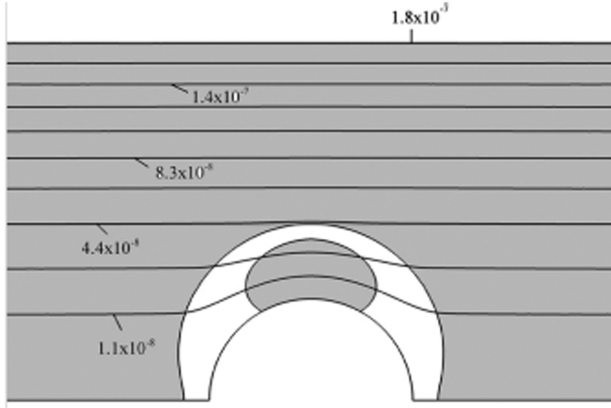


FIG. 34 Rise of a bubble in a Herschel-Bulkley fluid with $n = 0.7$ and negligible inertial or interfacial tension effects, $Y_g = 0.195$. Grey denotes unyielded fluid. (Dimakopoulos *et al.*, 2013). (N.B. Bn as defined in this paper is equivalent to $2Y_g/3$.) Reproduced with permission of Elsevier.

Frigaard, 2004) have employed the AL method to examine the computational issues in ducts with irregular cross-sections, including a maple leaf shape, as well as co-flows of various types. Figure 35 shows the computed flow at zero Reynolds number for a Bingham fluid in a plane channel with a cylinder that is offset from the centerplane using the Bercovier and Engleman regularization; this geometry is often used to test computational algorithms and constitutive equations for polymer melts. The flow is from left to right, and Bn based on the full channel width equals 125. The shaded regions are unyielded. The upstream and downstream flows approach the configuration that is expected in an infinite channel for such a large Bingham number, namely an unyielded plug across most of the channel cross-section and small sheared regions near the walls. There is no flow in the narrow gap between the cylinder and the near wall. The shaded “island” between the cylinder and the far wall is a consequence of the no-slip condition at the solid surfaces, which requires that there be a velocity maximum at an interior point in the channel where the derivative

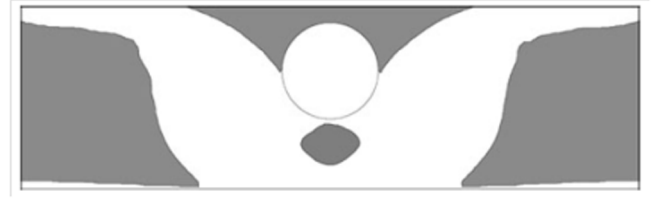


FIG. 35 Creeping flow of a Bingham liquid in a channel with an offset cylinder, $Bn = 125$. The flow is from left to right (Denn, 2008).

goes to zero; as long as the tensile stresses are sufficiently small, which is expected in this gradual contraction and expansion, the stress invariant will be below the critical value. This is therefore a region in space where the velocity is a constant and the von Mises criterion is satisfied everywhere on the surface, but the plug itself does not move; rather, fluid enters and leaves at a fixed velocity everywhere on the surface. We might think of this as analogous to a freezing/melting transition. Here, too, the fore-aft symmetry of the geometry is reflected in the solution.

3. The conceptual starting point

Most approaches to the analysis of complex flows of yield-stress fluids have started from a classical fluid mechanics perspective, with the Bingham or Oldroyd number viewed as a parameter that permits continuation from the classical inelastic solution. (Bhavaraju *et al.*, 1978), for example, studied the flow of a gas bubble in a Bingham fluid by means of a regular perturbation in Bn, and continuation in flow through a duct with a changing cross section, starting from the Newtonian fluid and progressing towards flow stoppage, is illustrated in the calculations of (Mitsoulis, 2007). There has been surprisingly little effort to utilize the motion of a plastic material as the base case, despite the extensive literature on plastic flow. The notion that the yield surfaces in Bingham flow might correspond to slip lines in classical plasticity was alluded to by (Beris *et al.*, 1985) with regard to the angle of departure of the outer yield surface from the axis of symmetry for flow past a sphere, and again by (Dimakopoulos *et al.*, 2013) regarding the intersection of the outer yield surface about a rising spherical bubble with the axis of symmetry. The connection between slip lines and yield surfaces, and especially the idea that the discontinuity at the slip line might then be smoothed by a boundary layer to obtain velocity continuity, seems to have been first suggested by Tanner in an unpublished discussion of (Denn, 1998). The connection between slip lines and yield surfaces is further developed in (Tanner, 2000), but the implementation of the plasticity solution as a base case does not seem to have been attempted.

4. Comparison with experiments in non-viscometric flows

Meaningful experimental data on the flow of yield-stress fluids in complex geometries has only recently become available. Most experiments have been done with various concentrations of neutralized Carbopol 940 in water, which is traditionally viewed as an “ideal” yield stress fluid without thixotropy. The earliest flow visualization experiments, by (Atapattu *et al.*, 1995), are notable in that a constant terminal velocity for a falling sphere could be obtained only after between four and ten individual spheres had been released consecutively at intervals of a few minutes. The time interval between successive spheres did not appear to influence the terminal velocity; only the number of spheres released was important. Atapattu and coworkers obtained velocity profiles and mapped apparent yield surfaces, but their experimental arrangement induced a substantial wall effect and it is not feasible to compare their results to available simulations. (Putz *et al.*, 2008) used particle image velocimetry to study the flow around a single sphere in both a Newtonian and yield-stress fluid. The flow pattern in the Newtonian fluid was consistent with the known analytical solution and exhibited fore-aft symmetry, as expected. The flow pattern for the yield-stress fluid, which was a 0.08% wt. neutralized aqueous solution of Carbopol 940, is shown in Fig. 36 for a Reynolds number reported as 2.0×10^{-3} and $Bn = 0.25$. There is clearly no fore-aft symmetry. This Carbopol does seem to have a very small region of hysteresis near the yield point in simple shear flow during a stress loop, but the authors note the similarity of the aft flow (a “negative wake”) to what is observed with polymer solutions and they attribute the phenomenon to probable viscoelasticity. A similar result for a 1% wt. carbopol 940 that is claimed to show no hysteresis was reported by (Ahonguio *et al.*, 2014). Similar behaviour was observed in an aging Laponite suspension (Gueslin *et al.*, 2006), but that system exhibits thixotropy and a Bingham-type model would not be expected to apply. (Tokpavi *et al.*, 2009) and (Josic *et al.*, 2013) have reported lack of fore-aft symmetry for creeping flow for the same 1% wt. Carbopol 940 solution about a cylinder and a disk, respectively. The evidence thus appears to be convincing that the classical continuum models have very limited utility for application in these complex flows, at least for the limited number of materials where detailed experiments have been reported, and the consensus among the experimentalists is that viscoelasticity is the reason for the discrepancy between simulation and experiment. (Viscoelasticity is a possible source of the observed normal stress in materials like Carbopol, but normal stresses can exist in systems that are not viscoelastic, such as non-Brownian suspensions.) Frigaard and coworkers have carried out a series of studies on co-current flows in straight and wavy channels in which one of the fluids has a yield stress, which

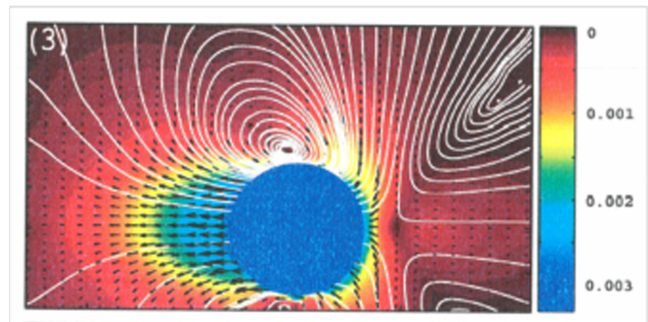


FIG. 36 Creeping flow of a neutralized 0.08% wt. Carbopol-940 solution about a sphere, $Bn = 0.25$. The sphere is moving from right to left. (Putz *et al.*, 2008), reproduced by permission of Elsevier.

is relevant to oil pipeline flow. As part of this work, (Hormozi *et al.*, 2014) recently simulated experiments in which a core fluid, either Newtonian or polymer solution, was pulsed while flowing concurrently with an outer Carbopol solution, creating complex patterns that appeared to be frozen into the interface. For this transient system their simulations using the Bingham model with the Bercovier and Engelman regularization did capture the essential features of the experiments, although there was no attempt at quantitative comparison.

C. Structure and Viscoelasticity

1. Structural continuum models

There have been numerous attempts to account for the time dependence of yield stress fluids through the introduction of a variable that characterizes the microstructure, in much the same way that transient network models have been used for entangled polymers [e.g. (Mewis and Denn, 1983)]. One example, the In the above, we have reviewed recent progress on our understanding of yield stress fluids. Much of the experimental is mainly due to simultaneous measurements of the flow structure and the mechanical properties. Techniques that allow elucidating the flow structure such as MRI, ultrasound and microscopy techniques have revealed a richness in the behavior of yield stress materials that was hitherto unsuspected, and have allowed for some novel insights. One of the main questions that has been around for many decades is whether the yield stress actually exists. We come to the conclusion here that it does, in any case on experimentally relevant timescales, and that different techniques of determining the yield stress yield similar values. However one of the novel insights is that not all yield stress materials behave ideally. A clear distinction needs to be made between two types of yield stress fluids: simple and thixotropic ones. For the latter, adequate experimental protocols need to be employed, that take

into account the time evolution of these materials: ageing and shear rejuvenation. If this is done, this solves the problem of the reproducible experimental determination of the yield stress. Tied in with the discussion of the yield stress is the shear localization that is generically observed in yield stress fluids. For simple yield stress fluids, shear banding is in general due to a stress heterogeneity. For thixotropic materials, the situation is qualitatively different: due to the interplay between ageing and shear rejuvenation, there exists a critical shear rate below which no stable homogeneous flow is possible. If then a shear rate is imposed macroscopically that is below the critical shear rate, a shear band is formed in which the material flows at the critical shear rate, the rest of the material remaining motionless. In addition, of course, wall slip may also be observed in thixotropic materials, and needs to be corrected for if it is present. In rheology, wall slip is usually defined as a viscosity that depends on the size of the gap of the measurement geometry, and this distinguishes it from the two types of shear localization discussed above; the correction can be done by comparing measurements with different gap sizes, and extrapolating to an infinite gap. Very recently, a different type of gap-dependent viscosity was uncovered for very small gaps i.e., microchannels with a size not very different from that of the drop size in the emulsion studied. Here, the gap dependence was attributed to a collective effects non-local rheology. There is still a lot of discussion on this topic, but it may challenge the simple view of yield stress materials sketched above. On the other hand, since the effect is only measurable if the gap is very small, it is probably not very important for most practical purposes. What is important for engineering purposes, on the other hand, is to have a predictive constitutive equation that allows for a general description of the flow (or not) of yield stress materials. For polymer systems a large number of such models have been derived from statistical mechanical models and are extensively used in practice. However, for yield stress materials, only 3D invariant versions of phenomenological (e.g., Bingham) models exist, and even these have not been fully tested in more complicated flows than simple shear. The latter is, at least in part, due to the lack of reliable data for other rheological parameters such as the normal stresses and the elongational viscosity, which remains an area for future research. The more fundamental problem is that a full elasto-visco-plastic theory of yield stress fluids seems to be out of reach for the moment because of our limited understanding of plasticity. One promising research direction to solve this problem is to borrow statistical mechanical models from the glass transition/soft matter physics communities such as mode-coupling theory or the Soft Glassy Rheology model. These would automatically include also ageing and shear rejuvenation as these are general features of the glass transition, and could thus in the end be the answer to the many remaining questions

posed in this review. λ -model, was introduced in Section III.B.2. Typically, the microstructural variable, which we will continue to denote λ (hence the term “ λ -models”), varies between zero and unity, where unity corresponds to the equilibrium structure and zero to complete structural breakdown. Some investigators prefer to permit $0 \leq \lambda \leq \infty$) (as in the form used in Section III.B.2). If the structure is anisotropic then we would require a structural tensor. The rate of structural breakdown is typically taken to depend on the magnitude of the deformation rate in the form $\lambda\dot{\gamma}^a$; the buildup rate is typically taken to depend on the distance from equilibrium and, in some cases, on the deformation rate, in the form $(1-\lambda)\dot{\gamma}^b$. The parameters a and b are typically taken to have integer values. If the rate of buildup is driven only by the distance from equilibrium then b would be expected to be zero, as is usually done in polymer network theories. For a simple shear flow we would then have a kinetic equation of the form

$$\frac{d\lambda}{dt} = k_1(1-\lambda)\dot{\gamma}^b - k_2\lambda\dot{\gamma}^a \quad (28)$$

For a general flow we would replace the time derivative d/dt by the substantial derivative $\frac{\partial}{\partial t} + \mathbf{v} \cdot \nabla$ and the shear rate $\dot{\gamma}$ by $\sqrt{\Pi_\Delta}$. There is a steady-state structure in a steady shear flow:

$$\lambda_{ss} = \left[1 + \frac{k_2}{k_1} \dot{\gamma}^{a-b} \right]^{-1} \quad (29)$$

Clearly, $a > b$ to ensure the correct limits $\lambda \rightarrow 1, 0$ as $\dot{\gamma} \rightarrow 0, \infty$ (Equations of this type for the structural variable do not generally appear to admit the possibility of avalanches). Many such models of structured liquids have been proposed, and they are reviewed in papers by (Mujumdar *et al.*, 2002) and (Mewis and Wagner, 2009); interestingly, the condition $a > b$ is violated by some of these models. Some models include two mechanisms for structure buildup, a Brownian term that depends only on $(1-\lambda)$ and a shear-dependent term. (Pinder, 1964) and (Coussot *et al.*, 2002b) assume a constant rate of buildup, which permits λ to become infinite; the latter formulation as discussed previously, does admit avalanches in a narrow parameter range.

In a conventional network model, like rubber elasticity, the modulus is proportional to the connectivity, so we would have $G = \lambda G_0$, where G_0 is the equilibrium modulus; for a fractal structure the form would be $G = \lambda^n G_0, n > 1$. It is likely that the yield stress would have the same dependence on λ as the modulus. The dependence of the dissipative parameters on λ would more than likely be taken initially to be a power-law; in fact, most of the models reviewed by Mewis and Wagner take the plastic viscosity to be proportional to λ . A minimal generalization of Eqs. 17 and 18 would then be of the

form:

$$\sigma = \left[\eta_p + \frac{\sigma_y}{\sqrt{\frac{1}{2}\Pi_\Delta}} \right] \Delta, \quad \frac{1}{2}\Pi_\Delta \geq \sigma_y^2 \quad (30)$$

$$\sigma = G\gamma, \quad \frac{1}{2}\Pi_\Delta < \sigma_y^2 \quad (31)$$

$$\frac{\partial \lambda}{\partial t} + \mathbf{v} \cdot \nabla \lambda = k_1(1 - \lambda)\left(\frac{1}{2}\Pi_\Delta\right)^{\frac{b}{2}} - k_2\lambda\left(\frac{1}{2}\Pi_\Delta\right)^{\frac{a}{2}} \quad (32)$$

$$G = \lambda^n G_0, \quad \sigma_y = \lambda^n \sigma_{y0}, \quad \eta_p = \lambda^k \eta_{p0} \quad (33)$$

For a strain-based yield criterion we would have:

$$\frac{1}{2}\Pi_y < \text{or} > \gamma_y^2 \quad (34)$$

and if the unyielded material is a linearly viscoelastic solid of Kelvin-Voigt form the constitutive equation prior to yielding would be

$$\sigma = G\gamma + \eta\Delta, \quad \frac{1}{2}\Pi_y < \gamma_y^2 \quad (35)$$

Incorporation of the structural variable into the conventional Bingham formulation, with $G \rightarrow \infty$, does not introduce new conceptual issues, whereas any attempt to include the viscoelastic deformation of the unyielded region appears to be incompatible with conventional regularization approaches.

While this approach has been used extensively to characterize simple shear flows it has been used only recently to describe a complex flow, namely the squeeze flow between parallel disks. (Alexandrou *et al.*, 2013) employed the Papanastasiou regularization and took the plastic viscosity to be a constant and the yield stress to be proportional to the structural parameter in the kinetic model. In Eq. (32) they took $b = 0$, $a = 1$, and they multiplied k_2 by $\exp\left(c\sqrt{\frac{1}{2}\Pi_\Delta}\right)$ for a better representation of the kinetics in the slurry they were modeling. Some computed profiles for both the thixotropic model and the basic Bingham model without structural kinetics are shown in Fig. 37. The unyielded regions at the axial stagnation points were identified by (Tanner, 2000) with plastic slip planes and are routinely seen in simulations of squeeze flow of Bingham and Herschel-Bulkley fluids. There was no comparison of these structural calculations with experiments. It is not known if a time-dependent but inelastic model of this type is sufficient to explain the loss of fore-aft symmetry in creeping flow past symmetric objects.

2. Viscoelastic modeling

There are two broad ways of formulating properly invariant continuum constitutive equations for viscoelastic materials. In one, the stress is expressed as an integral over the history of a strain function. In the other, the stress evolves according to a differential equation involving the rate-of-strain tensor. In certain limiting cases—a

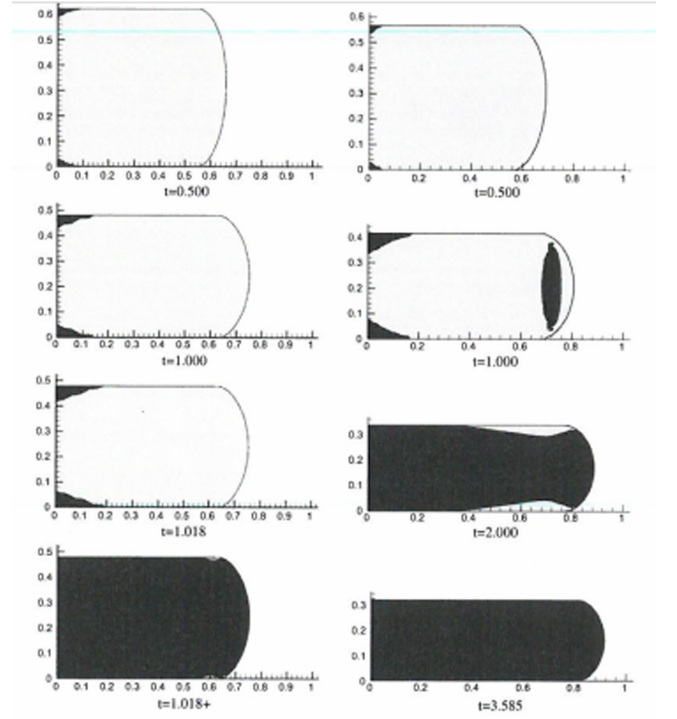


FIG. 37 Squeeze flow of a Bingham fluid without (left) and with (right) a structural parameter. The black regions are unyielded. The deformation prior to $t = 0.5$ is not shown. (Alexandrou *et al.*, 2013), reprinted with permission of Elsevier.

transient network model based on rubber elasticity, for example—the two approaches are equivalent. There is a strong tradition of formulations that include the kinetics of structure parameters or tensors. Differential equation stress models have been favoured for numerical applications, and differential equation approximations exist for most constitutive formulations originally developed in integral form. It is usual to write the stress as a sum $\sigma = -p\mathbf{I} + \tau + \eta_s\Delta$, where τ denotes the polymer contribution and η_s is a solvent viscosity or a way of representing the contribution from very rapid relaxation modes. Most models are generalization of a Maxwell model for the extra stress:

$$\theta \left[\frac{\partial \tau}{\partial t} + \mathbf{v} \cdot \nabla \tau + \nabla \mathbf{v}^T \cdot \tau - \tau \cdot \nabla \mathbf{v} + \right. \quad (36)$$

$$\left. \xi(\tau \cdot \Delta + \Delta \cdot \tau) \right] + Y(\tau)\tau = \theta G \Delta. \quad (37)$$

Here, θ is a characteristic time for stress relaxation, G is a shear modulus, and θG is the shear viscosity. ξ is a parameter that is bounded for a shear-thinning fluid between 0 and 2. Y is a function that serves to bound the extensional stresses; in the popular Phan Thien-Tanner model (Tanner, 2000) $Y = \exp(\epsilon \text{trace } \tau/G)$, where ϵ is typically of order 0.2. This equation is derivable from a network model, and it can be viewed as a properly invariant form of a mechanical system consisting of a

spring and dashpot in series. Real polymeric systems have multiple relaxation modes, so the stress would consist of a sum of partial stresses, each of which satisfies Eq. (37) or an appropriate generalization, with relaxation times and moduli characteristic of each mode. Integral formulations accommodate the multiple relaxation times through the time dependence of the memory integral. The Phan Thien-Tanner model has been used with considerable success in simulating the flow of polymer melts in complex geometries [see (Denn, 2008), for example].

The notion of combining viscoelasticity and yield behaviour was initially driven by the desire to describe the behaviour of polymers with high concentrations of carbon black. The first invariant formulation appears to be by (White, 1979), who incorporated a von Mises yield criterion into a memory integral constitutive equation. White's formulation did not include thixotropy, but he indicated that it could be accommodated by permitting the yield criterion to be history dependent. White's basic approach was applied to a more robust viscoelastic model by (Isayev and Fan, 1990), but it has only been employed to represent steady and transient shear and extensional rheology.

There have been several distinct efforts to incorporate yield behaviour into viscoelastic constitutive equations that can be used for computations in complex geometries. (Saramito, 2007) replaced $Y(\tau)$ in Eq. (37) by a term that enters only when the yield stress is exceeded, so prior to yielding τ represents a purely elastic deformation; Saramito subsequently generalized the formulation to include Herschel-Bulkley behaviour (Saramito, 2007). This formulation does not include any structural parameter to address thixotropy. (Cheddadi *et al.*, 2011) applied the model to the flow of wet and dry foams around a cylinder centered in a plane channel, assuming complete slip at the solid surfaces. Results for the wet channel flow are shown in Fig. 38 using an assumed yield strain of 0.1, which is typical for such foams. There is very good agreement between the calculation and the experiment. Notably, the absence of fore-aft symmetry and the negative wake are captured quantitatively. (Cheddadi and Saramito, 2013) have subsequently used the same experiments to validate a new computational scheme.

(de Souza Mendes, 2009, 2011) has developed a constitutive equation for τ with the general form of Eq. (37) with $Y = 1$; the rheological variables depend on a structure parameter that evolves according to the form of Eq. (32), with $a = b = 1$ but with k_2 replaced by a function of the stress and shear rate. The viscosity function takes the form of the Papanastasiou regularization, Eq. (27). The model has a maximum in the steady flow curve and exhibits the viscosity bifurcation in a series of constant stress calculations. (Fonseca *et al.*, 2013) have applied this equation to the flow past a cylinder centered in a channel, and (dos Santos *et al.*, 2014) have calculated the flow through a planar expansion followed by a con-

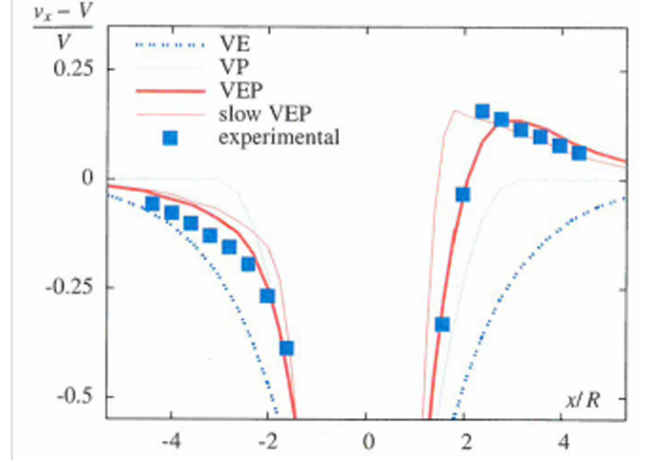


FIG. 38 Flow of a wet foam pasta cylinder. VEP denotes the elastoviscoplastic model, VP the Bingham model, and VE the purely viscoelastic fluid model ($Y = 1$). The slow VEP is a calculation in which the entrance velocity is reduced by a factor of 20 from the experimental value. (Cheddadi *et al.*, 2011). Reproduced by permission.

traction. Fore-aft symmetry is lost in both cases over a range of rheological parameters, but there is no comparison with experimental data.

(Renardy, 2010) has shown that a particular viscoelastic model of the general form of Eq. (37) that has a maximum and minimum in the steady flow curve (but not all such models) emulates the known behaviour of thixotropic yield-stress fluids as an elastic limit is approached. Yuriko Renardy and coworkers ((Maki and Renardy, 2010; Renardy and Grant, 2013) have examined the behaviour of the model in shear and extension. They have been able to model the hysteresis loop of a laponite suspension and the creep response of ketchup without including structural kinetics. The model has not been used to simulate flows in complex geometries, so the practical applicability is untested.

We can conclude this section with the observation that the development of useful constitutive equations is in its infancy. The classical Bingham and similar models are clearly deficient in being able to describe the most fundamental of three-dimensional flows of real yield stress materials, but the reason is unknown. Models based on viscoelastic equations derived for polymers do seem to capture some of the relevant mechanics, but they have not been adequately tested, even in their ability to predict normal stresses in shear of the correct magnitude and sign, and in any event the connection to underlying structure, which is at the heart of the polymer developments, seems to be absent in this case. There is still much to be done here.

VI. CONCLUSION

In the above, we have reviewed recent progress on the understanding of yield stress fluids. Most of recent experimental advances are due to simultaneous measurements of flow structure and mechanical properties. Techniques that allow elucidating the flow structure such as magnetic resonance imaging, ultrasound or optical microscopy techniques have revealed a richness in the behavior of yield stress materials that was hitherto unsuspected, and have allowed for some novel physical insights.

On the theoretical side, much progress has been accomplished to account for both the physical origin of solid behaviour in amorphous materials across a broad range of interparticle interaction producing glassy, jammed and gel behaviors. Simultaneously, computer simulations have demonstrated their efficiency in producing convincing particle-based models of yield stress materials, and have allowed detailed investigations of the rheological behavior of these systems in various geometries. By construction, such simulations allow for a direct study of both the macroscopic rheological response and the microscopic dynamics. These studies have in turn allowed the development of a new family of coarse-grained elasto-plastic models of yield stress materials, where exploration of larger-scale phenomena (such shear-banding and time-dependent flows) can be more easily studied than in particle-resolved simulations.

One of the main questions for many decades has been whether the yield stress actually exists. It is now well-established that it does, in any case on experimentally relevant timescales. Different techniques of determining the yield stress yield similar values provided care is taken to account for wall slip, flow heterogeneity and time-dependence. Indeed one of the novel insights is that not all yield stress materials behave ideally and that a distinction needs to be made between two types of yield stress fluids: simple and thixotropic ones. Simple yield stress fluids show a flow behaviour that is well reproduced by the Herschel-Bulkley law, with no significant time-dependence, while thixotropic ones show a pronounced time-dependence that arises from aging and shear rejuvenation phenomena. Adequate experimental protocols need to be employed, that take into account the time evolution of these materials, in order to get reproducible experimental estimates for the yield stress.

Tied in with the discussion of the yield stress is the shear localization that is generically observed in yield stress fluids. For simple yield stress fluids, shear banding is in general due to stress heterogeneity, and if not, it is only transient. For thixotropic materials, the situation is qualitatively different: due to the interplay between aging and shear rejuvenation, there exists a critical shear rate below which no stable homogeneous flow is possible. If a shear rate is then imposed macroscopically within the unstable regime, a shear band is formed in which the

material flows at the critical shear rate, the rest of the material remaining motionless.

In addition, of course, wall slip is commonly observed in thixotropic materials, and needs to be accounted for, when present. In rheology, wall slip is usually defined as a viscosity that depends on the size of the gap of the measurement geometry, and this distinguishes it from the two types of shear localization discussed above; the correction can be done by comparing measurements with different gap sizes, and extrapolating to an infinite gap. Besides complicating the interpretation of rheological measurements, wall slip also raises fascinating fundamental questions. Reaching a general understanding of slippage phenomena in yield stress materials appears as a challenging task for the future.

Recently, a different type of gap-dependent viscosity was uncovered for very small gaps e.g. for microchannels with a size close to that of the microstructural elements. Here, gap-dependence was attributed to collective effects or “spatial cooperativity” when the range of shear-induced rearrangements span the whole system. There is still a lot of discussion on this topic, but it may challenge the simple view of yield stress materials sketched above.

One last burning issue concerns the full characterization and understanding of the transient flow behavior of both categories of yield stress fluids. The way such materials *start* to flow is indeed of great practical interest. In spite of notable recent progress this question of the yielding dynamics mostly remains to be explored both at microscopic and mesoscopic levels, and both from experiments and theory.

What is also crucial, especially for engineering purposes, is to have a predictive constitutive equation that allows for a general description of the flow (or not) of yield stress materials. For polymer systems a large number of such models have been derived from statistical mechanical models and are extensively used in practice. However, for yield stress materials, only 3D invariant versions of phenomenological (e.g., Bingham) models exist, and even these have not been fully tested in more complicated flows than simple shear. The latter is, at least in part, due to the lack of reliable data for other rheological parameters such as the normal stresses and the elongational viscosity, which remains an area for future research. The more fundamental problem is that a full elasto-visco-plastic theory of yield stress fluids seems to be out of reach for the moment because of our limited understanding of plasticity. One promising research direction to solve this problem is to borrow statistical mechanical models from the glass transition/soft matter physics communities such as mode-coupling theory or the Soft Glassy Rheology model. These would automatically include also ageing and shear rejuvenation as these are general features of the glass transition, and could thus in the end be the answer to the many remaining questions posed in this review.

ACKNOWLEDGMENTS

We thank numerous colleagues for discussions on these matters over the years. We especially thank Catherine Barentin, Jean-Louis Barrat, Annie Colin, Philippe Coussot, Abdoulaye Fall, Marc-Antoine Fardin, Thomas Gibaud, Atsushi Ikeda, Sara Jabbari, Hamid Kellay, Jorge Kurchan, Anke Lindner, Jacques Meunier, Jan Mewis, Thijs Michels, Peder Moller, Guillaume Ovarlez, Peter Sollich, Hajime Tanaka, for interactions on this topic. The research leading to these results has received funding from the European Research Council under the European Unions Seventh Framework Programme (Grant No. FP7/2007-2013)/ERC Grant Agreement No 306845.

REFERENCES

- Ahonguio, F., L. Jossic, and A. Magnin (2014), *J. Non-Newtonian Fluid Mech.* **206**, 57.
- van Aken, G. (2001), *Colloids Surfaces A* **190**, 333.
- Alexandrou, A., G. Florides, and G. Georgiou (2013), *J. Non-Newtonian Fluid Mech* **193**, 103.
- Amarouchene, Y., D. Bonn, J. Meunier, and H. Kellay (2001), *Phys. Rev. Lett.* **86**, 3558.
- Andreotti, B., J.-L. Barrat, and C. Heussinger (2012), *Phys. Rev. Lett.* **109**, 105901.
- Andreotti, B., Y. Forterre, and O. Pouliquen (2013), *Granular media: between fluid and solid* (Cambridge University Press, Cambridge).
- Anna, S. L., G. H. McKinley, D. A. Nguyen, T. Sridhar, S. J. Muller, J. Huang, and D. F. James (2001), *J. Rheol.* **45**, 83.
- Aral, B., and D. Kalyon (1994), *J. Rheol.* **38**, 957.
- Astarita, G. (1990), *J. Rheol.* **34**, 275.
- Atapattu, D., R. Chhabra, and P. Uhlherr (1995), *J. Non-Newtonian Fluid Mech.* **59**, 245.
- Aytouna, M., J. Paredes, N. Shahidzadeh-Bonn, S. Moulinet, C. Wagner, Y. Amarouchene, J. Eggers, and D. Bonn (2013), *Phys. Rev. Lett.* **110**, 034501.
- Baldewa, B., and Y. M. Joshi (2012), *Soft Matter* **8**, 789.
- Ballauff, M., J. Brader, S. Egelhaaf, M. Fuchs, J. Horbach, N. Koumakis, M. Krüger, M. Laurati, K. Mutch, G. Petekidis, M. Siebenburger, T. Voigtman, and J. Zausch (2013), *Phys. Rev. Lett.* **110**, 215701.
- Ballesta, P., R. Besseling, L. Isa, G. Petekidis, and W. C. K. Poon (2008), *Phys. Rev. Lett.* **101**, 258301.
- Ballesta, P., G. Petekidis, L. Isa, W. Poon, and R. Besseling (2012), *J. Rheol.* **56**, 1005.
- Balmforth, N., and R. Craster (1999), *J. Non-Newtonian Fluid Mech.* **84**, 65.
- Balmforth, N., N. Dubash, and A. Slim (2010a), *J. Non-Newtonian Fluid Mech.* **165**, 1139.
- Balmforth, N., N. Dubash, and A. Slim (2010b), *J. Non-Newtonian Fluid Mech.* **165**, 1147.
- Balmforth, N. J., I. A. Frigaard, and G. Ovarlez (2014), *Ann. Review Fluid Mech.* **46**, 121.
- Baret, J., D. Vandembroucq, and S. Roux (2002), *Phys. Rev. Lett.* **89**, 195506.
- Barlett, P., L. Teece, and M. Faers (2012), *Phys. Rev. E* **85**, 021404.
- Barnes, H. (2007), *Appl. Rheol.* **17**, 43110.
- Barnes, H., and Q. Nguyen (2001), *J. Non-Newtonian Fluid Mech.* **98**, 1.
- Barnes, H. A. (1995), *J. Non-Newtonian Fluid Mech.* **56**, 221.
- Barnes, H. A. (1997), *J. Non-Newtonian Fluid Mech.* **70**, 1.
- Barnes, H. A. (1999), *J. Non-Newtonian Fluid Mech.* **81**, 133.
- Barnes, H. A., J. F. Hutton, and K. Walters (1989), *An Introduction to Rheology* (Elsevier (Amsterdam)).
- Barnes, H. A., and K. Walters (1985), *Rheol. Acta* **24**, 323.
- Barrat, J.-L., and A. Lemaitre (2011), “Dynamical heterogeneities in glasses, colloids and granular materials,” Chap. Heterogeneities in amorphous systems under shear (Oxford University Press, Oxford) pp. 264–297.
- Batista, A., A. Raymundo, I. Sousa, J. Empis, and J. Franco (2006), *Food Biophysics* **4**, 216.
- Bauer, T., J. Oberdisse, and L. Ramos (2006), *Phys. Rev. Lett.* **97**, 258303.
- Bécu, L., P. Grondin, S. Manneville, and A. Colin (2005), *Colloids Surfaces A* **263**, 146.
- Bécu, L., S. Manneville, and A. Colin (2006), *Phys. Rev. Lett.* **96**, 138302.
- Bengtzelius, U., W. Götze, and A. Sjolander (1984), *J. Phys. C: Solid State Phys.* **17**, 5915.
- Bercovier, M., and M. Engelman (1980), *J. Comput. Phys.* **36**, 313.
- Beris, A., J. Tsamopoulos, R. Armstrong, and R. Brown (1985), *J. Fluid Mech.* **158**, 219.
- Bernal, J. D., and J. Mason (1960), *Nature (London)* **188**, 910.
- Berthier, L. (2003), *J. Phys.: Condens. Matter* **15**, S933.
- Berthier, L., and J.-L. Barrat (2002), *Phys. Rev. Lett.* **89**, 095702.
- Berthier, L., J.-L. Barrat, and J. Kurchan (2000), *Phys. Rev. E* **61**, 5464.
- Berthier, L., and G. Biroli (2011), *Rev. Mod. Phys.* **83**, 587.
- Berthier, L., and G. Tarjus (2009), *Phys. Rev. Lett.* **103**, 170601.
- Berthier, L., and G. Tarjus (2011), *J. Chem. Phys.* **134**, 214503.
- Bertola, V., F. Bertrand, H. Tabuteau, D. Bonn, and P. Coussot (2003), *J. Rheol.* **47**, 1211.
- Besseling, R., L. I. P. Ballesta, G. Petekidis, M. Cates, and W. Poon (2010), *Phys. Rev. Lett.* **105**, 268301.
- Besseling, R., L. Isa, E. R. Weeks, and W. C. K. Poon (2009), *Adv. Colloid Interface Sci.* **146**, 1.
- Bhavaraju, S., R. Mashelkar, and H. Blanch (1978), *AIChE J.* **24**, 1063.
- Bibette, J., D. Roux, and B. Pouligny (1992), *J. Phys. II France* **2**, 401.
- Bingham, E. C. (1922), *Fluidity and Plasticity* (McGraw-Hill, New York).
- Bocquet, L., A. Colin, and A. Ajdari (2009), *Phys. Rev. Lett.* **103**, 036001.
- Bonn, D., P. Coussot, H. T. Huynh, F. Bertrand, and G. Debrégeas (2002a), *Europhys. Lett.* **89**, 786.
- Bonn, D., and M. Denn (2009), *Science* **324**, 1401.
- Bonn, D., S. Rodts, Groeninck, N. S.-B. S. Rafai, and P. Coussot (2008), *Annu. Rev. Fluid Mech.* **40**, 209.
- Bonn, D., S. Tanase, B. Abou, H. Tanaka, and J. Meunier (2002b), *Phys. Rev. Lett.* **89**, 015701.
- Bonnecaze, R., and M. Cloitre (2010), *Adv. Polym. Sci.* **236**, 117.

- Bouchaud, J.-P. (1992), J. Phys. I France **2**, 1705.
- Bouchaud, J.-P., and D. S. Dean (1995), J. Phys. I France **5**, 265.
- Bouchbinder, E., and J. S. Langer (2009a), Phys. Rev. E **80**, 031131.
- Bouchbinder, E., and J. S. Langer (2009b), Phys. Rev. E **80**, 031132.
- Bouchbinder, E., and J. S. Langer (2009c), Phys. Rev. E **80**, 031133.
- Boujlel, J., and P. Coussot (2012), Rheol. Acta **51**, 867.
- Boyer, F., E. Guazzelli, and O. Pouliquen (2011), Phys. Rev. Lett. **107**, 188301.
- Brader, J. M., M. Siebenbürger, M. Ballauff, K. Reinheimer, M. Wilhelm, S. J. Frey, F. Weysser, and M. Fuchs (2010), Phys. Rev. E **82**, 061401.
- Brambilla, G., D. E. Masri, M. Pierno, G. Petekidis, A. B. Schofield, L. Berthier, and L. Cipelletti (2009), Phys. Rev. Lett. **102**, 085703.
- Brenner, T., S. Matsukawa, K. Nishinari, and R. Johannsson (2013), J. Non-Newtonian Fluid Mech. **196**, 1.
- Burgos, G. R., A. N. Alexandrou, and V. Entov (1999), J. Rheol. **43**, 463.
- Buscall, R. (2010), J. Rheol. **54**, 1177.
- Buscall, R., T. H. Choudhury, M. A. Faers, J. W. Goodwin, P. A. Luckham, and S. J. Partridge. (2009), Soft Matter **5**, 1345.
- Buscall, R., J. McGowan, and A. MortonJones (1993), J. Rheol. **37**, 621.
- da C. Andrade, E. (1910), Proc. R. Soc. London A **84** (1).
- Callaghan, P. T. (2008), Rheol. Acta **47**, 243.
- Carrier, V., and G. Petekidis (2009), J. Rheol. **53**, 245.
- Cates, M. E., M. Fuchs, K. Kroy, W. C. K. Poon, and A. M. Puertas (2004), J. Phys.: Condens. Matter **16**, S4861.
- Caton, F., and C. Baravian (2008), Rheol. Acta **47**, 601.
- Chan, H., and A. Mohraz (2012), Phys. Rev. E **85**, 041403.
- Chan, H., and A. Mohraz (2013), Rheol. Acta **52**, 383.
- Chan, H., and A. Mohraz (2014), J. Rheol. **58**, 1419.
- Chang, C., Q. D. Nguyen, and H. Rønningsen (1999), J. Non-Newtonian Fluid Mech. **87**, 127.
- Charbonneau, P. (2014), Nature Comm. **5**, 3725.
- Chaudhuri, P., L. Berthier, and L. Bocquet (2012a), Phys. Rev. E **85**, 021503.
- Chaudhuri, P., L. Berthier, and S. Sastry (2010a), Phys. Rev. Lett. **104**, 165701.
- Chaudhuri, P., and J. Horbach (2013), Phys. Rev. E **88**, 040301(R).
- Chaudhuri, P., L. B. P. I. Hurtado, and W. Kob (2010b), Phys. Rev. E **81**, 040502.
- Chaudhuri, P., V. Mansard, A. Colin, and L. Bocquet (2012b), Phys. Rev. Lett. **109**, 036001.
- Cheddadi, I., and P. Saramito (2013), J. Non-Newtonian Fluid Mech. **202**, 13.
- Cheddadi, I., P. Saramito, B. Dollet, C. Raufaste, and F. Graner (2011), Eur. Phys. J. E **34**, 1.
- Cheddadi, I., P. Saramito, and F. Graner (2012), J. Rheol. **56**, 213.
- Chellamuthu, M., E. Arndt, and J. Rothstein (2009), Soft Matter **5**, 2117.
- Cheng, D. (1986), Rheol. Acta **25**, 542.
- Cheng, Z., J. Zhu, P. M. Chaikin, S.-E. Phan, and W. B. Russel (2002), Phys. Rev. E **65**, 041405.
- Cho, K. S. (2005), J. Rheol. **49**, 747.
- Christopoulou, C., G. Petekidis, B. Erwin, M. Cloitre, and D. Vlassopoulos (2009), Phil. Trans. R. Soc. A **367**, 5051.
- Clasen, C., and G. McKinley (2004), J. Non-Newtonian Fluid Mech. **124**, 1.
- Cloitre, M., R. Borrega, and F. M. L. Leibler (2003), Phys. Rev. Lett. **90**, 068303.
- Cloitre, M., R. Borrega, and L. Leibler (2000), Phys. Rev. Lett. **85**, 4819.
- Colombo, J., and E. D. Gado (2014), J. Rheol. **58**, 1089.
- Coussot, P. (2007), Soft Matter **3**, 528.
- Coussot, P. (2014), J. Non-Newtonian Fluid Mech. **211**, 31.
- Coussot, P., and C. Ancey (1999), *Rheophysics of Pastes and Suspensions* (EDP Sciences, Paris).
- Coussot, P., and S. Boyer (1995), Rheol. Acta **34**, 534.
- Coussot, P., Q. D. Nguyen, H. T. Huynh, and D. Bonn (2002a), Phys. Rev. Lett. **88**, 175501.
- Coussot, P., Q. D. Nguyen, H. T. Huynh, and D. Bonn (2002b), J. Rheol. **46**, 573.
- Coussot, P., and G. Ovarlez (2010), Eur. Phys. J. E **33** (3), 183.
- Coussot, P., J. S. Raynaud, F. Bertrand, P. Moucheron, J. P. Guibaud, H. T. Huynh, S. Jarny, and D. Lesueur (2002c), Phys. Rev. Lett. **88**, 218301.
- Coussot, P., H. Tabuteau, X. Chateau, L. Tocquer, and G. Ovarlez (2006), J. Rheol. **50**, 975.
- Coussot, P., L. Tocquer, C. Lanos, and G. Ovarlez (2009), J. Non-Newtonian Fluid Mech. **158**, 85.
- Covey, G., and B. Stanmore (1981), J. Non-Newtonian Fluid Mech. **8**, 249.
- Cruz, F. D., F. Chevoir, D. Bonn, and P. Coussot (2002), Phys. Rev. E **66**, 051305.
- Csikor, F., C. Motz, D. Weygand, M. Zaiser, and S. Zapperi (2011), Science **318**, 251.
- Cugliandolo, L., J. Kurchan, and L. Peliti (1997a), Phys. Rev. E **55**, 3898.
- Cugliandolo, L. F., and J. Kurchan (1993), Phys. Rev. Lett. **71**, 173.
- Cugliandolo, L. F., J. Kurchan, P. L. Doussal, and L. Peliti (1997b), Phys. Rev. Lett. **78**, 350.
- Dai, G., and R. Bird (1981), J. Non-Newtonian Fluid Mech. **8**, 349.
- Davies, G., and J. Stokes (2008), J. Non-Newtonian Fluid Mech. **148**, 73.
- Dawson, K., G. Foffi, M. Fuchs, W. Gotze, F. Sciortino, M. Sperl, P. Tartaglia, T. Voigtmann, and E. Zaccarelli (2000), Phys. Rev. E **63**, 011401.
- DeGiuli, E., E. Lerner, C. Brito, and M. Wyart (2014), Proc. Natl. Acad. Sci. USA **111**, 17054.
- DeGroot, J. J. V., C. W. Macosko, T. Kume, and T. Hashimoto (1994), J. Colloid Interface Sci. **166**, 404.
- Denkov, N., V. Subramanian, D. Gurovich, and A. Lips (2005), Colloids and Surfaces A: Physicochem. Eng. Aspects **263**, 129.
- Denn, M. (1998), *Dynamics of Complex Fluids*, edited by M. Adams, R. Mashelkar, J. Pearson, and A. Rennie (Imperial College Press and Royal Society, London).
- Denn, M. (2008), *Polymer melt processing: foundations in fluid mechanics and heat transfer* (Cambridge University Press, New York).
- Denn, M., and D. Bonn (2011), Rheol. Acta **50**, 307.
- Denn, M., and J. Morris (2014), Annu. Rev. Chem. Biomol. Eng. **5**, 203.
- Denn, M. M. (2001), Annu. Rev. Fluid Mech. **33**, 265.
- Dennin, M. (2008), J. Phys.: Condens. Matter **20**, 283103.
- Derec, C., G. Ducouret, A. Ajdari, and F. Lequeux (2003), Phys. Rev. E **67**, 061403.

- Dimakopoulos, Y., M. Pavlidis, and J. Tsamopoulos (2013), *J. Non-Newtonian Fluid Mech.* **200**, 34.
- Dimitriou, C., R. Ewoldt, and G. McKinley (2013), *J. Rheol.* **57**, 27.
- Dimitriou, C. J., and G. H. McKinley (2014), *Soft Matter*, .
- Divoux, T., C. Barentin, and S. Manneville (2011a), *Soft Matter* **7**, 8409.
- Divoux, T., C. Barentin, and S. Manneville (2011b), *Soft Matter* **7**, 9335.
- Divoux, T., V. Grenard, and S. Manneville (2013), *Phys. Rev. Lett.* **110**, 018304.
- Divoux, T., D. Tamarii, C. Barentin, and S. Manneville (2010), *Phys. Rev. Lett.* **104**, 208301.
- Divoux, T., D. Tamarii, C. Barentin, S. Teitel, and S. Manneville (2012), *Soft Matter* **8**, 4151.
- Donev, A., S. Torquato, F. H. Stillinger, and R. Connelly (2004), *Phys. Rev. E* **70**, 043301.
- Doshi, P., and O. Basaran (2004), *Phys. Fluids* **16**, 585.
- Durian, D. J. (1995), *Phys. Rev. Lett.* **75**, 4780.
- Edwards, S. (1987), *Dynamics of polymeric liquids vol. 1, fluid mechanics*, edited by R. Bird, C. Curtiss, R. Armstrong, and O. Hassager (Wiley Interscience, New York).
- Eggers, J. (1997), *Rev. Mod. Phys.* **69**, 865.
- Erwin, B. M., S. A. Rogers, M. Cloitre, and D. Vlassopoulos (2010), *J. Rheol.* **54**, 187.
- Evans, I. D. (1992), *J. Rheol.* **36**, 1313.
- Ewoldt, R. H. (2013), *J. Rheol.* **57**, 177.
- Ewoldt, R. H., A. E. Hosoi, and G. H. McKinley (2008), *J. Rheol.* **52**, 1427.
- Ewoldt, R. H., P. Winter, J. Maxey, and G. H. McKinley (2010), *Rheol. Acta* **49**, 191.
- Fabbian, L., W. Götze, F. Sciortino, P. Tartaglia, and F. Thiery (1999), *Phys. Rev. E* **59**, R1347.
- Falk, M. L., and J. S. Langer (1998), *Phys. Rev. E* **57**, 7192.
- Falk, M. L., and J. S. Langer (2011), *Annual Review of Condensed Matter Physics* **2**, 353.
- Falk, M. L., J. S. Langer, and L. Pechenik (2004), *Phys. Rev. E* **70**, 011507.
- Fall, A., F. Bertrand, G. Ovarlez, and D. Bonn (2009), *Phys. Rev. Lett.* **103**, 178301.
- Fall, A., A. Lemaître, F. B. Bonn, and G. Ovarlez (2010a), *Phys. Rev. Lett.* **105**, 268303.
- Fall, A., J. Paredes, and D. Bonn (2010b), *Phys. Rev. Lett.* **105**, 225502.
- Ferry, J. (1980), *Viscoelastic Properties of Polymers* (John Wiley & Sons, Inc.).
- Fielding, S. M., M. E. Cates, and P. Sollich (2009), *Soft Matter* **5**, 2378.
- Fielding, S. M., P. Sollich, and M. E. Cates (2000), *J. Rheol.* **44** (2), 323.
- Fiocco, D., G. Foffi, and S. Sastry (2013), *Phys. Rev. E* **88**, 020301.
- Foffi, G., C. de Michele, F. Sciortino, and P. Tartaglia (2005), *J. Chem. Phys.* **122**, 224903.
- Fonseca, C., S. Frey, M. Naccache, and P. de Souza Mendes (2013), *J. Non-Newtonian Fluid Mech.* **193**, 80.
- Fortin, M., and R. Glowinski (1983), *Augmented Lagrangian Methods* (North Holland).
- Frigaard, I., and C. Nouar (2005), *J. Non-Newtonian Fluid Mech.* **127**, 1.
- Fritschi, S., M. Fuchs, and T. Voigtmann (2014), *Soft Matter* **10**, 4822.
- Frölich, H., and R. Sack (1946), *Proc. R. Soc. Lond. A* **185**, 415.
- Fuchs, M., and M. E. Cates (2002), *Phys. Rev. Lett.* **89**, 248304.
- Fuchs, M., and M. E. Cates (2003), *Faraday Discuss.* **123**, 267.
- Fuchs, M., and M. E. Cates (2009), *J. Rheol.* **53**, 957.
- Fusco, C., T. Albaret, and A. Tanguy (2014), *Eur. Phys. J. E* **37**, 43.
- Gallot, T., C. Perge, V. Grenard, M.-A. Fardin, N. Taberlet, and S. Manneville (2013), *Review of Scientific Instruments* **84**, 045107.
- Ganeriwala, S. N., and C. A. Rotz (1987), *Polym. Eng. Sci.* **27**, 165.
- Gartling, D., and N. Phan-Thien (1984), *J. Non-Newtonian Fluid Mech.* **14**, 347.
- Geraud, B., L. Bocquet, and C. Barentin (2013), *Eur. Phys. J. E* **36**, 30.
- German, G., and V. Bertola (2010), *Phys. Fluids* **23**, 033101.
- Gibaud, T., C. Barentin, and S. Manneville (2008), *Phys. Rev. Lett.* **101**, 258302.
- Gibaud, T., C. Barentin, N. Taberlet, and S. Manneville (2009), *Soft Matter* **5**, 3026.
- Gibaud, T., D. Frelat, and S. Manneville (2010), *Soft Matter* **6**, 3482.
- Gilbreth, C., S. Sullivan, and M. Dennin (2006), *Phys. Rev. E* **74**, 051406.
- Gopalakrishnan, V., and C. Zukoski (2007), *J. Rheol.* **51**, 623.
- Götze, W. (2008), *Complex Dynamics of Glass-Forming Liquids: A Mode-Coupling Theory* (Oxford University Press, Oxford).
- Goyon, J., A. Colin, and L. Bocquet (2010), *Soft Matter* **6**, 2668.
- Goyon, J., A. Colin, G. Ovarlez, A. Ajdari, and L. Bocquet (2008), *Nature* **454**, 84.
- Graham, M. (1995), *J. Rheol.* **39**, 697.
- Grenard, V., T. Divoux, N. Taberlet, and S. Manneville (2014), *Soft Matter* **10**, 1555.
- Grenard, V., N. Taberlet, and S. Manneville (2011), *Soft Matter* **7**, 3920.
- Griffith, A. (1921), *Phil. Trans. R. Soc. A* **221**, 163.
- Gueslin, B., L. Talini, B. Herzhaft, Y. Peysson, and C. Allain (2006), *Phys. Fluids* **18**, 103101.
- Gutowski, I., D. Lee, J. de Bruyn, and B. Frisken (2012), *Rheol. Acta* **51**, 441.
- Habibi, M., J. Paredes, M. M. Denn, and D. Bonn (2015), “Wall slip correction and normal stress measurement in foams and emulsions,” *J. Rheol.*, submitted.
- Hansen, J. P., and I. R. McDonald (2006), *Theory of Simple Liquids* (Academic, London).
- Hartman Kok, P., S. Kazarian, B. Briscoe, and C. Lawrence (2004), *J. Colloid Interface Sci.* **280**, 511.
- Hartman Kok, P., S. Kazarian, C. Lawrence, and B. Briscoe (2002), *J. Rheol.* **46**, 481.
- Hartnett, J., and R. Hu (1989), *J. Rheol.* **33**, 671.
- Hatano, T. (2010), *Prog. Theor. Phys. Suppl.* **184**, 143.
- Hébraud, P., F. Lequeux, J.-P. Munch, and D. J. Pine (1997), *Phys. Rev. Lett.* **78**, 4657.
- van Hecke, M. (2010), *J. Phys.: Condens. Matter* **22**, 033101.
- Hermes, M., and P. Clegg (2013), *Soft Matter* **9**, 7568.
- Hermes, M., and M. Dijkstra (2010), *Europhys. Lett.* **89**, 38005.
- Herschel, W., and R. Bulkley (1926), *Kolloid Zeitschrift* **39**, 291.
- Hess, A., and N. Aksel (2011), *Phys. Rev. E* **84**, 051502.

- Hohenemser, K., and W. Prager (1932), *Z. Ang. Mat. Mech.* **12**, 216.
- Höhler, R., and S. Cohen-Addad (2005), *Journal of Physics: Condensed Matter* **17**, R1041.
- Hormozi, S., G. Dunbrack, and I. A. Frigaard (2014), *Phys. Fluids* **26**, 093101.
- Huang, N., G. Ovarlez, F. Bertrand, S. Rodts, P. Coussot, and D. Bonn (2005), *Phys. Rev. Lett.* **94**, 028301.
- Huilgol, R., and Z. You (2005), *J. Non-Newtonian Fluid Mech.* **128**, 126.
- Huisman, F., S. Friedman, and P. Taborek (2012), *Soft Matter* **8**, 6767.
- Husband, D. M., N. Aksel, and W. Gleissle (1993), *J. Rheol.* **37**, 215.
- Hyun, K., S. H. Kim, K. H. Ahn, and S. J. Lee (2002), *Journal of Non-Newtonian Fluid Mechanics* **107** (13), 51.
- Hyun, K., M. Wilhelm, C. Klein, K. Cho, J. Nam, K. Ahn, S. Lee, R. Ewoldt, and G. McKinley (2011), *Progress in Polymer Science* **36**, 1697.
- Ianni, F., R. D. Leonardo, S. Gentilini, and G. Ruocco (2007), *Phys. Rev. E* **75**, 011408.
- Ianni, F., R. D. Leonardo, S. Gentilini, and G. Ruocco (2008), *Phys. Rev. E* **77**, 031406.
- Ikeda, A., and L. Berthier (2013), *Phys. Rev. E* **88**, 052305.
- Ikeda, A., L. Berthier, and P. sollich (2012), *Phys. Rev. Lett.* **109**, 018301.
- Ikeda, A., L. Berthier, and P. sollich (2013), *Soft Matter* **9**, 7669.
- Illa, X., A. Puisto, A. Lehtinen, M. Mohtaschemi, and M. Alava (2013), *Phys. Rev. E* **87**, 022307.
- Irani, E., P. Chaudhuri, and C. Heussinger (2014), *Phys. Rev. Lett.* **112**, 188303.
- Isa, L., R. Besseling, and W. C. K. Poon (2007), *Phys. Rev. Lett.* **98**, 198305.
- Isayev, A., and X. Fan (1990), *J. Rheol.* **34**, 35.
- Jagla, E. A. (2007), *Phys. Rev. E* **76**, 046119.
- James, A., D. Williams, and P. Williams (1987), *Rheol. Acta* **26**, 437.
- Jana, S., B. Kapoor, and A. Acrivos (1995), *J. Rheol.* **39**, 1123.
- Jop, P., Mansard, P. Chaudhuri, L. Bocquet, and A. Colin (2012), *Phys. Rev. Lett.* **108**, 148301.
- Jossic, L., F. Ahonguio, and A. Magnin (2013), *J. Non-Newtonian Fluid Mech.* **191**, 14.
- Kabla, A., S. J., and G. Debrégeas (2007), *J. Fluid Mech.* **587**, 45.
- Kalyon, D. (2005), *J. Rheol.* **49**, 621.
- Kalyon, D., P. Yaras, B. Aral, and U. Yilmazer (1993), *J. Rheol.* **37**, 35.
- van Kao, S., L. Nielsen, and C. Hill (1975), *J. Colloid Interface Sci.* **53**, 358.
- Karppinen, A., T. Saarinen, J. Salmela, A. Laukkanen, M. Nuopponen, and J. Seppälä (2012), *Cellulose* **19**, 1807.
- Katgert, G., A. Latka, M. Möbius, and M. van Hecke (2009), *Phys. Rev. E* **79**, 066318.
- Katgert, G., M. Möbius, and M. van Hecke (2008), *Phys. Rev. Lett.* **101**, 058301.
- Kawasaki, T., D. Coslovich, A. Ikeda, and L. Berthier (2015), *Phys. Rev. E* **91**, 012203.
- de Kee, D., R. Chhabra, M. Powley, and S. Roy (1990), *Chem. Eng. Comm.* **96**, 229.
- Keentok, M. (1982), *Rheol. Acta* **21**, 325.
- Keim, N. C., and P. Arratia (2014), *Phys. Rev. Lett.* **112**, 028302.
- Khan, S. A., C. A. Schnepper, and R. C. Armstrong (1988), *Journal of Rheology* **32**, 69.
- Kiljański, T. (1989), *Rheol. Acta* **28**, 61.
- Kim, J., D. Merger, M. Wilhelm, and M. E. Helgeson (2014), *J. Rheol.* **58** (5), 1359.
- Kirkpatrick, T. R., and D. Thirumalai (1987), *Phys. Rev. Lett.* **58**, 2091.
- Klein, C. O., H. W. Spiess, A. Calin, C. Balan, and M. Wilhelm (2007), *Macromolecules* **40**, 4250.
- Knowlton, E. D., D. J. Pine, and L. Cipelletti (2014), *Soft Matter* **10**, 6931.
- Kogan, M., L. Ducloué, J. Goyon, X. Chateau, O. Pitois, and G. Ovarlez (2013), *Rheol. Acta* **52**, 237.
- Koumakis, N., J. F. Brady, and G. Petekidis (2013), *Phys. Rev. Lett.* **110**, 178301.
- Koumakis, N., M. Laurati, S. Egelhaaf, J. Brady, and G. Petekidis (2012), *Phys. Rev. Lett.* **108**, 098303.
- Koumakis, N., and G. Petekidis (2011), *Soft Matter* **7**, 2456.
- Kraynik, A. (1988), *Annu. Rev. Fluid Mech.* **20**, 325.
- Kumar, A., A. D. Stickland, and P. J. Scales (2012), *Korea-Aust. Rheol. J.* **24**, 105.
- Labiausse, V., R. Höhler, and S. Cohen-Addad (2007), *J. Rheol.* **51**, 479.
- Lang, E., and C. Rha (1981), *J. Text. Studies* **12**, 47.
- Larson, R. G. (1999), *The Structure and Rheology of Complex Fluids* (Oxford University Press).
- Laurati, M., S. Egelhaaf, and G. Petekidis (2011), *J. Rheol.* **55**, 673.
- Laurati, M., S. U. Egelhaaf, and G. Petekidis (2014), *J. Rheol.* **58** (5), 1395.
- Lavrenteva, O., and A. Nir (2010), *Rev. Chem. Eng.* **26**, 149.
- Lawn, B. (1993), *Fracture of Brittle Solids* (Cambridge University Press).
- Le Grand, A., and G. Petekidis (2008), *Rheol. Acta* **47** (5-6), 579.
- Lehtinen, A., A. Puisto, X. Illa, M. Mohtaschemi, and M. J. Alava (2013), *Soft Matter* **9**, 8041.
- Lequeux, F., and A. Ajdari (2001), *Phys. Rev. E* **63**, 030502.
- Lerner, E., G. Düring, and M. Wyart (2012), *Proc. Natl. Acad. Sci. USA* **109**, 4798.
- Letwimolnun, W., B. Vergnes, G. Ausias, and P. Carreau (2007), *J. Non-Newtonian Fluid Mech.* **141**, 167.
- Lidell, P., and D. V. Boger (1996), *J. Non-Newtonian Fluid Mech.* **63**, 235.
- Lin, S.-F., and R. Brodkey (1985), *J. Rheol.* **29**, 147.
- Lin-Gibson, S., J. A. Pathak, E. A. Grulke, H. Wang, and E. K. Hobbie (2004), *Phys. Rev. Lett.* **92**, 048302.
- Lindström, S., T. Kodger, J. Sprakel, and D. Weitz (2012), *Soft* **8**, 3657.
- Lipscomb, G., and M. Denn (1984), *J. Non-Newtonian Fluid Mech.* **14**, 337.
- Liu, A., and S. R. Nagel (1998), *Nature* **396**, 21.
- Liu, A. J., and S. R. Nagel, Eds. (2001), *Jamming and rheology* (Taylor and Francis, London).
- Liu, B., S. Muller, and M. Denn (2002), *J. Non-Newtonian Fluid Mech.* **102**, 179.
- Loewenberg, M., and J. Hinch (1996), *J. Fluid. Mech.* **321**, 395.
- Lois, G., J. Blawdziewicz, and C. S. O'Hern (2008), *Phys. Rev. Lett.* **100**, 028001.
- Louvet, N., D. Bonn, and H. Kellay (2014), *Phys. Rev. Lett.* **113**, 218302.
- Lu, P., E. Zaccarelli, F. Ciulla, A. B. Schofield, F. Sciortino, and D. A. Weitz (2008), *Nature* **453**, 499.

- Lubchenko, V. (2009), Proc. Natl. Acad. Sci. USA **106**, 11506.
- Lubchenko, V., and P. G. Wolynes (2007), Annu. Rev. Phys. Chem. **58**, 235.
- Macosko, C. (1994), *Rheology. Principles, measurements, and applications*. (Wiley - VCH, New York).
- Magda, J. J., H. El-Gendy, K. Oh, M. D. Deo, A. Montesi, and R. Venkatesan (2009), Energy & Fuels **23** (3), 1311, <http://pubs.acs.org/doi/pdf/10.1021/ef800628g>.
- Magnin, A., and J. Piau (1990), J. Non-Newtonian Fluid Mech. **36**, 85.
- Majumdar, S., R. Krishnaswamy, and A. Sood (2011), Soft Matter **7**, 7805.
- Maki, K., and Y. Renardy (2010), J. Non-Newtonian Fluid Mech. **165**, 1373.
- Maloney, C. E., and A. Lemaitre (2006), Phys. Rev. E **74**, 016118.
- Manley, S., H. M. Wyss, K. Miyazaki, J. C. Conrad, V. Trappe, L. J. Kaufman, and D. R. Reichman (2005), Phys. Rev. Lett. **95**, 238302.
- Manneville, S. (2008), Rheol. Acta **47**, 301.
- Manneville, S., L. Bécu, and A. Colin (2004), Eur. Phys. J. AP **28**, 361.
- Mansard, V., and A. Colin (2012), Soft Matter **8**, 4025.
- Martens, K., L. Bocquet, and J.-L. Barrat (2012), Soft Matter **8**, 4197.
- Martinie, L., H. Buggisch, and N. Willenbacher (2013), J. Rheol. **57**, 627.
- Marunaka, R., and M. Kawaguchi (2014), Colloids and Surfaces A: Physicochemical and Engineering Aspects **456** (0), 75.
- Marze, S., D. Langevin, and A. Saint-Jalmes (2008), J. Rheol. **52**, 1091.
- Mas, R., and A. Magnin (1994), J. Rheol. **38**, 889.
- Mason, T. G., J. Bibette, and D. A. Weitz (1996), J. Colloid Interface Sci. **179**, 439.
- Masselon, C., J.-B. Salmon, and A. Colin (2008), Phys. Rev. Lett. **100**, 038301.
- Meeker, S. P., R. T. Bonnecaze, and M. Cloitre (2004a), J. Rheol. **48**, 1295.
- Meeker, S. P., R. T. Bonnecaze, and M. Cloitre (2004b), Phys. Rev. Lett. **92**, 198302.
- Mewis, J., and M. Denn (1983), J. Non-Newtonian Fluid Mech. **12**, 69.
- Mewis, J., and A. Spaul (1976), Adv. Colloid Interface Sci. **6**, 173.
- Mewis, J., and N. J. Wagner (2009), Advances in Colloid and Interface Science **147–148**, 214.
- Michaels, A., and J. Bolger (1962), Ind. Eng. Chem. Fundam. **1**, 153.
- MiDi, G. (2004), Eur. Phys. J. E **14**, 341.
- Miguel, M.-C., L. Laurson, and M. Alava (2008), Eur. Phys. J. B **64**, 443.
- Miguel, M.-C., A. Vespignani, M. Zaiser, and S. Zapperi (2002), Phys. Rev. Lett. **89**, 165501.
- Min Kim, J., A. P. R. Eberle, A. Kate Gurnon, L. Porcar, and N. J. Wagner (2014), J. Rheol. **58** (5), 1301.
- Mitsoulis, E. (2007), *Rheology Reviews*, edited by D. Binding, N. Hudson, and R. Keunings (British Society of Rheology, Glasgow).
- Miyazaki, K., and D. R. Reichman (2002), Phys. Rev. E **66**, 050501.
- Möbius, M. E., G. Katgert, and M. van Hecke (2010), Europhys. Lett. **90**, 44003.
- Mohan, L., R. Bonnecaze, and M. Cloitre (2013a), Phys. Rev. Lett. **111**, 268301.
- Mohan, L., C. Pellet, M. Cloitre, and R. Bonnecaze (2013b), J. Rheol. **57**, 1023.
- Mohraz, A., and M. Solomon (2005), J. Rheol. **49**, 657.
- Mohtaschemi, M., A. Puisto, X. Illa, and M. J. Alava (2014), Soft Matter **10**, 2971.
- Møller, P. C. F., A. Fall, and D. Bonn (2009a), Europhys. Lett. **87**, 38004.
- Møller, P. C. F., A. Fall, V. Chikkadi, D. Derks, and D. Bonn (2009b), Phil. Trans. R. Soc. Lond. A **367**, 5139.
- Møller, P. C. F., J. Mewis, and D. Bonn (2006), Soft Matter **2**, 274.
- Møller, P. C. F., S. Rodts, M. A. J. Michels, and D. Bonn (2008), Phys. Rev. E **77**, 041507.
- Montesi, A., A. P. na, and M. Pasquali (2004), Phys. Rev. Lett. **92**, 058303.
- Mooney, M. (1931), J. Rheol. **2**, 210.
- Moorcroft, R., M. Cates, and S. Fielding (2011), Phys. Rev. Lett. **106**, 055502.
- Moorcroft, R., and S. Fielding (2013), Phys. Rev. Lett. **110**, 086001.
- Mora, S. (2011), Soft Matter **7**, 4908.
- Moyers-Gonzalez, M., and I. Frigaard (2004), J. Non-Newtonian Fluid Mech. **122**, 227.
- Mujumdar, A., A. N. Beris, and B. Metzner (2002), J. Non-Newtonian Fluid Mech. **102**, 157.
- Nagamanasa, K. H., S. Gokhale, A. K. Sood, and R. Ganapathy (2014), Phys. Rev. E **89**, 062308.
- Nagase, Y., and K. Okada (1986), J. Rheol. **30**, 1123.
- Navarrete, R., L. Scriven, and C. Macosko (1996), J. Colloid Interface Sci. **180**, 200.
- Navickis, L., and E. Bagley (1983), J. Rheol. **27**, 519.
- Negi, A., and C. Osuji (2009), Rheol. Acta **48**, 871.
- Negi, A., and C. Osuji (2010a), Europhys. Lett. **90**, 28003.
- Negi, A., and C. Osuji (2010b), J. Rheol. **54**, 943.
- Negi, A., and C. Osuji (2010c), Phys. Rev. E **82**, 031404.
- Nguyen, Q., T. Akroyd, D. de Kee, and L. Zhu (2006), Korea-Australia Rheol. J. **18**, 15.
- Nguyen, Q., and D. Boger (1983), J. Rheol. **27**, 321.
- Nguyen, Q., and D. Boger (1992), Annu. Rev. Fluid Mech. **24**, 47.
- Nichol, K., and M. van Hecke (2012), Phys. Rev. E **85**, 061309.
- Nichol, K., A. Zanin, R. Bastien, E. Wandersman, and M. van Hecke (2010), Phys. Rev. Lett. **104**, 078302.
- Nickerson, C., and J. Kornfield (2005), J. Rheol. **49**, 865.
- Nordstrom, K., E. Verneuil, P. Arratia, A. Basu, Z. Zhang, A. Yodh, J. Gollub, and D. Durian (2010), Phys. Rev. Lett. **105**, 175701.
- Nott, P., and J. Brady (1994), J. Fluid Mech. **275**, 157.
- Oldroyd, J. (1947a), Proc. Camb. Philos. Soc. **43**, 100.
- Oldroyd, J. (1953), Proc. R. Soc. Lond. A **218**, 122.
- Oldroyd, J. G. (1947b), Math. Proc. Cambridge **43**, 383.
- Olmsted, P. D. (2008), Rheol. Acta **47**, 283.
- Olsson, P., and S. Teitel (2007), Phys. Rev. Lett. **99**, 178001.
- Olsson, P., and S. Teitel (2011), Phys. Rev. E **83**, 030302.
- Olsson, P., and S. Teitel (2012), Phys. Rev. Lett. **109**, 108001.
- Oppong, F. K., L. Rubatat, B. J. Frisken, A. E. Bailey, and J. R. de Bruyn (2006), Phys. Rev. E **73**, 041405.
- Osuji, C. O., C. Kim, and D. A. Weitz (2008), Phys. Rev. E **77**, 060402(R).
- Ovarlez, G., F. Bertrand, and S. Rodts (2006), J. Rheol. **50**, 259.

- Ovarlez, G., and X. Chateau (2008), *Phys. Rev. E* **77**, 061403.
- Ovarlez, G., S. Cohen-Addad, K. Krishan, J. Goyon, and P. Coussot (2013a), *J. Non-Newtonian Fluid Mech.* **193**, 68.
- Ovarlez, G., K. Krishan, and S. Cohen-Addad (2010), *Europhys. Lett.* **91**, 68005.
- Ovarlez, G., F. Mahaut, F. Bertrand, and X. Chateau (2011), *J. Rheol.* **55**, 197.
- Ovarlez, G., S. Rodts, X. Chateau, and P. Coussot (2009), *Rheol. Acta* **48**, 831.
- Ovarlez, G., S. Rodts, A. Ragouilliaux, P. Coussot, J. Goyon, and A. Colin (2008), *Phys. Rev. E* **78**, 036307.
- Ovarlez, G., L. Tocquer, F. Bertrand, and P. Coussot (2013b), *Soft Matter* **9**, 5540.
- Papanastasiou, T. (1987), *J. Rheol.* **31**, 385.
- Papenhuijzen, J. (1972), *Rheol. Acta* **11**, 73.
- Paredes, J. (2013), *Understanding the Rheology of Yield Stress Materials.*, Ph.D. thesis (Univ. of Amsterdam).
- Paredes, J., M. M. Denn, and D. Bonn (2015), "On different ways of measuring "the" yield stress," To appear in *Journal of Rheology*.
- Paredes, J., M. A. J. Michels, and D. Bonn (2013), *Phys. Rev. Lett.* **111**, 015701.
- Paredes, J., N. Shahidzadeh-Bonn, and D. Bonn (2011), *J. Phys.: Condens. Matter* **23**, 284116.
- Parisi, G., and F. Zamponi (2010), *Rev. Mod. Phys.* **82**, 789.
- Park, J., and K. Ahn (2013), *Soft Matter* **9**, 11650.
- Perchikov, N., and E. Bouchbinder (2014), *Phys. Rev. E* **89**, 062307.
- Pérez-González, J., J. López-Durán, B. Marín-Santibáñez, and F. Rodríguez-González (2012), *Rheol. Acta* **51**, 937.
- Perge, C. (2014), *Ultrasonic imaging in soft materials*, Ph.D. thesis (École Normale Supérieure de Lyon).
- Perge, C., N. Taberlet, T. Gibaud, and S. Manneville (2014), *J. Rheol.* **58**, 1331.
- Persello, J., A. Magnin, J. Chang, J. Piau, and B. Cabane (1994), *J. Rheol.* **38**, 1845.
- Petekidis, G., A. Moussaid, and P. Pusey (2002), *Phys. Rev. E* **66**, 051402.
- Petekidis, G., D. Vlassopoulos, and P. Pusey (2003), *Faraday Discuss.* **123**, 287.
- Petekidis, G., D. Vlassopoulos, and P. Pusey (2004), *J. Phys. Condens. Matter* **16**, S3955.
- Peyneau, P.-E., and J.-N. Roux (2008), *Phys. Rev. E* **78**, 011307.
- Pham, K., G. Petekidis, D. Vlassopoulos, S. Egelhaaf, P. Pusey, and W. Poon (2006), *Europhys. Lett.* **1975**, 624.
- Pham, K. N., S. U. Egelhaaf, P. N. Pusey, and W. C. K. Poon (2004), *Phys. Rev. E* **69**, 011503.
- Pham, K. N., A. M. Puertas, J. Bergenholtz, S. U. Egelhaaf, A. Moussaid, P. N. Pusey, A. B. Schofield, M. E. Cates, M. Fuchs, and W. C. K. Poon (2002), *Science* **296**, 104.
- Picard, G., A. Ajdari, L. Bocquet, and F. Lequeux (2002), *Phys. Rev. E* **66**, 051501.
- Picard, G., A. Ajdari, F. Lequeux, and L. Bocquet (2004), *Eur. Phys. J. E* **15**, 371.
- Picard, G., A. Ajdari, F. Lequeux, and L. Bocquet (2005), *Phys. Rev. E* **71**, 010501(R).
- Pignon, F., A. Magnin, and J.-M. Piau (1996), *J. Rheol.* **40**, 573.
- Pinder, K. (1964), *Can. J. Chem. Eng.* **42**, 132.
- Pipkin, A. C. (1972), *Lectures on Viscoelasticity Theory* (Springer, New York).
- Plazek, D. (1960), *J. Colloid Sci.* **15**, 50.
- Pomeau, Y. (1992), *C.R. Acad. Sci. Ser. II* **314**, 553.
- Poulos, A. S., J. Stellbrink, and G. Petekidis (2013), *Rheol. Acta* **52**, 785.
- Poumaere, A., M. Moyers-González, C. Castelain, and T. Burghellea (2014), *J. Non-Newtonian Fluid Mech.* **205**, 28.
- Prager, W. (1961), *Introduction to mechanics of continua* (Ginn, Boston).
- Pratt, E., and M. Dennin (2003), *Phys. Rev. E* **67**, 051402.
- Princen, H. M. (1985), *J. Colloid Interface Sci.* **105**, 150.
- Princen, H. M., and A. D. Kiss (1987), *J. Colloid Interface Sci.* **112**, 427.
- Princen, H. M., and A. D. Kiss (1989), *J. Colloid Interface Sci.* **128**, 176.
- Puertas, A. M., and M. Fuchs (2009), in *Structure and functional properties of colloidal systems*, edited by R. Hidalgo-Alvarez (Taylor and Francis, London).
- Puertas, A. M., E. Zaccarelli, and F. Sciortino (2005), *J. Phys.: Condens. Matter* **17**, L271.
- Pusey, P. N., and W. van Megen (1986), *Nature (London)* **320**, 340.
- Pusey, P. N., and W. van Megen (1987), *Phys. Rev. Lett.* **59**, 2083.
- Putz, A., T. Burghellea, I. Frigaard, and D. Martinez (2008), *Phys. Fluids* **20**, 033102.
- Putz, A., and I. Frigaard (2010), *JNNFM* **165**, 263.
- Putz, A., I. Frigaard, and D. Martinez (2009), *J. Non-Newtonian Fluid Mech.* **163**, 62.
- Rabideau, B., and C. L. L. Coussot (2009), *Rheol. Acta* **48**, 517.
- Ragouilliaux, A., B. Herzhaft, F. Bertrand, and P. Coussot (2006), *Rheol. Acta* **46**, 261.
- Ragouilliaux, A., G. Ovarlez, N. Shahidzadeh-Bonn, B. Herzhaft, T. Palermo, and P. Coussot (2007), *Phys. Rev. E* **76**, 051408.
- Rainone, C., P. Urbani, H. Yoshino, and F. Zamponi (2015), *Phys. Rev. Lett.* **114**, 015701.
- Reddy, K. A., Y. Forterre, and O. Pouliquen (2011), *Phys. Rev. Lett.* **106**, 108301.
- Regev, I., T. Lookman, and C. Reichhardt (2013), *Phys. Rev. E* **88**, 062401.
- Renardy, M. (2010), *J. Non-Newtonian Fluid Mech.* **165**, 519.
- Renardy, M., and Y. Renardy (2004), *J. Non-Newtonian Fluid Mech.* **122**, 302.
- Renardy, Y., and H. Grant (2013), *Rheol. Acta* **52**, 867.
- Renou, F., J. Stellbrink, and G. Petekidis (2010), *J. Rheol.* **54**, 1219.
- Roberts, G., and H. Barnes (2001), *Rheol. Acta* **40** (5), 499.
- Rodney, D., A. Tanguy, and D. Vandembroucq (2011), *Modelling Simul. Mater. Sci. Eng.* **19**, 083001.
- Rogers, M., K. Chen, L. Andrzejewski, S. Narayanan, S. Ramakrishnan, R. Leheny, and J. Harden (2014), *Phys. Rev. E* **90**, 062310.
- Rogers, S. A., B. M. Erwin, D. Vlassopoulos, and M. Cloitre (2011a), *J. Rheol.* **55**, 733.
- Rogers, S. A., B. M. Erwin, D. Vlassopoulos, and M. Cloitre (2011b), *J. Rheol.* **55**, 435.
- Rogers, S. A., D. Vlassopoulos, and P. T. Callaghan (2008), *Phys. Rev. Lett.* **100**, 128304.
- Rottler, J., and M. O. Robbins (2005), *Phys. Rev. Lett.* **95**, 225504.
- Rouyer, F., S. Cohen-Addad, and R. Höhler (2005), *Colloids Surfaces A* **263**, 111.

- Royall, C., W. Poon, and E. Weeks (2013), *Soft Matter* **9**, 17.
- Royall, C. P., S. R. Williams, T. Ohtsuka, and H. Tanaka (2008), *Nature Mater.* **7**, 556.
- Royall, C. P., S. R. Williams, and H. Tanaka (2015), “The nature of the glass and gel transitions in sticky spheres,” *ArXiv:1409.5469*.
- Saint-Jalmes, A., and D. Durian (1999), *J. Rheol.* **43**, 1411.
- Salmon, J.-B., L. Bécu, S. Manneville, and A. Colin (2003a), *Eur. Phys. J. E* **10**, 209.
- Salmon, J.-B., S. Manneville, A. Colin, and B. Pouligny (2003b), *Eur. Phys. J. AP* **22**, 143.
- dos Santos, D., S. Frey, M. Naccache, and P. de Souza Mendes (2014), *Rheol. Acta* **53**, 31.
- Saramito, P. (2007), *J. Non-Newtonian Fluid Mech.* **145**, 1.
- Saunders, B., and B. Vincent (1999), *Adv. Colloid Interface Sci.* **80**, 1.
- Sausset, F., G. Biroli, and J. Kurchan (2010), *J. Stat. Phys.* **140**, 718.
- Schall, P., D. A. Weitz, and F. Spaepen (2007), *Science* **318**, 1895.
- Schmitt, V., C. M. Marques, and F. Lequeux (1995), *Phys. Rev. E* **52**, 4009.
- Schowalter, W., C. Chaffey, and H. Brenner (1968), *J. Colloid Interface Sci.* **26**, 152.
- Schurz, J. (1990), *Rheol. Acta* **29**, 170.
- Schwartz, L., and H. Princen (1987), *J. Colloid Interface Sci.* **118**, 201.
- Sciortino, F. (2002), *Nature Materials* **1**, 145.
- Sciortino, F., and P. Tartaglia (2005), *Adv. Phys.* **54**, 471.
- Sciortino, F., P. Tartaglia, and E. Zaccarelli (2003), *Phys. Rev. Lett.* **91**, 268301.
- Segré, G., and A. Silberberg (1961), *Nature* **189**, 209.
- Seth, J., M. Cloitre, and R. Bonnecaze (2008), *J. Rheol.* **52**, 1241.
- Seth, J., C. Locatelli-Champagne, F. Monti, R. Bonnecaze, and M. Cloitre (2012), *Soft Matter* **8**, 140.
- Seth, J., L. Mohan, C. Locatelli-Champagne, M. Cloitre, and R. Bonnecaze (2011), *Nature Materials* **10**, 838.
- Shahin, A., and Y. Joshi (2010), *Langmuir* **26**, 4219.
- Shahin, A., and Y. Joshi (2012), *Langmuir* **28**, 15674.
- Shaukat, A., M. Kaushal, A. Sharma, and Y. Joshi (2012a), *Soft Matter* **8**, 10107.
- Shaukat, A., A. Sharma, and Y. M. Joshi (2012b), *Journal of Non-Newtonian Fluid Mechanics* **167–168** (0), 9.
- Shi, Y., M. B. Katz, H. Li, and M. L. Falk (2007), *Phys. Rev. Lett.* **98**, 185505.
- Siebenbürger, M., M. Ballauf, and T. Voigtman (2012), *Phys. Rev. Lett.* **108**, 255701.
- Siebenbürger, M., M. Fuchs, and M. Ballauff (2012), *Soft Matter* **8**, 4014.
- Singh, J., and M. Denn (2008), *Phys. Fluid* **20**, 040901.
- Sollich, P. (1998), *Phys. Rev. E* **58** (1), 738.
- Sollich, P., and M. E. Cates (2012), *Phys. Rev. E* **85**, 031127.
- Sollich, P., F. Lequeux, P. Hébraud, and M. E. Cates (1997), *Phys. Rev. Lett.* **78**, 2020.
- Soltani, F., and U. Yilmazer (1998), *Journal of Applied Polymer Science* **70**, 515.
- de Souza Mendes, P. (2009), *J. Non-Newtonian Fluid Mech.* **64**, 66.
- de Souza Mendes, P. (2011), *Soft Matter* **7**, 2471.
- Spaans, R., and M. Williams (1995), *J. Rheol.* **39**, 241.
- Speers, R., K. Holme, M. Tung, and W. Williamson (1987), *Rheol. Acta* **26**, 447.
- Spenley, A., M. E. Cates, and T. C. B. McLeish (1993), *Phys. Rev. Lett.* **71**, 939.
- Sprakel, J., S. Lindström, T. Kodger, and D. Weitz (2011), *Phys. Rev. Lett.* **106**, 248303.
- Szamel, G. (2010), *Europhys. Lett.* **91**, 56004.
- Tabuteau, H., S. Mora, G. Porte, M. Abkarian, and C. Ligoure (2009), *Phys. Rev. Lett.* **102**, 155501.
- Tanguy, A., F. Leonforte, and J.-L. Barrat (2006), *Eur. Phys. J. E* **20**, 355.
- Tanner, R. (2000), *Engineering Rheology*, 2nd ed. (Oxford).
- Teece, L. J., M. A. Faers, and P. Bartlett (2011), *Soft Matter* **7**, 1341.
- Testard, V., L. Berthier, and W. Kob (2011), *Phys. Rev. Lett.* **106**, 125702.
- Tighe, B. P., E. Woldhuis, J. J. C. Remmers, W. van Saarloos, and M. van Hecke (2010), *Phys. Rev. Lett.* **105**, 088303.
- Tiu, C., and D. Boger (1974), *J. Text. Studies* **5**, 329.
- Tokpavi, D. L., P. Jay, A. Magnin, and L. Jossic (2009), *J. Non-Newtonian Fluid Mech.* **164**, 35.
- Torquato, S., and F. H. Stillinger (2010), *Rev. Mod. Phys.* **82**, 2633.
- Truzzolillo, D., D. Vlassopoulos, and M. Gauthier (2013), *Journal of Non-Newtonian Fluid Mechanics* **193** (0), 11, viscoplastic Fluids: From Theory to Application.
- Uhlherr, P., J. Guo, C. Tiu, X.-M. Zhang, J.-Q. Zhou, and T.-N. Fang (2005), *J. Non-Newtonian Fluid Mech.* **125**, 101.
- Vandembroucq, D., and S. Roux (2011), *Phys. Rev. B* **84**, 134210.
- Vanel, L., S. Ciliberto, and P.-P. Cortet (2009), *J. Phys. D: Appl. Phys.* **42**, 214007.
- Varnik, F., L. Bocquet, and J.-L. Barrat (2004), *J. Chem. Phys.* **120**, 2788.
- Varnik, F., L. Bocquet, J.-L. Barrat, and L. Berthier (2003), *Phys. Rev. Lett.* **90**, 095702.
- Viasnoff, V., and F. Lequeux (2002), *Phys. Rev. Lett.* **89**, 065701.
- Vinogradov, G., G. Froishteter, and K. Trilisky (1978), *Rheol. Acta* **17**, 156.
- Vinogradov, G., G. Froishteter, K. Trilisky, and Y. Smorodinsky (1975), *Rheol. Acta* **14**, 765.
- Voigtman, T. (2014), “Nonlinear glassy rheology,” To appear in *Current Opinion in Colloid & Interface Science*.
- Wagner, C., Y. Amarouchene, D. Bonn, and J. Eggers (2005), *Phys. Rev. Lett.* **95**, 164504.
- Walls, H., S. Caines, A. Sanchez, and S. Khan (2003), *J. Rheol.* **47**, 847.
- Walton, I., and S. Bittleston (1991), *J. Fluid Mech.* **222**, 39.
- Wein, O., and V. Tovchigrechko (1992), *J. Rheol.* **36**, 812.
- West, A., J. Melrose, and R. Ball (1994), *Phys. Rev. E* **49**, 4237.
- White, J. (1979), *J. Non-Newtonian Fluid Mech* **5**, 177.
- Whittle, M., and E. Dickinson (1997), *J. Chem. Phys.* **107**, 10191.
- Wilhelm, M. (2002), *Macromol. Mater. Eng.* **287**, 83.
- Wilhelm, M., K. Reinheimer, and J. Kübel (2012), *Z. Phys. Chem.* **226**, 547.
- Wyss, H., K. Miyazaki, J. Mattsson, Z. Hu, D. Reichman, and D. Weitz (2007), *Phys. Rev. Lett.* **98**, 238303.
- Xu, N., and C. S. O’Hern (2006), *Phys. Rev. E* **73**, 061303.
- Yan, Y., Z. Z. Z. Cheneler, J. Stokes, and M. Adams (2010), *Rheol. Acta* **49**, 255.
- Yildirim, O. E., and O. A. Basaran (2006), *J. Non-Newtonian Fluid Mech.* **136**, 17.

- Yilmazer, U., and D. Kalyon (1989), *J. Rheol.* **33**, 1197.
- Yoshimura, A. S., and R. K. Prud'homme (1988), *J. Rheol.* **32**, 53.
- Yoshino, H., and M. Mézard (2010), *Phys. Rev. Lett.* **105**, 015504.
- Yoshino, H., and F. Zamponi (2014), *Phys. Rev. E* **90**, 022302.
- Zaccarelli, E. (2007), *J. Phys.: Condens. Matter* **19**, 323101.
- Zaccarelli, E., S. V. Buldyrev, E. L. Nave, A. J. Moreno, I. Saika-Voivod, F. Sciortino, and P. Tartaglia (2005), *Phys. Rev. Lett.* **94**, 218301.
- Zaccarelli, E., and W. C. K. Poon (2009), *Proc. Natl. Acad. Sci. USA* **106**, 15203.
- Zausch, J., J. Horbach, M. Laurati, S. Egelhaaf, J. Brader, T. Voigtmann, and M. Fuchs (2008), *J. Phys. Condens. Matter* **20**, 404210.
- Zhu, L., N. Sun, K. Papadopoulos, and D. D. Kee (2001), *J. Rheol.* **45**, 1105.